MSG & Metop Satellite Measurements for Thunderstorm Predictions

Jonas Kvist Andersen, June 2017

DTU Space
National Space Institute

Abstract

This report investigates the characteristics of atmospheric instability indices and their predictive capabilities in relation to severe weather events, such as thunderstorms. Specifically, a series of three indices, denoted the Global Instability Index (GII), is investigated. One operational retrieval of the GII in clear-sky environments is done through measurements from the MSG. For the purpose of this project, two new GII retrievals based on measurements from the Metop satellites was implemented. One of these retrievals allowed for GII computation in all-sky environments (regardless of clouds). The GII retrievals are investigated against lightning data from various detection networks and severe weather reports through qualitative case studies. Furthermore, the three retrievals are compared against each other. Based on the case studies of the report it is concluded that predictive capabilities certainly exist for the GII, however with some flaws and room for improvement.

Contents

1 Introduction

Forecasting severe convective weather events such as thunderstorms, tornadoes, or large hail storms is of obvious interest, since an effective forecast may ultimately save large amount of property damage and even (in case of very severe storms) human lives. Especially societies in developing countries could potentially benefit from effective short-range forecasting, as buildings in these areas might not be sophisticated enough to withstand a thunderstorm or heavy rainfall. This is where the advantages of satellite measurements prove useful: In developing areas, or simply in very remote areas, there is rarely enough interest (and thus economical support) to install sophisticated ground-based forecast tools or monitoring systems such as lightning locating systems (for the purpose of studying lightning activity in the given region). Satellites may cover these regions just as easily as Europe or the United States, where interest in developing forecasting systems is higher, depending on the type of orbit of the satellite.

EUMETSAT's Meteosat Second Generation (MSG) satellite system, consisting of three satellites, has been operational since 2002, with the primary satellite (the one used in the case studies of this report) continuously measuring the entirety of Europe and Africa from a geostationary orbit centered at 0°. One of the applications of MSG is to provide measurements of the air-stability in pre-convective environments (that is, prior to any storm development). This is done in the shape of so-called instability indices. These indices are described further in section 2.1 - essentially, they allow for predictions of the convective potential over a given region, providing an indication of whether a thunderstorm should be expected or not, typically within a few hours to half a day (Koenig & de Coning, 2008). This type of very short-range forecasting is more accurately labelled as *nowcasting*. MSG provides a product called the Global Instability Index (GII), comprising a series of instability indices, which is also described further in sections 2.1-2.2.

The Metop satellite system, also operated by EUMETSAT, consists of two satellites in a sun-synchronous orbit, meaning that global coverage is achieved over the course of a day (this is explained in detail in section 2.3). The Metop satellites do not provide the GII product, however, they do provide the necessary measurements to compute the GII. For this report, a Metop GII (denoted IASI GII, after the primary instrument aboard Metop) was developed - an essential feature of the IASI GII, and one of the main motivations of this study, is that it can be computed both in cloud-free and cloudy conditions. A further description is provided in sections 2.3-2.4.

The main purpose of this report is to investigate the different GII retrievals and their use as nowcasting tools for thunderstorm (and other severe weather events often associated with thunderstorms). This is done through a series of case studies, in which the GII is investigated early in the day and compared to the observed weather conditions during the remaining day and evening hours. Section 3 describes the types of data, mainly measurements of lightning activity, that is utilized to monitor severe weather. Section 4 provides a short introduction to the programs created for GII processing. These data processing routines are part of the "product" of this project, as they will allow for quick implementation of MSG/Metop GII measurements for use in other studies **or as auxiliary data for the ASIM Data Center**.
The case studies are provided in section 5, while a discussion of results and prospects of future studies is provided in section 6. Finally, a brief conclusion of the findings of the report will be provided in section 7.

2 Computing instability indices utilizing MSG and Metop measurements

This section introduces the concept of instability indices as well as a series of specific instability indices that comprise a product denoted the GII (Global Instability Index). Then follows an outline of how measurements from two different satellites both (independently of each other) provide the necessary input to compute the GII. Finally, a description of how the satellite measurements are used to compute the GII is given.

2.1 Instability indices

A vast amount of indices for indication of instability and convection exist. Some have been used for several decades while others have been modified and yet other indices have simply fallen out of meteorologists' favor. What these indices generally have in common, is that they provide a value for a given point on Earth, which is then used to asses the stability of the atmosphere above this point and hence the potential for severe convective

weather events to occur (other types of instability indices exist, where the dimensionality in which values are assigned is not two dimensional latitude vs. longitude, however in this report all instability are of the type described in the former.)

EUMETSAT (responsible for both MSG and Metop, the satellite systems used in this report) has combined the instability indices obtained by the processing of MSG (SEVIRI) data into a product titled the Global Instability Index - it comprises the K-index, Lifted index, Total Precipitable Water content, KO-index, and the Maximum Buoyancy. In this study, three instability indices, derived independently from two different satellite systems (MSG and Metop), are investigated for a series of case studies across Europe. The indices are the K-index, Lifted index, and Total Precipitable Water content. The KO-index and Maximum Buoyancy are not investigated. The KO-index was discarded due to the fact that its computation requires the temperature at 1000 hPa, making it very often undefined for even slightly lifted terrain, and the Maximum Buoyancy was discarded due to its seemingly smaller popularity in literature. As such, for the purpose of this study, the Global Instability Index is taken to comprise the K-index, Lifted index, and Total Precipitable Water content. In this section follows an introduction of each of the three chosen instability indices, how they are computed, and how their physical interpretations relate to convection and thunderstorm potential. Usually, certain threshold values are introduced for the instability indices, meaning that values above (or below) this threshold indicates unstable conditions - it must be stressed, that these thresholds are empirical in nature and may vary with geographic location, season, and other conditions. Thus, for a given area, the instability indices provide an indication of the likelihood of convection and *not* an absolutely certain prediction.

Important to note is that for a given point on Earth, all three instability indices can be computed when vertical profiles of atmospheric temperature and water vapor content (humidity) versus pressure are known over the given point. Figure 1 shows a basic sketch of the dimensions of the vertical profiles - vertical temperature and humidity profiles are, for a given area on the Earth's surface, provided for a certain amount of pressure levels. For IASI, the temperature/humidity profile product is denoted as the IASI Level 2 product - in this report, Level 2 data shall be understood as vertical temperature and humidity profiles. Sections 2.2 and 2.3 describe how this data is obtained by the MSG and Metop satellites, respectively, and section 2.4 outlines how the instability indices are computed from these vertical profiles.

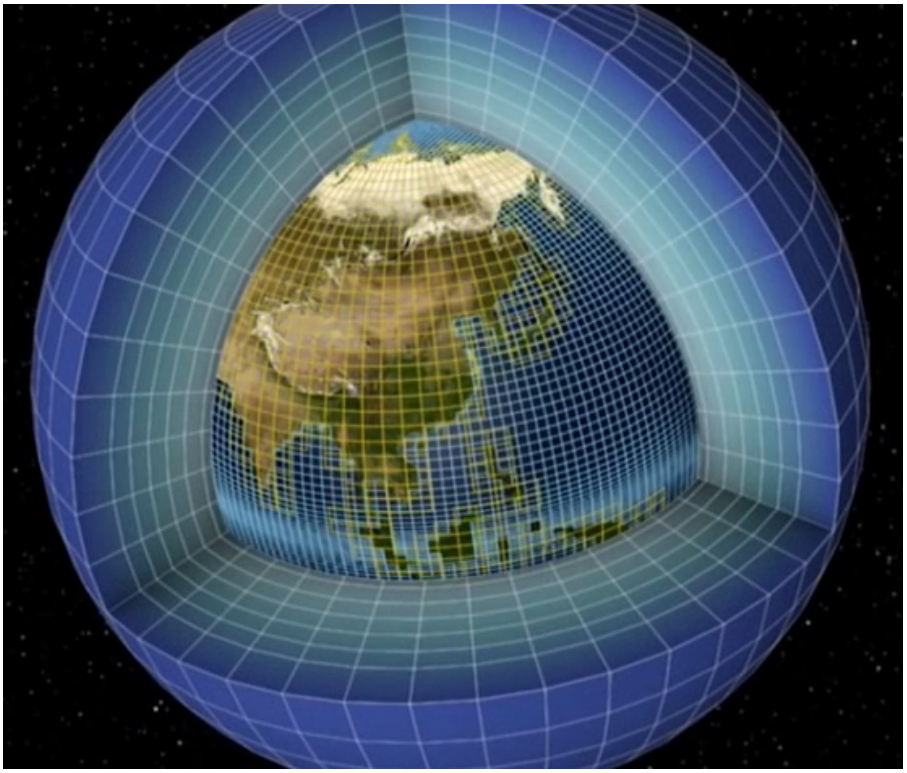

Figure 1: Illustration of a three dimensional grid in the Earth's atmosphere. The size of each grid cell is not to scale - the figure is purely shown to give an illustration of the dimnesionality of the vertical temperature and humidity profiles needed to compute the GII. (Image taken from video on the EUMETSAT website[1].)

2.1.1 K-index (KI)

The K-index was developed by American meteorologist J. J. George in 1960 as a measure of thunderstorm potential over continental areas in summertime. For a column of the atmosphere it is defined as:

$$K = (T_{850} - T_{500}) + TD_{850} - (T_{700} - TD_{700}) \tag{1}$$

where T is air temperature and TD is dew point temperature. The subscripts indicate pressure level in hPa - thus, T_{850} is the air temperature at 850 hPa and so on. The K-index combines information on the vertical temperature lapse rate, moisture content in the lower atmosphere, and the vertical extent of the low-level moisture. The vertical temperature is reflected by the term in the first parentheses, namely the difference in temperature between 850 hPa and 500 hPa - a steeper temperature difference from the lower, warmer atmosphere to the higher, colder atmosphere yields a higher K-index. The dew point temperature at 850 hPa yields information about the low atmosphere moisture level - the higher the dew point temperature, the more moisture will be present in the lower atmosphere, resulting in a higher K-index. Finally, the term in the final parentheses (the difference between temperature and dew point temperature, also known as the temperature-dew point depression, at 700 hPa) reflects the vertical extent of the low-level moisture - a smaller difference between temperature and dew point temperature implies a higher level of humidity and a higher K-index. Thus, in short, a high K-index is found in an atmosphere where the temperature lapse rate is high and a large part of the lower atmosphere contains a high level of moisture. K-index is usually given in degrees Celsius (Peppler, 1988).

George designed the index based on rawinsonde measurements in the Eastern US and found that a K-index > 20 °C was indicative of an increased frequency in air mass thunderstorms. Another study, conducted in the Western US, suggested that a K-index in the range 15 °C $< K <$ 20 °C indicated a probability of thunderstorms of less than 20%, whereas $K > 40$ °C indicated a thunderstorm probability of nearly 100%. Yet another study found that the K-index was a relatively poor predictor of severe thunderstorms but one of the best predictors of less severe summertime thunderstorms and various types of rainfall (Peppler, 1988).

[1] `http://www.eumetsat.int/website/home/Satellites/CurrentSatellites/Metop/MetopDesign/IASI/index.html`

2.1.2 Lifted index (LI)

The Lifted index was developed by J. G. Galway in 1956 as an indicator of latent atmospheric instability in the afternoon/evening hours, yielding a prediction index for severe storms. It is a modification of another instability index (the Showalter index) and was developed for the prediction of storms over the United States. Generally, the Lifted index is expressed simply as:

$$LI = T_{500} - T_{500}^{\text{lifted from surface}} \tag{2}$$

where T_{500} is the air temperature at 500 hPa and $T_{500}^{\text{lifted from surface}}$ represents the temperature of a surface air parcel lifted adiabatically to 500 hPa. Galway defined the surface air parcel as the lowest 3000 ft (914.4 m) of the atmosphere and assigned it the mean mixing ratio (humidity) of this layer and the forecasted maximum afternoon temperature, making Galway's Lifted index a prediction index. Many variations of the Lifted index have been implemented. In this study, the surface air parcel is defined as the lowest 100 hPa of the atmosphere and assigned the mean mixing ratio *and* the mean air temperature of this layer. This variation is therefore known as a static index, as no forecasted temperature is used. It is a fairly common modification used in several other studies (Peppler, 1988, Haklander & van Delden, 2003) as well as in the operational MSG SEVIRI GII computation of the Lifted index (EUMETSAT, Global Instability Index: Product Guide, reference given in section 9) - this is explained further in section 2.4.
If the surface air parcel temperature upon adiabatic lifting to 500 hPa is higher than the ambient air temperature at 500 hPa the air parcel will (theoretically) continue to rise, leading to convective storm development. This is indicated by a negative Lifted index. No specific threshold value for the Lifted index was developed by Galway, however typical upper bounds for severe thunderstorm activity lie in the interval -2 to $+2$ - that is, potential for severe storms increases with decreasing Lifted index (Peppler 1988). Furthermore, a low Lifted index has been utilized as an indicator of potential for tornado outbreaks (Ferguson 1983).

2.1.3 Total Precipitable Water (TPW)

A key element in the development of convective storms is the presence of water vapor in the atmosphere. Computing the Total Precipitable Water is a straightforward way of evaluating the extent of the atmospheric humidity - it is simply the total water vapor content of a column of the atmosphere (measured in kg/m^2). As such, TPW is more accurately labeled as an air mass parameter, rather than an empirical index. Given a profile of the atmospheric water vapor mixing ratio, $q(p)$, pressure, p, as well as the gravitational acceleration, $g(z, \phi)$ (dependent on altitude, z, and latitude, ϕ), the Total Precipitable Water content (TPW) is computed as:

$$TPW = \int_{\text{surface}}^{\text{top of atmosphere}} \frac{q(p)}{g(z, \phi)} dp \tag{3}$$

Given a humidity profile of M pressure levels, the integral can be evaluated as a summation - this is explained in further detail in section 2.4.3.

Seeing as the TPW content is not an empirical index designed for the purpose of detecting instability, determining approximative threshold levels corresponding to likelihoods of certain degrees of thunderstorm activity (as has been done for the K-index and Lifted index) is not quite feasible. Instead, the TPW content of a given area is considered in relation to the average TPW of the surrounding - an area showing TPW values high above the average TPW of the surroundings are interpreted as potentially unstable, whereas an area with TPW values far below the average TPW of the surroundings is considered most likely stable. In the case studies of section 5 the highest observed TPW values were typically in the range 40-50 kg/m^2, whereas the lowest values were typically in the vicinity of 5-10 kg/m^2. The TPW content is commonly included in an anlysis of instability indices (see for example Koenig & de Coning, 2008 and de Coning et al., 2011).

2.2 MSG SEVIRI retrieval of temperature & humidity profiles

The Meteosat Second Generation (MSG) consists of three operational satellites: Meteosat 8, 9, and 10 (formerly known as Meteosat 1, 2, and 3, respectively) - all in a geostationary orbit (roughly 36,000 km altitude).
The instrument, which provides the data of interest, is the main payload of the MSG satellites and is known as the Spinning Enhanced Visible and InfraRed Imager (SEVIRI). In this section, the process of data gathering and processing of SEVIRI, leading to vertical temperature and humidity profiles, is outlined.

Meteosat 10, situated at 0° longitude, scans the full disc of the Earth, providing a new image every 15 minutes, and is the primary satellite of the MSG. Meteosat 9 provides a Rapid Scanning Service over a subsection of Europe and Africa, providing a new image every five minutes, whereas Meteosat 8 operates over the Indian Ocean (41.5°E) and provides the same services as Meteosat 10 for this area. Only data provided by the 0° Meteosat 10 satellite is utilized in this study. Figure 2 shows an illustration of the SEVIRI instrument aboard MSG-10 scanning the Earth. In the section below a basic overview of the processing of data from the SEVIRI instrument aboard the MSG satellites, leading to the generation of atmospheric temperature and humidity profiles, is provided.

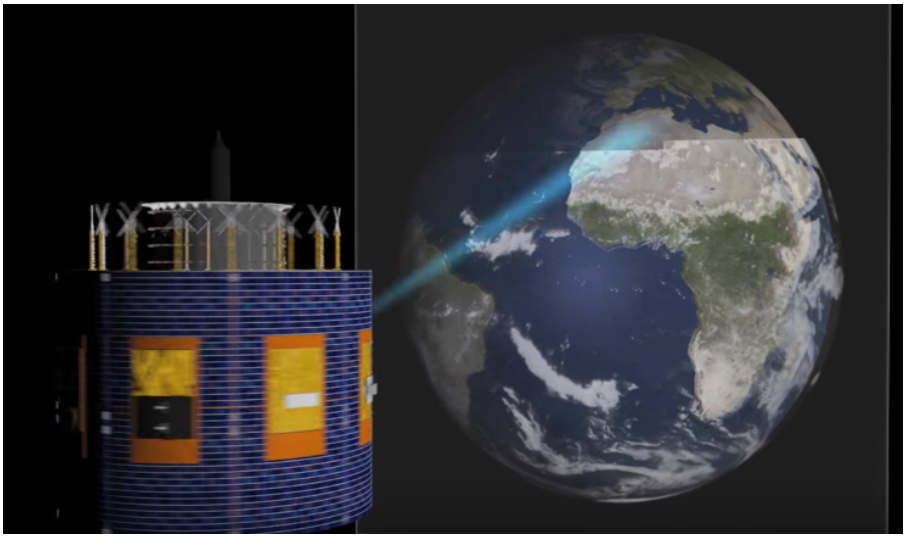

Figure 2: Illustration showing SEVIRI, aboard MSG-10, scanning the Earth from its geostationary orbit centered at 0°. (Image taken from the EUMETSAT website[2]).

2.2.1 SEVIRI retrieval algorithm

The SEVIRI instrument scans the radiance from Earth in 12 channels - 1 high resolution visible channel, 2 visible channels, and 9 infrared (IR) channels. A list showing all the SEVIRI channels is found in figure 3. A full scan of the Earth is completed every 15 minutes and the spatial resolution (pixel size) is 3 km (except for the high resolution visbile channel, which has a resolution of 1 km, however this channel is not utilized in the temperature/humidity profile retrieval). The channel radiances can be converted into brightness temperatures, T_B, via the Planck formula (EUMETSAT, IASI Level 2 Product: Generation Specification). Each channel radiance (or brightness temperature) provides information on a specific set of characteristics of the atmosphere (for instance, the two channels centered at 6.2 μm and 7.2 μm, respectively, provide information on atmospheric water vapor content at different levels - accordingly, they are referred to as the *water vapor channels*). In the following, the vertical temperature and humidity profiles (the output that is to be retrieved) are combined in a state vector, $\boldsymbol{x}$. The basic idea behind the algorithm for obtaining the temperature and humidity profiles is to determine the state vector, that is most likely to produce the observed brightness temperatures.

[2] `http://www.eumetsat.int/website/home/Satellites/CurrentSatellites/Meteosat/MeteosatDesign/index.html`

Spectral Channel	*Central Wavelength*	*Range*	*Spatial Sampling Distance (SSD)*
VIS 0.6	0.635 µm	0.56 – 0.71 µm	3.0 km
VIS 0.8	0.810 µm	0.74 – 0.88 µm	3.0 km
NIR 1.6	1.600 µm	1.50 – 1.78 µm	3.0 km
IR 3.9	3.920 µm	3.48 – 4.36 µm	3.0 km
WV 6.2	6.325 µm	5.35 – 7.15 µm	3.0 km
WV 7.3	7.350 µm	6.85 – 7.85 µm	3.0 km
IR 8.7	8.700 µm	8.30 – 9.10 µm	3.0 km
IR 9.7	9.660 µm	9.38 – 9.94 µm	3.0 km
IR 10.8	10.800 µm	9.80 – 11.80 µm	3.0 km
IR 12.0	12.000 µm	11.00 – 13.00 µm	3.0 km
IR 13.4	13.400 µm	12.40 – 14.40 µm	3.0 km
HRV	-	0.5 – 0.9 µm	1.0 km

Figure 3: List of the 12 channels of observation of the SEVIRI instrument. Only a subset of the channels are used for computing temperature and humidity profiles. (Taken from EUMETSAT, Algorithm Theoretical Basis Document for the GII/TOZ Product - see full reference in section 9).

In the retrieval of temperature and humidity profiles, six SEVIRI channels are used: IR8.7, IR10.8, IR12.0, WV6.2 and WV7.3 (the two water vapor channels), and the CO_2 channel IR13.4. The brightness temperatures of these six channels do not constitute sufficient information to establish the state vector - an infinite amount of different state vectors could result in the observed brightness temperature. To solve this problem, a *first-guess* (or *background*) state vector , $\boldsymbol{x}_0$ is used to impose constraints on the resulting state vector. This first-guess state vector is taken from the European Centre for Medium-Range Weather Forecasts (ECMWF) global model forescasts, which have a resolution of 1°latitude by 1°longitude and are provided every 6 hours (thus, the profiles must be interpolated to the time of the given SEVIRI image). With a background state vector and a series of observed channel brightness temperatures in place, the algorithm, which is based on the *standard retrieval equation* (Rodgers 1976), can make its first iteration: First, the brightness temperatures of the six SEVIRI channels are *simulated* from the background profiles and compared to the *observed* brightness temperatures. If the difference between simulated and observed brightness temperature is below a certain RMS threshold, the current state vector (the background state vector, x_0) is taken as the correct one. If the difference is above the threshold, the standard retrieval equation is solved for the updated state vector, x_{n+1} (in this case x_1). This process is then repeated in a second iteration, first comparing simulated brightness temperatures of the updated state vector with observed brightness temperatures and so on. Iterations of the algorithm are continued until a state vector that simulates brightness temperatures that are satisfactorily close to the observed ones has been determined.

A very important and essential limitation of the SEVIRI temperature and humidity profile retrieval algorithm is that it only functions in *cloud-free* conditions: In cloud covered areas the atmospheric radiance in the wavelengths of the six SEVIRI channels are blocked since they are infrared (very thin cloud covers may still permit the signals to pass through). For this reason, the SEVIRI processing also utilizes the MSG Cloud Mask product to asses the extent of cloud cover over each pixel - if less than 50% of the pixel is covered by clouds, the temperature and humidity profiles may still be computed (Koenig & de Coning 2008).

It should be noted, that the reliance of the SEVIRI retrieval algorithm on Numerical Weather Prediction (NWP) in the shape of the first-guess state vector from ECMWF forecasts results in a predisposition of the final state vector: The final state vector tends to retain the general features of the first-guess state vector - if the first-guess state vector is far from the correct state, the algorithm will likely not be able to rectify the error. Thus, the final SEVIRI temperature and humidity profiles (and accordingly also the GII) are dependent on a first-guess state vector that is reasonably close to the correct state of the atmosphere.

This outlines the general function of the SEVIRI retrieval algorithm as well as its limitations. For the purpose of this study, it suffices for the reader to have a basic understanding of the temperature and humidity profile retrieval of the SEVIRI instrument. For a more thorough walkthrough of the generation of temperature and humidity profiles through the SEVIRI processing the reader is referred to Koenig & de Coning 2008, which provides both a slightly more detailed summary of the retrieval algorithm as well as a validation study of the SEVIRI GII, and for a complete, detailed description of the retrieval algorithm the reader is referred to the Algorithm Theoretical Basis Document for the MSG GII/TOZ Product (version 3, May 2013) (cf. section 8 for complete references). Section 2.4 outlines how the temperature and humidity profiles are used to compute the GII.

2.3 Metop IASI retrieval of temperature & humidity profiles

The EUMETSAT Polar System (EPS) consists of the two Metop satellites, Metop A (launched October 2006) and Metop B (launched September 2012) with a third satellite, Metop C, planned for launch in late 2018. The satellites are in a low Earth polar orbit (roughly 817 km altitude), which is sun-synchronous with local time of ascending note of 9:30. This means, that everytime the satellite passes the Equator from south to north, the local time beneath the satellite (at nadir) is 21:30 and when the satellite passes Equator from north to south, the local time is 09:30 - in other words, the local time of descending is 09:30. The ground track repeat cycle is 29 days (412 orbits). Because the satellite instrument of interest (IASI) measures the Earth in a broad swath across the satellites track (to be clarified in the present section), measurements are not made exclusively at nadir. This means, that every point on Earth is monitored twice a day - once in the morning and once in the evening (at Equator once at 09:30 and once at 21:30 - away from Equator these times will of course be slightly different due to the Earth rotating). The nadir point of the satellite will vary from day to day, resetting after 29 days, however this is unimportant, as the IASI instrument measures in a swath that extends on both sides of the nadir point. Metop-A and Metop-B are in co-planar orbits, however they are 174 degrees out of phase with respect to the ground track repeat cycle. This means that the two satellites trace the exact same tracks on Earth, they simply do so roughly 2 weeks (the 174 degree offset translates to approximately half the ground track repeat cycle) apart.

The main payload instrument aboard Metop, responsible for the retrieval of atmospheric temperature and humidity profiles, is the Infrared Atmospheric Sounding Interferometer (IASI). This section describes the processing of IASI measurements for the generation of temperature and humidity profiles. Some parts of the processing is similar (even practically identical) to the SEVIRI processing, however there are some essential differences between the two types of processing and between the two final products. It is stressed, as it was for the section above on SEVIRI processing above, that this outline is meant to give a basic understanding of the methods implemented by the IASI processing to obtain atmospheric temperature and humidity profiles - as such, certain parts and details are omitted. For a comprehensive description of the IASI temperature and humidity profile retrieval algorithm the reader is referred to the IASI Level 2 Product Generation Specification, issue V8C, 2016 (the full reference including an EUMETSAT document number is provided in section 9).

2.3.1 IASI retrieval algorithm

The Infrared Atmospheric Sounding Interferometer (IASI) is a Michelson interferometer and is the main payload instrument of the Metop satellites. As a Metop satellite orbits Earth, IASI scans an area across the satellite track - this track consists of 15 so-called Elementary Fields of View (EFOV), each consisting of 4 Instantaneous Fields of View (IFOV), on each side of the nadir point (see figure 4), resulting in 120 individual measurement points per scan line. The width of the scan line is roughly 2200 km (edge to edge) and the diameter of an IFOV is 12 km at nadir (increasing when approaching the edge of the scan line).

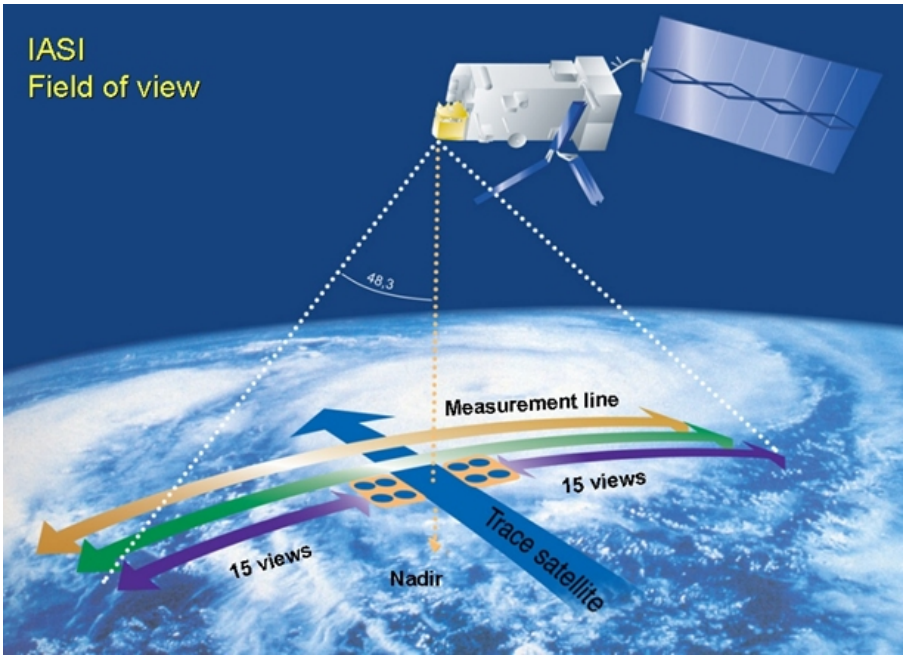

Figure 4: Illustration of the view of IASI aboard a Metop satellite.

IASI scans the Earth and its atmosphere in 8461 infrared channels - an immense amount of channels compared to the 12 channels of the SEVIRI instrument. The IASI channels are divided into three main bands and table 1 shows an overview of the wavelengths as well as the main applications of these three bands. As can be seen in the table, IASI also provides information on trace gasses such as CH_4, N_2O, and SO_2 as well as surface emissivity and cloud parameters. For the purpose of this study, however, the interest lies in obtaining the temperature and humidity profiles.

Band	Wavelength range	Main applications
1	8.26 μm - 15.50 μm	Temperature profile, ozone levels, surface and cloud properties
2	5.00 μm - 8.26 μm	Humidity profile, trace gas levels (CH_4, NO_2, SO_2)
3	3.62 μm - 5.00 μm	Temperature profile, trace gas levels, surface and cloud properties

Table 1: Table showing wavelength range and main applications of the three main bands of the IASI channels.

The essential difference between the IASI and SEVIRI retrieval of the atmospheric temperature and humidity profiles lies in the fact that IASI, with its extensive amount of channels, is able to retrieve temperature and humidity profiles *without* the use of a first-guess state vector from NWP. With the addition of measurements in the microwave spectrum from the Advanced Microwave Sounding Unit (AMSU) and Microwave Humidity Sounder (MHS), also aboard Metop, the IASI processing uses a Piece-Wise Linear Regression (PWLR) model, which takes the IASI/AMSU/MHS radiance measurements as input and retrieves temperature and humidity profiles for the entire measurement area *regardless of cloud cover*. This is possible due to the utilization of measurements in the microwave spectrum, which, as opposed to the infrared radiation, are not blocked by a cloud cover. Thus, information from under the clouds of cloudy areas are obtained by the AMSU and MHS measurements. This feature, obtaining all-sky temperature and humidity profiles purely from measurements, was implemented relatively recently (November 2014) in Version 6 of the IASI Level 2 processing (cf. IASI Level 2 Product Generation Specification issue V8C, 2016). Two aspects of this retrieval is interesting: First, and perhaps most importantly, this IASI retrieval makes it possible to compute the instability indices of the GII for all areas, regardless of the presence of clouds - this is *not* possible with the SEVIRI temperature and humidity profile retrieval. Second, the IASI retrieval is independent on NPW - the retrieval is performed using only measurements from IASI and the auxiliary data from AMSU/MHS, as opposed to the SEVIRI retrieval, which must have temperature and humidity first-guess profiles available from ECMWF forecasts.

Part of the IASI processing, and part of the final IASI Level 2 product, is a mapping of the cloud cover and cloud parameters (such as cloud top pressure etc.). In the final part of the IASI processing, the cloud cover

mapping is used to determine areas of clear sky. With this information acquired, the IASI processing performs the same optimal estimation retrieval for cloud-free areas that was described for the SEVIRI processing. Instead of obtaining the necessary background state vector (temperature and humidity profiles) from NWP, the IASI version of the retrieval simply uses the all-sky temperature and humidity profiles that was obtained from IASI/AMSU/MHS measurements as a first-guess state vector. The iterative optimal estimation algorithm is then performed using the measured brightness temperatures from a subset of IASI channels - again, the algorithm only functions in cloud-free areas because the infrared radiation cannot penetrate a cover of clouds.

In conclusion, the IASI processing consists of two retrievals: The all-sky temperature and humidity profiles obtained purely from infrared (IASI) and microwave (AMSU/MHS) measurements (via the PWLR method) and the purely clear-sky temperature and humidity profiles resulting from the optimal estimation retrieval, which uses the all-sky profiles as first-guess (or background) profiles. From here on, the all-sky temperature and humidity profiles shall be referred to as the *first-guess IASI profiles*, whereas the clear-sky (post optimal estimation retrieval) profiles shall be referred to as the *final IASI profiles*.

2.4 Computing GII from temperature & humidity profiles (Level 2 data)

This section provides a description of how each of the investigated instability indices are computed for a given area, when vertical temperature and humidity profiles are available. While this computation is done in the SEVIRI processing by EUMETSAT (and delivered as a "GII product"), this is not the case for the IASI processing - hence, the computations described below were used to develop a program for calculating the first-guess IASI GII (based on the first-guess IASI temperature/humidity profiles) as well as the final IASI GII (based on the final IASI temperature/humidity profiles). The computations of the K-index and Lifted index are based mainly on the Algorithm Theoretical Basis Document for the MSG GII/TOZ Product, while the computation of the TPW content is based on formulas and approximative expressions from ASI Level 2 Product Generation Specification (cf. section 9 for complete references).

To avoid any confusion, Section 2.5 provides a summary of the three GII retrieval types and their characteristics.

2.4.1 Lifted index

The Lifted index is the difference between air temperature at 500 hPa and the temperature of a surface air parcel (the lowest 100 hPa) lifted to 500 hPa, as described by expression (2). Upon obtaining temperature and humidity profiles from SEVIRI and IASI the first term is easily computed: The temperature profile is interpolated linearly in temperature and logarithmically in pressure (as pressure decreases exponentially with height). The SEVIRI temperature and humidity profiles typically consists of 43 pressure levels (cf. the Algorithm Theoretical Basis Document for the MSG GII/TOZ Product), whereas IASI profiles comprise 101 pressure levels (this is true for IASI data from May 2015 and onwards, meaning that IASI profiles contain 101 pressure levels in all the analysed cases studies). Obtaining the temperature, T, at a specific pressure level, p, from the pressures, p_0, p_1, and temperatures, T_0, T_1, of the level above and below p is achieved through the interpolation (EUMETSAT, IASI Level 2: Product Generation Specification):

$$T = T_0 + \frac{T_1 - T_0}{\ln\left(\frac{p_1}{p_0}\right)} \ln\left(\frac{p}{p_0}\right) \tag{4}$$

where p_0 and p_1 are pressure levels surrounding the pressure level p - the temperatures T_0, T_1, and T are the corresponding temperatures at these pressure levels.

The second term, $T_{500}^{\text{lifted from surface}}$, is determined by first establishing the surface air parcel with the characteristics of the surface pressure and the average temperature and water vapor content of the lowest 100 hPa - the averaging of temperature and water vapor content is done linearly with pressure. In the SEVIRI GII computation an interpolation is performed, obtaining the average of exactly the lowest 100 hPa. In the IASI GII computation a linear averaging over the lowest four pressure levels, corresponding to roughly 100 hPa (with a surface pressure of 1013 hPa, the four lowest pressure levels cover a range of 109 hPa, whereas the range is 102 hPa when the surface pressure is 802 hPa - thus, the temperature and humidity are in almost all situations, barring areas of very high topography, averaged over slightly more than 100 hPa), was implemented. The error generated by not doing quite a proper interpolation for this calculation is deemed inconsequential in the GII analyses of this report. Once characterised, the surface air parcel is lifted dry adiabatically from the surface

to the lifting condensation level. The lifting condensation level temperature is determined by the empirical relation:

$$T_{\text{lift}} = \frac{1}{\frac{1}{T_{\text{sfc}}-55} - \frac{\ln(RH_{\text{sfc}}/100)}{2840}} \tag{5}$$

where T_{sfc} is the surface air parcel temperature (the average of the 100 hPa lower layer) and RH_{sfc} is the relative humidity of the parcel (which is obtainable when temperature, water vapor mixing ratio, and pressure are known). The pressure at the lifting condensation level is obtained as:

$$p_{\text{lift}} = \frac{p_{\text{sfc}}}{\left(\frac{T_{\text{sfc}}}{T_{\text{lift}}}\right)^{R/c_p}} \tag{6}$$

In case the lifting condensation level lies below the 500 hPa height (that is, $p_{\text{lift}} > 500$ hPa) the surface air parcel is simply lifted dry adiabatically from the surface to 500 hPa. This is, however, virtually never the case. Therefore, the surface air parcel must first be lifted dry adiabatically to the lifting codensation level and *then* lifted moist adiabatically from the lifting condensation level to 500 hPa. The empirical regression scheme that accomplishes this is described in detail in (EUMETSAT, Algorithm Theoretical Basis Document for the GII/TOZ Product) and is omitted here since it is somewhat tedious. It is exactly this regression scheme that has been implemented for the IASI Lifted index computation. Thus, the only difference between the SEVIRI and IASI Lifted index computation lies in the evaluation of the T_{500} temperature and the surface air parcel temperature/humidity, T_{sfc} and q_{sfc}, where the IASI computation simply uses values from the pressure level closest to 500 hPa (496.6 hPa when IASI profiles have 101 pressure levels, which is the case for post-2015 data) and averages over the four lowest pressure levels (corresponding to slightly more than 100 hPa, depending on surface altitude, but never exceeding a deviation of 10 hPa) to obtain T_{sfc} and q_{sfc}, instead of performing interpolations as the SEVIRI computation.

2.4.2 K-index

To evaluate the K-index, as given by expression (1), the atmospheric temperature at three different pressure levels (850 hPa, 700 hPa, and 500 hPa) must be evaluated. These temperatures are determined by interpolation of the given temperature profiles from SEVIRI and IASI, respectively - the only difference between the SEVIRI and IASI computation is the amount of pressure levels, on which the temperature is provided. Furthermore, the dew point temperature, TD, must be evaluated at pressure levels 850 hPa and 700 hPa. An empirical formula for the calculation of the dew temperature (in unit K) is given by (EUMETSAT, Algorithm Theoretical Basis Document for the GII/TOZ Product):

$$TD = \frac{243.5 \cdot a - 440.8}{19.48 - a} + 273.15 \tag{7}$$

where,

$$a = \ln \frac{E(T) \cdot RH}{100} \tag{8}$$

$E(T)$ is the saturation vapor pressure (dependent on temperature) and RH is the relative humidity. The saturation vapor pressure has the following empirical relation to the air temperature:

$$E(T) = 6.11 \cdot 10^{7.5 \cdot (T-273.15)/(T-273.15+237.3)} \tag{9}$$

Temperature T is expressed in units K, and the resulting vapour pressure is in units hPa. In order to compute the relative humidity, RH, at a given pressure level, the water vapor mixing ratio at this pressure level must be known. Since both the water vapor mixing ratio and the pressure decrease exponentially with height, the interpolation that must be implemented to obtain the water vapor mixing ratio at a certain pressure level is double logarithmic (IASI Level 2: Product Generation Specification):

$$\ln(q) = \ln(q_0) + \frac{\ln\left(\frac{q_1}{q_0}\right)}{\ln\left(\frac{p_1}{p_0}\right)} \ln\left(\frac{p}{p_0}\right) \tag{10}$$

where p_0 and p_1 are pressure levels below and above the height of pressure level p (that is, $p_0 > p > p_1$). q_0, q_1, and q are the corresponding water vapor mixing ratios.

With the temperatures and dew point temperatures known, the K-index is easily computed by expression (1). The K-index is traditionally given in units of °C (so 273.15 should be subtracted from the final result in case temperatures and dew points are given in Kelvin).

2.4.3 Total Precipitable Water

The Total Precipitable Water content is (for both SEVIRI and IASI processing) evaluated as the following summation:

$$TPW = \sum_i \frac{\overline{q}_i(p)}{g(\overline{z}, \phi)} \Delta p \tag{11}$$

where the subscript i refers to the pressure layer, i. Units of pressure should be Pa, gravitational acceleration should be m/s^2, and water vapor mixing ratio kg/kg (or g/g). The average humidity of pressure layer i is simply given by[3]:

$$\overline{q}_i = \frac{q_i + q_{i+1}}{2} \tag{12}$$

and the difference in pressure is of course $\Delta p = p_i - p_{i+1}$. The local gravitational acceleration, $g(\overline{z}_i, \phi)$ (dependent on latitude ϕ and the mean altitude $\overline{z}_i$ of layer i), is computed as:

$$\begin{aligned} g(\overline{z}_i, \phi) = 9.80616 \cdot (1 - 0.0026373 \cdot \cos(\phi) + 0.0000059 \cdot \cos^2(\phi)) - (3.085462 \cdot 10^{-6} + 2.27 \cdot 10^{-9} \cdot \cos(\phi)) \cdot \overline{z}_i \\ + (7.254 \cdot 10^{-13} + 10^{-20} \cdot \cos(\phi)) \cdot \overline{z}_i^2 - (1.517 \cdot 10^{-19} + 6 \cdot 10^{-22} \cdot \cos(\phi)) \cdot \overline{z}_i^3 \end{aligned} \tag{13}$$

An empirical approximative formula for the mean altitude is given by:

$$\overline{z}_i = -4000 \left(\ln \left(\frac{p_i}{1013} \right) + \ln \left(\frac{p_{i+1}}{1013} \right) \right) \tag{14}$$

where p_i and p_{i+1} are the pressures at the boundary to layer i and $i + 1$, respectively, given in hPa.

The only difference in the TPW computation of SEVIRI and IASI is the number of pressure levels - more pressure levels makes the summation a better approximation of the integral in expression (3), however in this case the between the SEVIRI and IASI computation is most likely negligible. The empirical formulas of this section were taken from (EUMETSAT, IASI Level 2: Product Generation Specification).

2.5 Summary of GII retrievals

At this point it is deemed appropriate to provide a quick overview of the three different GII retrievals investigated in this report and how they are obtained. The SEVIRI GII is delivered as a finished product by EUMETSAT. The first-guess and final IASI GII retrieval was developed for this report - it uses the first-guess and final temperature and humidity profiles, that are delivered in the IASI Level 2 product, to compute the instability indices of the GII as described in section 2 above. Table 2 below gives a summary of the characteristics of each GII retrieval.

[3] ERROR IN IASI PGS EQUATION 95!

GII retrieval type	Satellite	Coverage area and time	Coverage type	Data delivered by EUMETSAT
SEVIRI	MSG-10	Full Earth disk centered at 0°(Europe and Africa). Continuous coverage (new image every 15 minutes)	Clear-sky	GII product
First-guess IASI	Metop-A/Metop-B	A given area is covered roughly twice a day (local morning and local evening)	All-sky (regardless of cloud-cover)	Temperature/humidity profiles
Final IASI	Metop-A/Metop-B	A given area is covered roughly twice a day (local morning and local evening)	Clear-sky	Temperature/humidity profiles

Table 2: Overview of the three different GII retrievals investigated in this report. Note that the SEVIRI GII product is computed by EUMETSAT, whereas the IASI (final and first-guess) GII has been computed for this reported using temperature/humidity profiles delivered in the IASI Level 2 product.

3 Lightning and severe weather as convection indicators

The instability indices are meant to indicate unstable conditions in the atmosphere. More specifically, the indices can be said to rate the likelihood of the atmosphere to develop convective phenomena. Atmospheric convection is the result of mixing of parcels of air with different levels of humidity and thus different temperature lapse rates. This mixing of air parcels increases wind speeds and leads to cloud development, however in areas where the atmosphere is moist enough, convective phenomena such as thunderstorms, heavy rainfall, hail storms, and tornadoes may develop. As described in section 2.1, it is these types of severe convective phenomena that the instability indices included in the GII seek to predict.

In order to evaluate the usefulness of the SEVIRI and IASI GII, an indicator of atmospheric instability is needed. For this purpose lightning data is employed. As all the instability indices in the GII are assumed indicators of thunderstorms, lightning data is an obvious choice for evaluation of the GII. In addition to lightning data, data from the European Severe Weather Database was used in the case studies to locate other severe weather events such as tornadoes and hail storms. Data from several different lightning networks were available for the different studied cases. Having full coverage from the same lightning networks for all the case studies would obviously have been prefered, however most lightning data networks are commercial, meaning that data comes at a cost. Lightning data from the LINET and Ebro Valley LMA (to be described presently) networks for a few specific thunderstorm events studied in a previous project (Andersen & Kristensen, 2016) was available and so these storms were obvious candidates to include in the case studies. GLD360 data was available for an area covering roughly all of southern and central Europe for all but one of the case studies. Finally, data from Blitzortung.org (a nearly global network, mapping lightning activity using a large number of amateur lightning detection systems, often operated by university students etc.) was available for all case studies. In this section a very basic summary of lightning terminology is provided. Then, the different lightning locating systems are briefly introduced and their advantages and limitations are outlined. Finally, a description of the data obtained from the European Severe Weather Database is provided.

3.1 Brief summary of lightning terminology

Lightning occurs due to the accumulation of positive or negative charges in different layers of a cloud, mainly in the form of positive/negative atmospheric ions attached to water droplets, highlighting the necessity of atmospheric water vapor content for thunderstorms to occur. The charged layers create high electric potentials both intra-cloud (inside the cloud itself), inter-cloud (between different clouds), and between the cloud and ground. During the development of a thunderstorm, the difference in potential can become so high, that the air may exceed its dielectric strength, resulting in breakdown, and the air may then act partially as a conductor, allowing the charged cloud to discharge through the air as if it were a wire. If the potential difference (for instance between a cloud and the ground) is sufficiently high, the electric breakdown of air may result in an electric arc bridging the gap between cloud and ground during the discharge - this, essentially, is how lightning occurs. If the discharge occurs from a cloud to ground it is termed cloud-to ground lightning (CG), if the discharge is between two parts of the same cloud it is termed intra-cloud (IC) lightning, and finally, discharge between two different clouds are termed cloud-to-cloud (CC) lightning (Uman, 2001). For the purpose of this study, IC and CC lightning may be considered the same phenomenon and so from here on either of these lightning types shall

be referred to as IC lightning.

In order to illustrate how lightning events are detected, a common CG lightning event (also known as a CG flash) is described in the following - CG lightning is the type that is best understood and easiest measured. A sketch showing the temporal evolution of a CG lightning flash with negative polarity (far more common than positive polarity lightning) is provided in figure 5. In short, the CG flash occurs as a result of the stepped leader propagating from the negatively charges lower layer of the cloud towards the ground (which has an induced positive charge) step-wise through the air that has undergone electric breakdown. Once the stepped leader is sufficiently close to ground the attachment process ensues, in which charges from the ground connects with the stepped leader. When the attachment is complete, the return stroke occurs - this is where the bright flash and loud thunder take place. Upon the first return stroke, the event may cease. Alternatively, the dart leader (the stepped leader connected all the way to the ground) may remain and a second return stroke may occur - this process can reiterate, spawning even more return strokes (the temporal separation between two return strokes is usually around 20 ms).

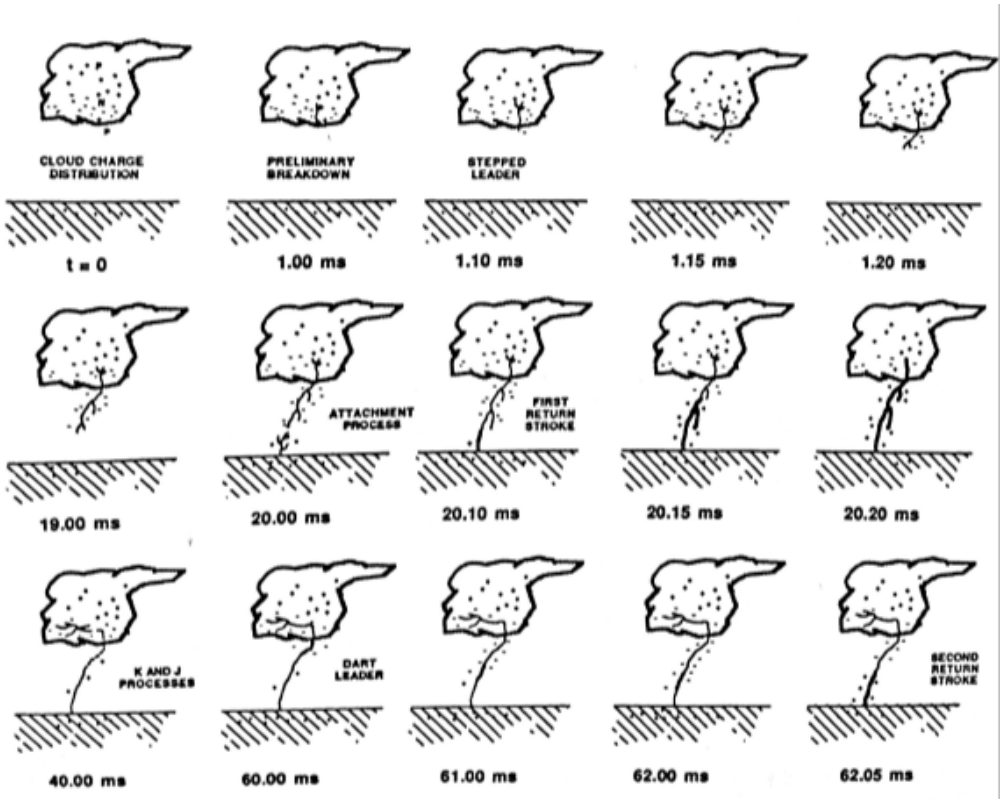

Figure 5: Illustration showing the evolution of a typical CG (cloud-to-ground) flash. (Figure taken from Uman, 2001).

Different lightning locating systems detect different parts of lightning events. The step-wise propagation of the stepped leader emits signals primarily in the VHF band (very high frequency, 30 MHz - 300 MHz). Thus, lightning locating systems that wish to map lightning events in three dimensions must use VHF sensors in order to map the propagating stepped leader. The return strokes emit strong signals in the VLF band (very low frequency, 3 kHz - 30 kHz). An advantage in tracking VLF signals is that they may propagate between the ground and ionosphere, continually bouncing between the two, allowing VLF sensors to measure signals from a great distance. Conversely, VHF sensors must measure VHF signals from a direct line of sight, which obviously limits the size of the coverage area of a VHF lightning locating system. Measuring the lightning VLF signals does, however, not yield a three dimensional mapping of lightning - only return stroke signals are measured. Usually, lightning locating systems that operate in the VLF band utilize a waveform discrimination to only include CG return strokes (ignoring any IC return strokes), providing a two dimensional mapping of CG lightning events. The difference in propagation of VLF and VHF signals is illustrated in figure 6.

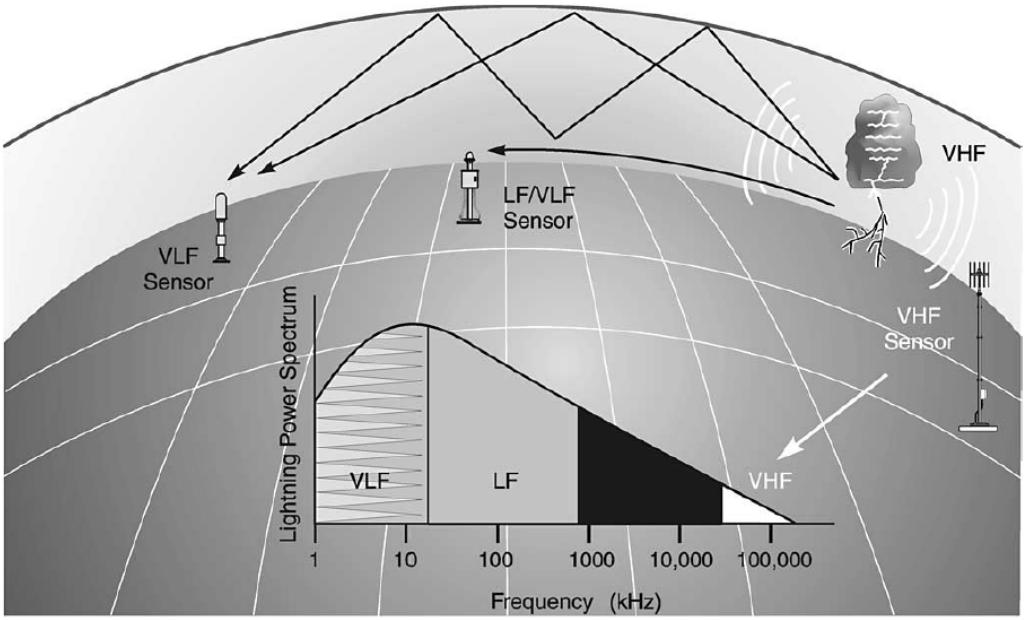

Figure 6: Illustration showing the difference between propagation of VLF and VHF signals from a lightning event. Figure from (Cummins & Murphy, 2009).

The following subsections provide a brief introduction of the basic characteristics of the lightning locating systems used in the case studies of section 5. It is noted, that the exact measurement and mapping of lightning events (both spatial and temporal) is a huge scientific subject on its own, still in rapid evolution. For the purpose of this study, exact lightning mappings and specific characteristics of storms are not of high importance: As will become clear in the case studies, and as is demonstrated in other studies on the subject (Koenig & de Coning, 2008, de Coning et al., 2011, Peppler & Lamb, 1989), the comparison between instability indices and lightning activity is often quite qualitative in nature. The lightning data is simply used as an indicator of highly convective weather: For a given area, a high amount of lightning data is taken to indicate a severe storm, whereas a low amount is taken to indicate a less severe storm, and no lightning data at all (assuming no other severe weather activities were observed on the European Severe Weather Database) is taken to mean that no (severe) convection occurred. Nevertheless, lightning terminology and descriptions of the lightning locating systems are included in order to provide a more complete account of the comparison between the GII and lightning activity.

3.2 Global Lightning Dataset 360

The Global Lightning Dataset 360 lightning locating system (GLD360, or simply GLD) consists of a number of VLF sensors situated around the world, providing global coverage. It detects CG return strokes (due to its VLF sensors, cf. section 3.1). GLD is a commercial network operated by Vaisala (data is purchasable) and for this reason, a complete mapping of the station locations is not available. Also, literature evaluating the accuracy and efficiency of the network is scarce. According to Vaisala, the timing precision of each sensor is 1 μm and the maximum detection distance of a sensor is 6000 km (Vaisala, 2015). This is due to the effect of VLF signals reflecting off of the ground and ionosphere that was (cf. figure 6) and due to the utilization of both TOA (time of arrival) and azimuth angle measurements of the VLF signals by each sensor. The application of the arrival azimuth angle of a signal is called Magnetic Direction Finding (MDF) and makes it possible for just two sensors to locate a CG stroke. In the region of southern Europe GLD reportedly achieves a detection efficiency of 70-80% (that is, 70-80% of CG return strokes are measured by the network) and a location accuracy of 2-3 km, though these values stem from an extrapolation of results of testing in the United States[4]. Analysis performed in a previous project showed reasonable (but not great) coherence between GLD360 and Ebro Valley LMA measurements in the area around the Ebro Valley LMA network (Andersen & Kristensen, 2016). Thus, location accuracy and detection efficiency values should only be considered estimates, however as an approximative indicator of thunderstorm severity, this level of detection efficiency and location accuracy is certainly acceptable.

[4]Personal communication with Ryan Said, Vaisala, 14th June 2016

GLD data was available for a region comprising most of southern and central Europe (latitude: 35°N - 51°N, longitude: 10°W - 25°E) for the period of June 2015 to December 2016, meaning that GLD data was available for southern/central Europe for all but one of the five case studies of section 5.

3.3 Blitzortung.org

Blitzortung is an online community of volunteering participants, accumulating data from all participants into a central processing server, which then provides users of the Blitzortung website with near real-time lightning data as well as archives containing older data. The basic concept of Blitzortung is to create an extensive world wide lightning locating network operated by volunteers. To achieve this, each sensor unit is sold relatively cheap to the volunteering station operators - in exchange, each station operator is provided with raw data from the entire network and may use this data for any non-commercial purpose. The sensors are VLF sensors, measuring signal time of arrival, meaning that the Blitzortung network is much like the GLD network, in that it maps CG strokes in two dimensions (longitude, latitude) by use of long range VLF sensors (since the MDF technology is not applied in the Blitzortung sensors, at least four sensors are required to locate a source). Of course, since Blitzortung is reliant on operators volunteering for the project, it cannot necessarily plan out the most efficient geographical setup of stations and the detection efficiency and location accuracy will naturally vary heavily with area - in fact, no specific detection efficiencies or location accuracies are provided for any areas. Again, even though the network accuracy is likely not quite on par with more sophisticated networks, as a simple indicator of thunderstorm severity the Blitzortung network is definitely useful.

Blitzortung data was available for all the case studies of the report. For a thorough description of the Blitzortung project and network see (Wanke et al., 2014).

3.4 Ebro Valley Lightning Mapping Array

The Ebro Valley Lightning Mapping Array (from here on abbreviated as LMA) consists of 13 VHF sensors spread over an area around Ebro Valley, Spain. The VHF sensors make it possible for the LMA to measure the propagation of stepped leaders of both CG and IC lightning, locating the three dimensional position of each step of the leader. This results in a retrieval of longitude, latitude, and altitude for every detected step of a leader, making it possible to map out the shape of a CG/IC stroke (assuming enough measurements are captured by the network). This feature is very valuable for studies on specific characteristics of individual lightning strokes, however when the interest lies in simply measuring the extent of lightning activity, having three dimensional mapping of the signals is not of particular interest. Instead, one may simply inspect the density of measurements in a two dimensional (longitude, latitude) plane and interpret a high density as a sign of heavy thunderstorm activity. In a more exact study of lightning activity one must be aware that not all received VHF signals stem from lightning - icy particles colliding with airplanes, for instance, may cause the same type of signals and appear in the LMA measurements (Thomas et al., 2004).

LMA data was available from noon to midnight on July 24th 2015, where heavy thunderstorm activity was observed in the coverage area of the LMA network (as well as in many other parts of Europe outside the network coverage area). Therefore, this date was chosen for analysis in the case studies. An important thing to note, however, is that on this day, only 5 out of the 13 sensors were active. This causes the size of the area, in which the network provides reasonable location accuracy and detection efficiency, to significantly decrease, due to the decrease in network baseline length. A map showing the location of the active LMA stations is seen in figure 7. In a previous project (Andersen & Kirstensen, 2016) an area was suggested for the specific date, inside which measurements were reasonably reliable - measurements outside this area were discarded. This adaptation shall be used in the case study of this report as well.

For a detailed description of the LMA network, its location accuracy, and its data processing see (Thomas et al., 2004).

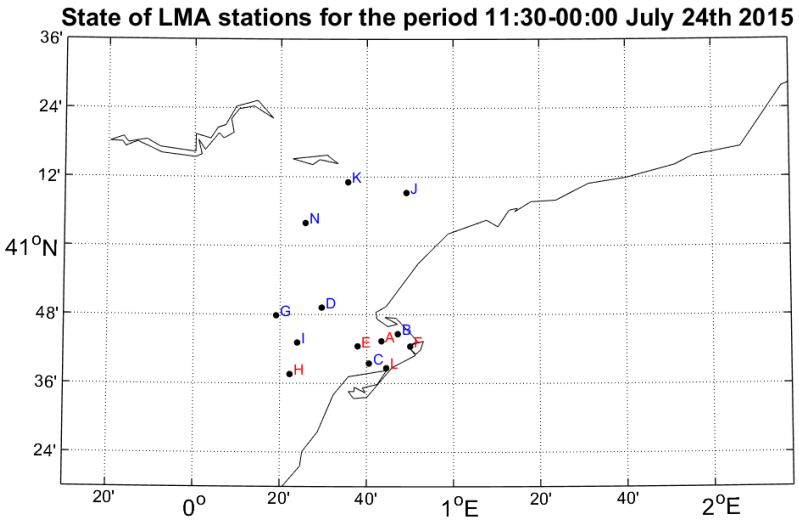

Figure 7: Map showing the location of the sensor stations of the Ebro Valley LMA. The letters are a short-hand way of identifying the different stations in the datasets - the color indicates the state of the sensor in the time frame of the available data: Red indicates an active station while blue indicates an inactive station.

3.5 LINET

The European LINET lightning detection network consists of LF/VLF (where LF stands for low frequency, 30 kHz to 300 kHz) sensors located around Europe - the sensor density is significantly higher in Germany (see figure 8). The network is able to detect total lightning (that is, both CG return strokes and IC stepped leader processes), providing a three dimensional mapping of lightning activity. This is achieved due to a special technology used in the LF/VLF sensors - most importantly, the sensors have a very high sensitivity, so even though the stepped leader processes do not emit particularly strong signals in the LF/VLF spectrum, the sensors are often able to pick them up, especially in areas where the density of sensor stations is high. Due to the LINET network being commercial, the exact technology behind the sensors is not publicly available - some of the basic principles, along with other information on LINET, are outlined in (Betz et al., 2009). LINET is also capable of distinguishing between IC and CG signals, allowing for them to be analyzed separately. As an indicator of thunderstorm severity, for the comparison with instability indices, it is most interesting to investigate the CG strokes, as a heavy amount of this type of lightning is associated with a severe thunderstorm.

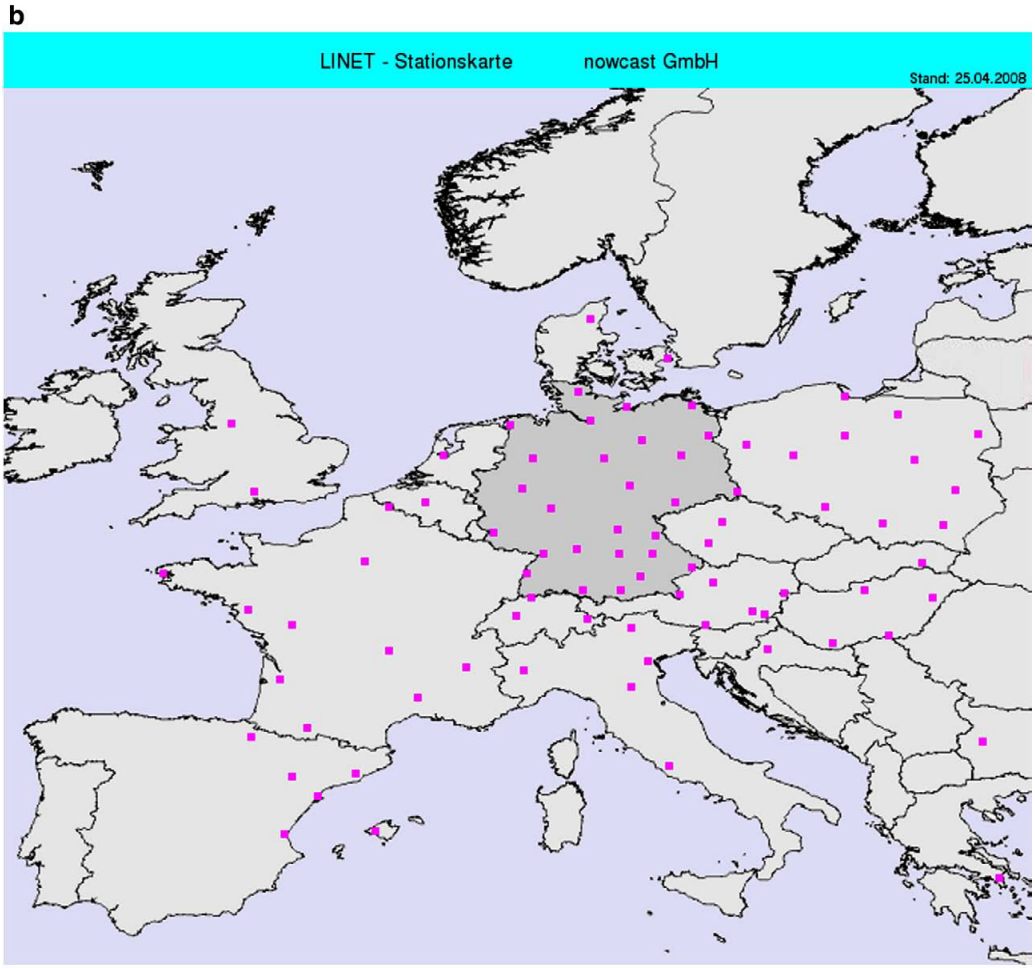

Figure 8: Map showing the sensor station locations for the European LINET network as of 2008. As can be seen, the sensor density is significantly higher in and around Germany.

LINET data was available for two specific thunderstorms in two different cases of the case studies (that is, very small areas around each thunderstorms) - one in northern Germany and one in Venice, both regions where the LINET sensor station density is quite high, prompting high accuracy and detection efficiency. Although it has been concluded that a high accuracy and detection efficiency may not be essential in the comparison of thunderstorm severity and instability indices, the storms with LINET data coverage are still chose for analysis in the case studies, as the increased accuracy and efficiency may prove useful in case of poor coverage from the other detection networks - also, a higher accuracy lightning locating system, measuring total lightning, may be of interest in other (perhaps more local) types of analysis of instability indices in a future study.

3.6 European Severe Weather Database

Although lightning data is chosen as the main indicator of severe convection in this study, it is supplemented with data from the European Severe Weather Database (ESWD). This is partly due to the fact, that case studies were sought to cover a wide range of different storms - including occurrences of tornadoes, large hail, and heavy rainfall. As will be seen in the first of the five case studies, the ESWD data also occasionally compliment the lightning data in the sense that severe weather may occur *without* the presence of lightning activity. Although the instability indices of the GII are mainly studied to predict lightning (see for instance Koenig & de Coning, 2008 and de Coning et al. 2011), severe storms that exhibit little or no lightning activity should theoretically also be predictable through the instability indices (cf. the description of the indices in section 2.1).

The ESWD consists of archived reports of severe weather, submitted both by meteorological institutes and organizations as well as by civilian users. Each report then receives a quality label, depending on the level of confidence with which the severe weather event can be asserted. A report that is simply reported by a civilian

user receives the lowest quality label, called level Q0. A simple plausibility check is made by sorting through other reports from the same area along with a rough comparison with weather forecasts from the area (for instance, a heavy snowstorm likely did not occur if weather forecasts predicted clear skies and temperatures of and 20°C) - reports that pass this test obtain the quality level Q0+. The most important quality check is the level Q1 quality check, which means that the report is confirmed by a reliable source (such as a national meteorological institute or the like - reports coming straight from such an institute receives the level Q1 quality label immediately). The final quality label, level Q2, is reserved for weather events that have been extensively studied, verifying every detail (exact time and location, extent of damages caused etc.) of the event - this quality level is typically only assigned to severe weather events that have been part of a scientific study. For the case studies of this report, only reports carrying a quality label of Q1 or Q2 have been used. One thing to note about the ESWD reports is that they often vary quite a bit in accuracy of time and location of occurrence - some reports consist of a video recording of the event, typically resulting in a quite exact time and location of the event, while others may consist of measurements (carrying uncertainties) or perhaps an image without a timestamp. Still, as explained in the description of lightning data, precision in the form exact time and location of an event is not of crucial importance and thus simply knowing that, for instance, a hail storm occurred in the late afternoon in southern Germany or heavy rain was observed in the evening in Slovenia is typically enough information to make a reasonable analysis of the GII versus severe weather events. For each of the case studies, the most notable ESWD reports and their (approximate) time of occurrence are summarised in a short section along with a presentation of the lightning data.

A legend for the ESWD plots is shown in figure 9.

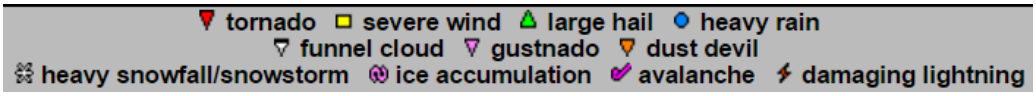

Figure 9: Legend showing which symbols are used to indicate different types of events.

4 Program Architecture and Manual

The SEVIRI GII data and the IASI Level 2 Product are not exactly straightforward to read. Nor is the IASI GII processing routine uncomplicated. Thus, part of the "product" of this project is the Python programs written to perform the reading, processing, and plotting of the different GII retrievals. The full programs will not be inserted into this report, however a quick overview of the programs written is given in the appendix in section 8.

5 Case studies

This section features a collection of case studies, comparing three different GII retrievals to observed lightning data and severe weather reports as well as to each other. The three GII retrievals are the SEVIRI GII, the first-guess IASI GII, based on first-guess IASI temperature/humidity profiles, and the final IASI GII, based on the final IASI temperature/humidity profiles. As has been mentioned throughout the report, the comparison between GII and observed convection indicators is done very qualitatively and, in most cases, done in a very low temporal and spatial resolution: Due to the nature of the SEVIRI and IASI measurements (SEVIRI obtains a new image of Europe every 15 minutes, whereas IASI obtains one morning and one evening sweep, roughly, per day for a given area) it becomes difficult to obtain SEVIRI and IASI GII measurements at *exactly* the same time. One IASI Level 2 data file comprises one full IASI orbit (one full sweep) and the naming of each IASI data includes the start time of the sweep. During the initial analysis of the IASI data, it was observed, that each "Europe sweep" (again, the time of the IASI sweep that covers the majority of Europe changes from day to day as well as the exact area covered by this sweep, due to the nature of the sun-synchronous orbit with a 29 day ground track repeat cycle) begins around northern Sweden/Finland and descends towards Equator (recall that the local time of descending is 09:30, meaning that the satellite will cross the Equator at 09:30 *local time*). Depending on how far the satellite is in the ground track repeat cycle, this sweep will start (around northern Sweden/Finland or somewhere in the vicinity) at sometime between roughly 08:30-09:30 UTC. This makes for a somewhat inconvenient "search" for the orbit that covers the desired area, however with two satellites (Metop-A and Metop-B) the chances of finding an orbit covering all desired regions is doubled (recall that Metop-A and

-B are 174 degrees apart in the ground track repeat cycle). Obviously, if a continous processing of IASI Level 2 data were to be desired, a program could be developed to track the satellites movement with respect to the ground track repeat cycle by time and date, expediting the process of finding the appropriate IASI data file. In these case studies, first the appropriate IASI sweep was identified (depending on the area of interest). Then, depending on the start time of the IASI orbit, the appropriate SEVIRI GII image was chosen: This was simply done by choosing the SEVIRI GII image of roughly 15-20 minutes *after* the start orbit time of IASI. The logic of this decision is based on the fact that, as mentioned earlier, the IASI orbits covering Europe around morning time start somewhere over northern Scandinavia. 15-20 minutes is then an approximation of the time taken by the Metop satellite to sweep over the entirety of Europe (recall that the orbital period of Metop is 101 minutes). Although this is, of course, a somewhat imprecise approximation, it will become clear in the following case studies (especially in section 5.6) that the GII does not, generally, vary significantly in short timeframes such as 10-30 minutes - often, only minor differences are observed even over the course of an hour. The low temporal resolution of the case studies is also reflected in the use of lightning and severe weather data: Exact timestamps of lightning flashes or severe weather reports are not of interest in these case studies - instead, the time of occurrence of convection indicators shall be referred to more loosely ("an increase in lightning activity is observed around 16:00-17:00", "a tornado was observed at approximately 19:30" etc.). Similarly, what is meant by the low spatial resolution of the case studies, is that, generally, regions will be distributed into areas of "high K-index" or "very low TPW content" and so on, as opposed to noting specific values and gradients within a small area. Although this is the type of analysis performed in these case studies, it certainly cannot be rejected that interesting observations could potentially be made in a case study focusing on more local areas and specific convection indicators.

Sections 5.1-5.5 present five case studies, each investigating the GII and severe weather activity of one day - each case was chosen due to specific characteristics of the weather conditions on the given day. All the case studies investigate summer days, as this is the season of frequent storm development and the season, during which most instability indices were originally tested when developed, cf. section 2.1, and all in Europe). The general structure of the case studies consists of a presentation of why this specific case was chosen followed by a description of the available lightning and severe weather data. Then proceeds a meticulous description of each index (K-index, Lifted index, and TPW content) as observed by each of the three GII retrieval types. The main aim of this description is to provide a comparison between each index and the observed lightning/severe weather activity, however the agreement/differences between the differetn GII retrievals are also commented. Finally, a short summary, outlining the most interesting observations of the given case study, is provided.

In these case studies, the lightning data (along with the data from ESWD) are considered the "true" indicators of severe convection (though this data obviously has intrinsic uncertainties), while the ability of the SEVIRI/IASI GII to predict the locations of severe convection is investigated. When performing tests of this kind, a *false alarm* is often defined as a case where the predictor (in this case the GII) predicts instability but the true indicator (the lightning/severe weather data) shows stable conditions. Conversely, if the predictor predicts stable conditions and the true indicator shows instability it is regarded as a *miss*.

One final note before commencing the case studies concerns the area of the Alps: The reader will observe that for a large part of this area, the K-index is never available, neither in clear-sky or cloudy conditions. This is of course due to the high topography of the Alps - recall that the K-index is not defined when surface pressure is below 850 hPa. Also, due to the natural decrease in humidity with altitude, tends to show very low TPW values.

5.1 Stable day across Europe 2016-08-13

This day was chosen for analysis due to predominantly stable weather conditions prevailing throughout Europe. This allows for investigation of the GII in large areas where no subsequent thunderstorm activity (or other severe weather events) took place. Important to note, is that in order to cover the entire area of Europe, two consecutive IASI sweeps have been plotted together. This of course means that there is a gap in time between the measurements of first sweep and measurements of the second sweep. Again, this timing difference is assumed relatively negligible - the SEVIRI image is chosen at a time right between the two IASI sweeps. This method is only case studies, in which two IASI sweeps are used in the same plot.

Lightning activity and severe weather reports: For this case only Blitzortung and GLD data was available.

Plots showing this data for the entire day are found in figures 10 and 11, respectively. Both networks observe no lightning data in the entirety of central and western Europe. Only two locations inside the analysis area show lightning activity: Blitzortung data shows some activity in the southern parts of Sweden (outside the area of GLD data availability) during the afternoon and evening hours and both Blitzortung and GLD observe a low amount of activity in Greece slightly before noon (the activity in the Aegean Sea is ignored, since it takes place in the very early morning hours, before the SEVIRI/IASI measurements).

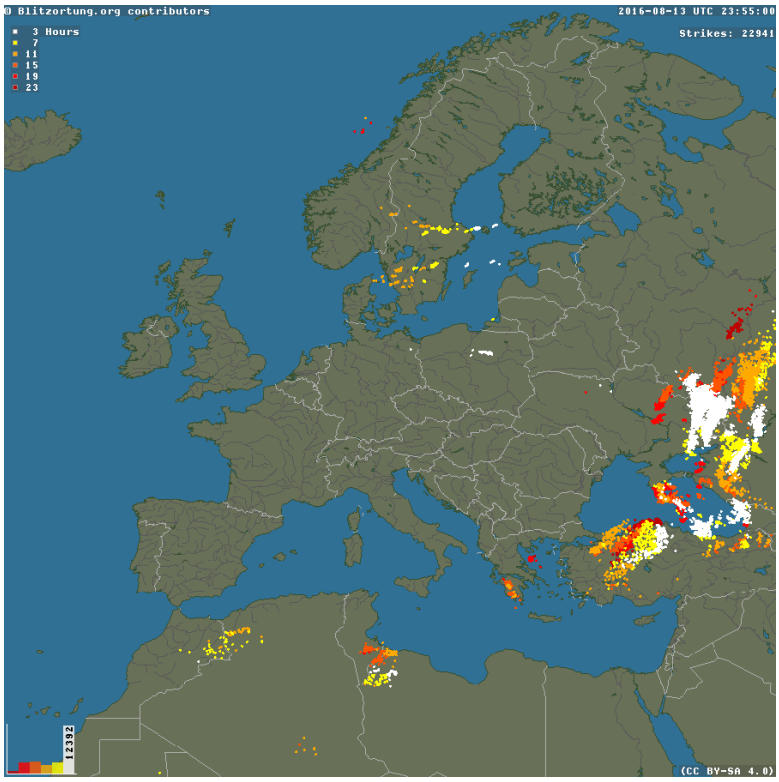

Figure 10: Blitzortung lightning data for the entire day 2016-08-13. Note how the time of the activity is indicated: A time is given in the top right corner (23:55 of the analysed day) - the colour of each point then indicates roughly how many hours *prior to* 23:55 this point was measured. Thus, dark red points were measured at roughly 01:00, while white points occurred at roughly 21:00 etc. All Blitzortung plots in this report use 23:55 as the "reference time".

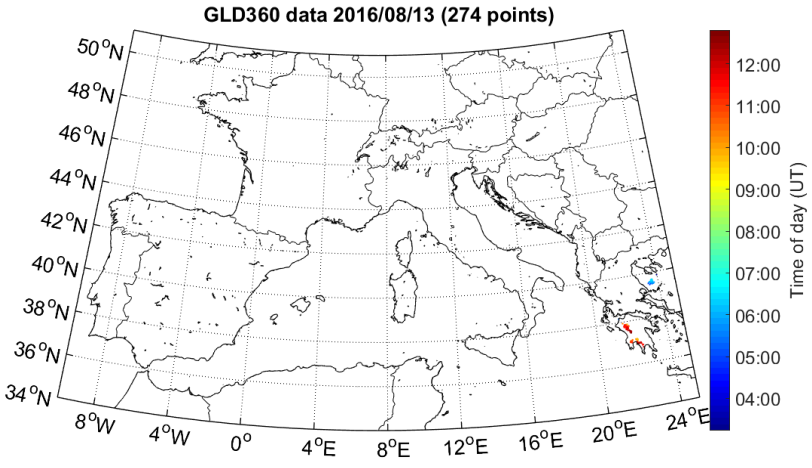

Figure 11: GLD lightning data for the entire day (and full available area) 2016-08-13.

The ESWD show no reports of any severe weather events in southern Sweden or Greece, however it does contain a report of two tornadoes accompanied by moderate rainfall: One in the very northern parts of Sweden at about 05:00 (that is, *before* the IASI/SEVIRI measurements) and one off the coast of Estonia around noon (both outside the area of GLD availability). Furthermore, severe winds were reported around the border between Germany and France around noon (see figure **??**) - no lightning activity was observed by Blitzortung or GLD in either of these areas.

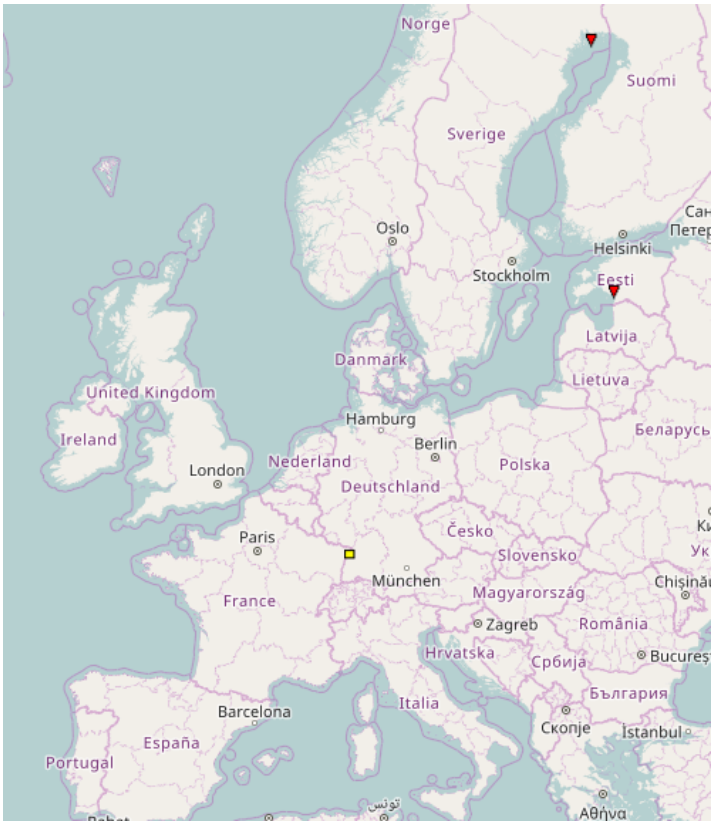

Figure 12: ESWD reports on 2015-05-05 showing hail storms (green triangles), strong winds (yellow squares), heavy rainfall (blue circles), tornadoes (red triangles), and damaging lightning (lightning symbol).

The first-guess IASI, final IASI, and SEVIRI GII are shown in figure 13. As mentioned above, two consecutive IASI sweeps are plotted - the sweep starting in the east (around Estonia) is the first orbit, commencing at roughly 08:33 UTC, whereas the second sweep commences at roughly 10:12 UTC. The SEVIRI image of 09:30 UTC is therefore chosen for the analysis, as this image is acquired roughly in the middle of the time period taken to acquire the two IASI sweeps. All times are given in UTC - the time given in the title of all IASI plots is the time of the orbit start (in this special case the given time is the start time of the first of the two orbits).

K-index: SEVIRI observes quite high K-index values over Greece (approx. 30 °C), agreeing well with the observed lightning data. Most of Sweden is missing SEVIRI coverage, however some data is present in the central/southern parts and this data does indeed show moderately a high K-index (values of approx. 20-25 °C). A moderate K-index is also observed in Germany and northern Spain - none of theses areas showed any severe weather activity and would be expected to show lower K-index values. A quite high K-index is observed around the Alps, where no lightning or severe weather is observed - severe winds were, however, observed at the German/French border north of the Alps and so it is possible that the atmosphere of this entire region was in fact quite unstable. Still, with a K-index this high one would generally expect some thunderstorm activity to occur. SEVIRI is missing data for the area of the Estonia tornado/rainfall. The remaining areas of Europe, where cloud cover did not obstruct the view of SEVIRI, show reasonably low K-index values, suggesting stable conditions.
Looking at the K-index of the final IASI GII one notes the same general tendencies as observed for the SEVIRI K-index. High K-index values are observed for the parts of Sweden that observed subsequent lightning activity

(and is not under cloud cover at the time of the sweep). The IASI K-index is missing coverage over the part of Greece that saw lightning activity, however the few data points that are available in northern Greece as well as over the Aegean Sea do indicate a high K-index in this area. Otherwise, high values are observed in parts of Germany, Spain, and around the Alps, as also observed by SEVIRI. It is noted, however, that these IASI K-index values (especially the ones observed in the area around the Alps) are significantly lower than the ones observed by SEVIRI.
The K-index of the first-guess IASI GII shows some interesting observations. High instability is predicted over Greece and southern Sweden, as would be expected based on lightning data. However a high K-index is also observed for an enormous part of the remaining Scandinavia and northern Germany, where no lightning activity or severe weather events were observed. Interestingly, the part of northern Sweden where a tornado took place a few hours *before* the SEVIRI/IASI measurements leading to the GII also shows high K-index values. One could argue that it seems reasonable for this area to remain unstable a while after the tornado occurred. High instability is also predicted over Estonia/Latvia/Lithuania as well as Poland and the Czech Republic. Although unstable weather was observed in Estonia, making an observation of high K-index reasonable, no thunderstorms or other severe weather types were observed in the remaining countries. As for the K-index of the final IASI GII, the areas around the Alps and in Spain, showing a high SEVIRI K-index, present significantly lower values for the first-guess IASI K-index.

Lifted index: The SEVIRI Lifted index shows very negative values locally around the area of Greece, in which lightning activity was observed around noon. This is the lowest Lifted index observed by SEVIRI in Europe. Moderately low values are also observed around the Alps (including further north, around the German/French border where strong winds occurred). The part of southern Sweden that was not covered by clouds, and where lightning activity occurred in the afternoon/evening, actually shows a positive Lifted index. The Lifted index of the final IASI GII also shows very negative values in the area around Greece, however the exact location of lightning activity is not in the coverage area (due to a shift in cloud coverage most likely). Moderately negative values are observed in a large part of Germany (including the border to France, where strong winds were observed) all the way south to the area around the Alps. Interestingly, the IASI Lifted index is lower for the southern Germany than over the Alps, whereas for SEVIRI this is basically reversed - this could possibly be attributed simply to the shift in time between the two (due to having combined two IASI sweeps in order to cover Europe fully). The clear-sky area of southern Sweden shows values very close to zero - slightly lower than what is observed by SEVIRI, however still not low enough to be considered indacting likely instability.
The Lifted index of the first-guess IASI GII also shows very negative values around Greece, however whereas the SEVIRI Lifted index showed much more local instability around the area of subsequent lightning activity, the first-guess IASI Lifted index shows negative values in a much larger area, including the coast of northern Greece and the entire Aegean Sea. The clear-sky areas correspond very closely to the final IASI Lifted index. The area of northern Sweden, where the final IASI and SEVIRI Lifted index are unavailable, shows a positive Lifted index. Interestingly, the area off the coast of Estonia shows a very local negative Lifted index at the exact location of the tornado, surrounded by positive values. Moderately negative values are also observed over Poland and the Czech Republic.

Total Precipitable Water: SEVIRI observes a fairly high TPW content in the area around Greece (> 30 kg/m^2). For the area in Sweden, where lightning activity was also observed, the SEVIRI TPW is observed to be around 20 kg/m^2, roughly the same value that is found for most of France, Germany, and over most of the oceans, suggesting that the atmosphere over this part of Sweden isn't particularly moist, compared to areas that did not undergo thunderstorm activity. As already seen in the K-index and Lifted index analyses, the area around Estonia was not observable by SEVIRI.
The final IASI GII TPW agrees very well with SEVIRI in areas that are very dry (TPW < 15 kg/m^2). In the area of southern Sweden were the GII was computable, however, the IASI TPW is somewhat lower than what was obtained by SEVIRI. Again, the final IASI GII is missing some coverage in the area around Greece, where lightning activity was observed, however data over the Aegean Sea indicate a lower IASI TPW compared to the SEVIRI TPW.
The first-guess IASI GII obtains TPW values for the area around Estonia, where a tornado and moderate rainfall were observed. These values are quite high (approx. 35 kg/m^2), indicating a very moist atmosphere, especially for the coastal area, where the tornado was reported, but also for areas off the coast of Latvia and Lithuania. The first-guess IASI GII also obtains TPW values over Scandinavia and the large area of the Czech Republic/Germany/Lithuania/Letvia, where cloud cover prevented SEVIRI/final IASI GII retrieval. These areas show very low and intermediate TPW contents, respectively. Interestingly, the TPW values of the area

around the northern Sweden tornado and rainfall event is quite low - arguably, this seems rather reasonable, seeing as a large amount of precipitation just occurred (translating water from the atmosphere to the ground). In general, areas with low TPW values agree quite well for all three retrievals (final IASI, IASI, and SEVIRI GII). Interestingly, the first-guess IASI TPW content over the Aegean Sea east of Greece, over which SEVIRI was observed to detect quite high values and the final IASI TPW somewhat lower values, the first-guess IASI TPW is observed to lie somewhere in the middle, slightly higher than the final IASI TPW yet lower than the SEVIRI values.

Summary and notable observations: For all retrieval types, the K-index correctly predicts unstable conditions in Sweden and Greece (as well as Estonia, though no thunderstorm activity was observed here), however instability is also predicted in large parts of Scandinavia, Germany and Poland, where no severe weather was observed, meaning that the K-index is plagued by some false alarms. Lifted index predicts instability in Greece but not in Sweden or Estonia, constituting misses by the Lifted index with respect to the lightning and severe weather data. TPW is high over Estonia, where moderate rainfall and a tornado was reported, as expected - moderate values are also observed in the eastern parts of Greece, where lightning activity was observed in the general area. Conversely, the TPW showed low values over southern Sweden, where thunderstorm activity did occur.

This case serves the purpose of investigating locations where no severe convective activity was observed throughout the day - in these cases one would expect the GII to indicate stable conditions in the morning time. Aside from a fairly large amount of false alarm locations of the K-index and the Lifted index seemingly failing to predict activity in Sweden and Estonia, the morning time SEVIRI/IASI GII compared reasonably to the subsequently observed severe weather. In general, the SEVIRI, final IASI, and first-guess IASI GII compare very well - only in specific, local cases are differences between the three detected.

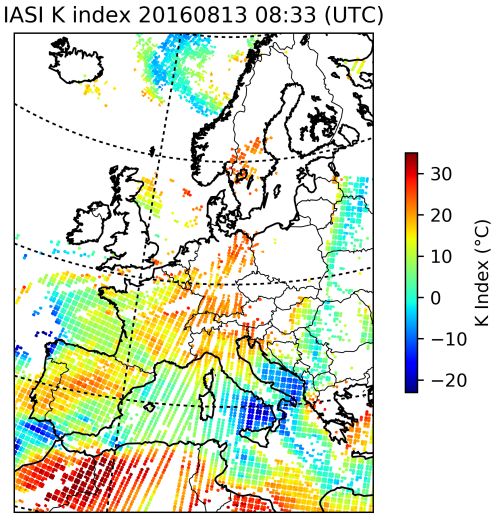

(a) IASI K-index

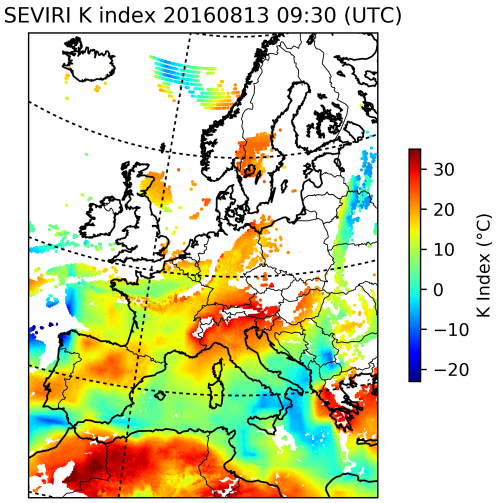

(b) SEVIRI K-index

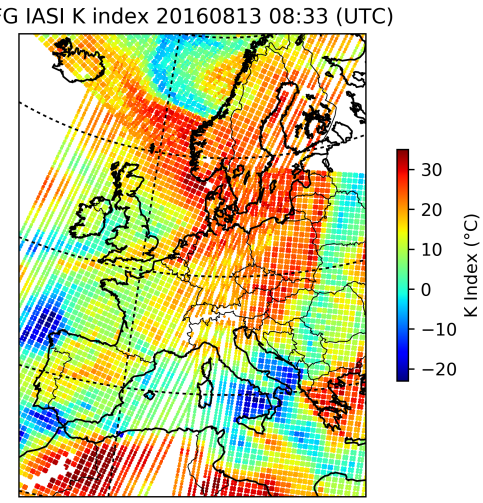

(c) FG IASI K-index

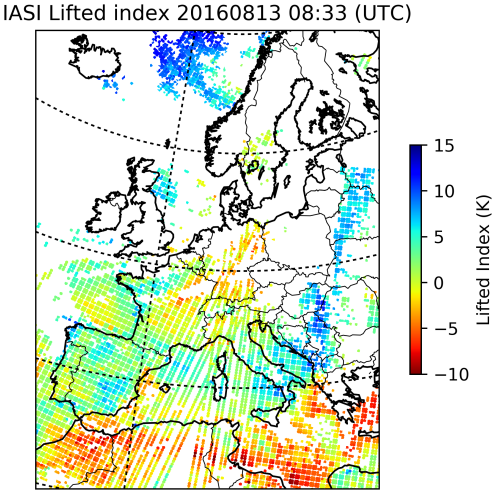

(d) IASI Lifted index

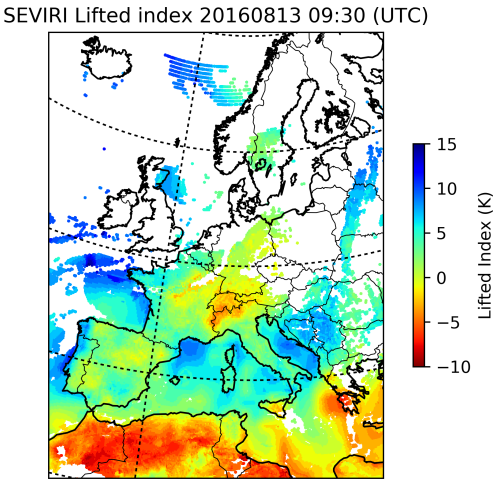

(e) SEVIRI Lifted index

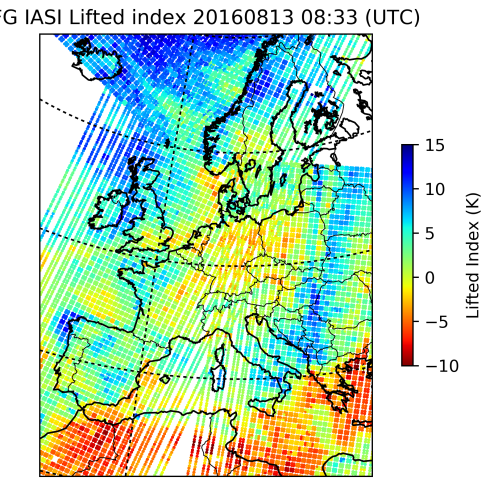

(f) FG IASI Lifted index

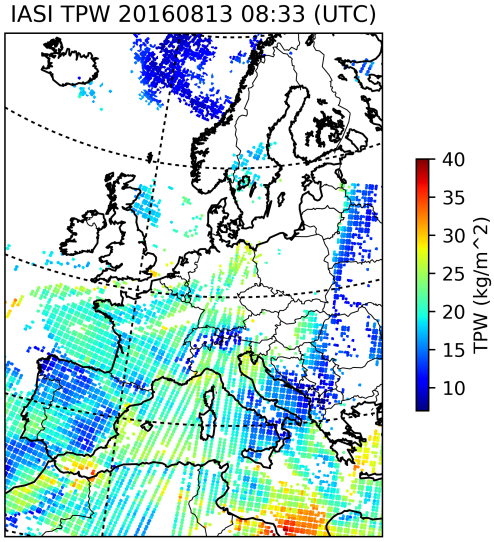

(g) IASI TPW

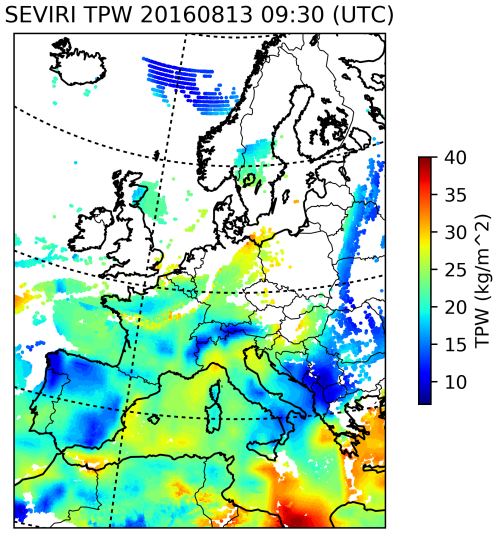

(h) SEVIRI TPW

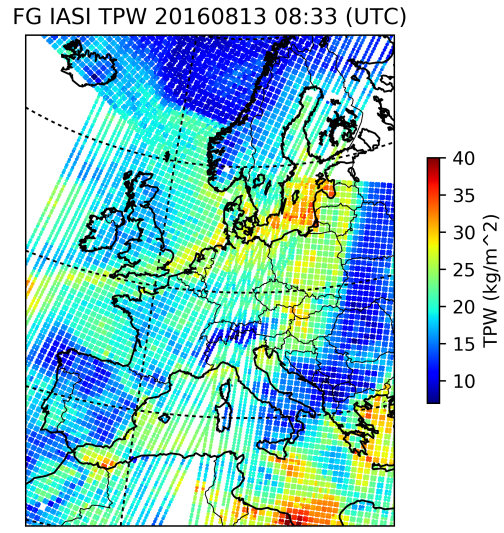

(i) FG IASI TPW

Figure 13: Final IASI, SEVIRI, and first-guess (FG) IASI GII retrievals 2016-08-13.

5.2 Tornado in Germany 2015-05-05

This day was chosen for analysis due to a severe thunderstorm occurring over a very large area including the Netherlands, Denmark, and the northern parts of Germany. Tornadoes were observed in northern Germany and large hail were reported in the Netherlands. Another interesting feature of the storm is that it lasted pretty much the entire day, propagating from west to east.

Lightning activity and severe weather reports: Seeing as the storm in question occurred in the northern part of Europe, GLD data was unavailable. Data from LINET was however available (which is also part of the reason this storm was chosen for the case studies) but only for a very local area (latitude 51°N - 55°N and longitude 3°E - 15°E). As a supplement, Blitzortung data was used. Plots of the lightning data are found in figures 14 (Blitzortung) and 15 (LINET).
Blitzortung shows the general evolution of the very large scale thunderstorm: It develops over France in the morning, then propagates to the Netherlands, northern Germany and Denmark, and finally Poland/the Batlic Sea. A seemingly separate thunderstorm of much smaller scale is observed in the area of Switzerland, Austria, southern Germany, and the Czech Republic. Since the large scale storm was clearly ongoing at the time of the IASI morning sweep (around 09:00), it is noted already at this point, that clear-sky conditions are quite unlikely for most of the northern Europe area (and clear skies is certainly not the case for northern Germany/Netherlands where the storm is ongoing in the morning hours). This is also indicated by LINET data, which provides a close-up look at the lightning activity of over Germany and the Netherlands.

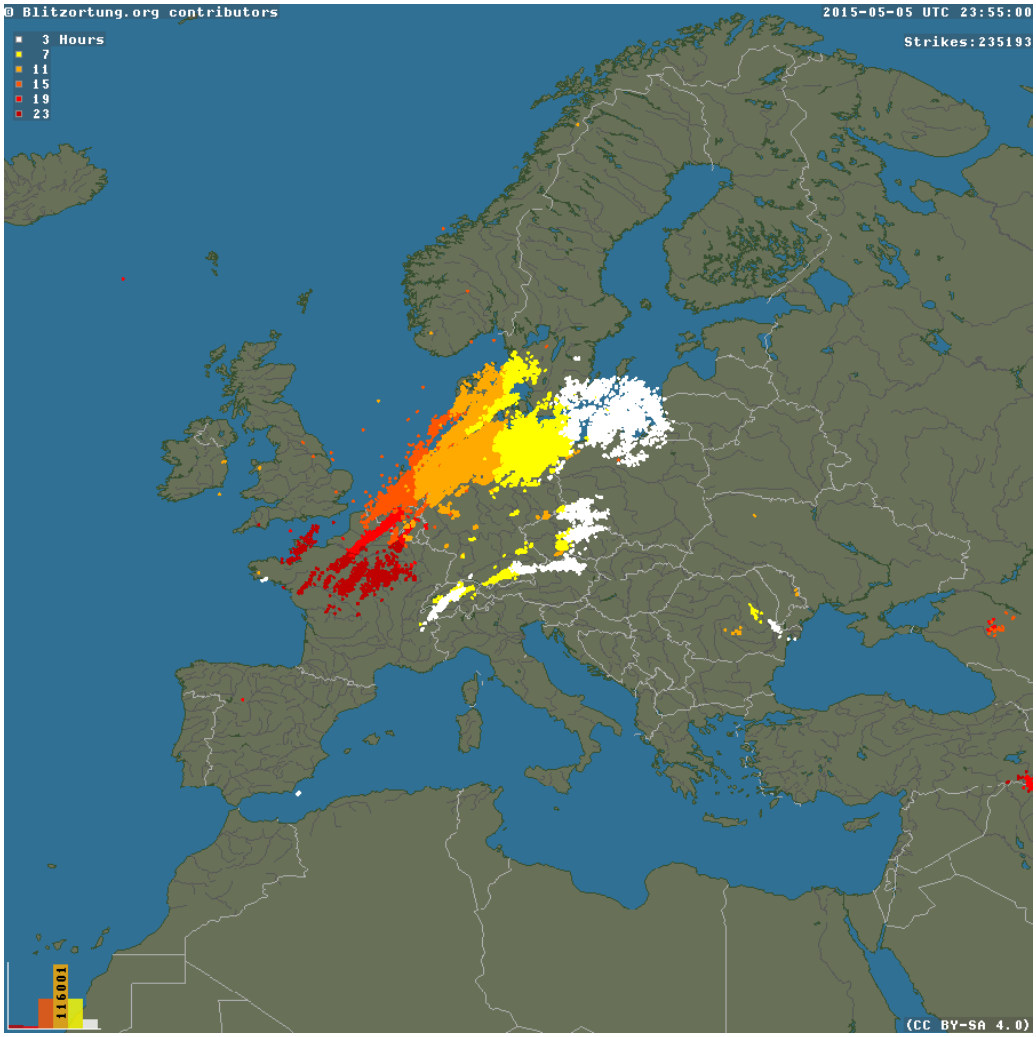

Figure 14: Blitzortung lightning data for the entire day 2015-05-05.

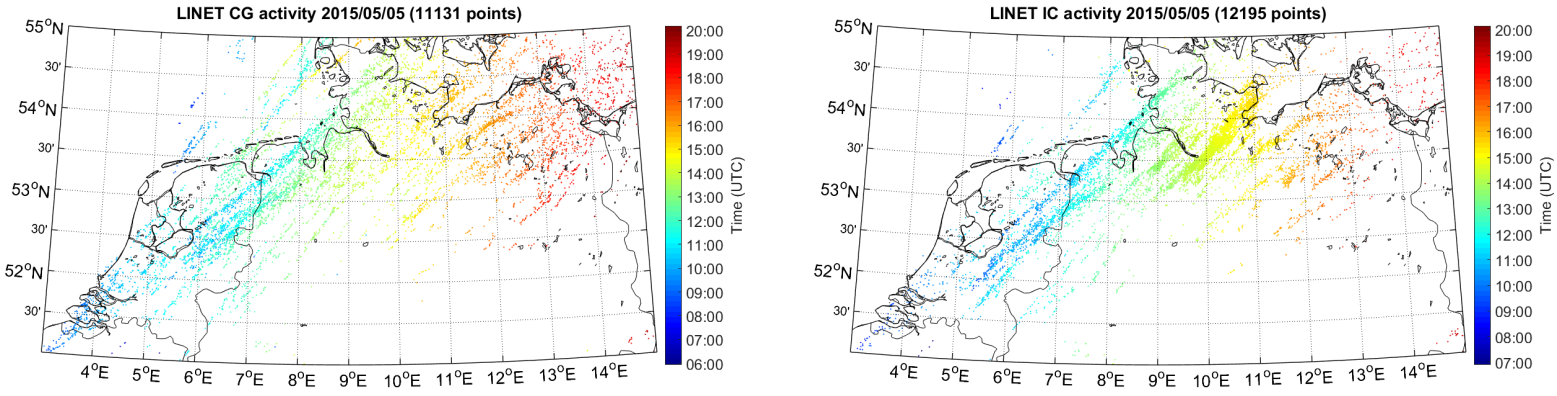

(a) LINET CG activity

(b) LINET IC activity

Figure 15: LINET CG and IC activity for the available area and time period on 2015-05-05.

The ESWD shows, most notably, reports of large hail in the Netherlands and several reports of tornadoes in north Germany, accompanied by strong winds and heavy rainfall. All of the tornadoes were reported to have occurred in the timeframe 16:00-17:30 and the large hail reportedly occurred at 12:00-13:30.

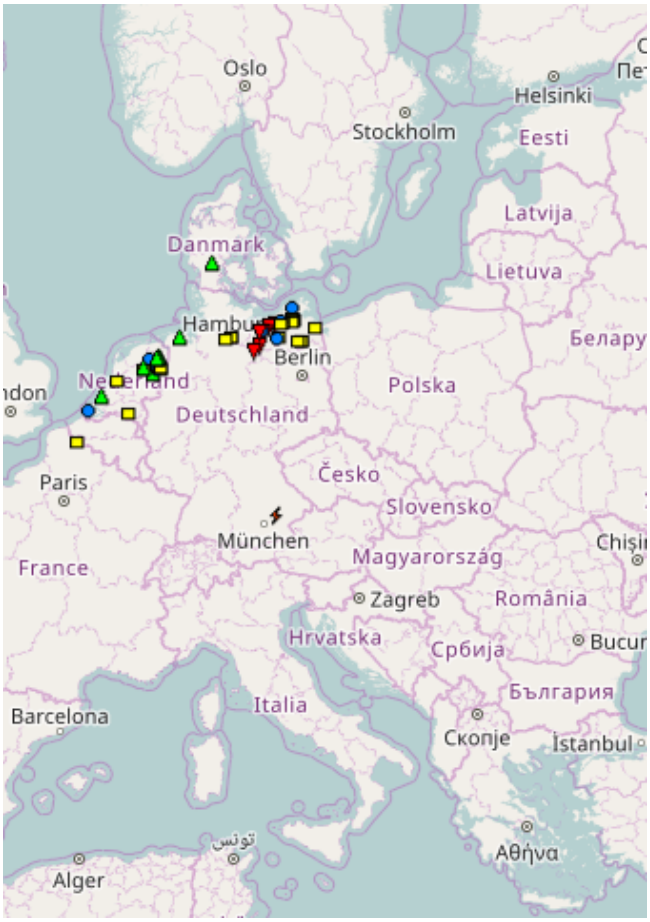

Figure 16: ESWD reports on 2015-05-05 showing hail storms (green triangles), strong winds (yellow squares), heavy rainfall (blue circles), tornadoes (red triangles), and damaging lightning (lightning symbol).

SEVIRI and final IASI GII coverage: The three GII retrievals are shown in figure 17. As was already alluded to above, the fact that the same very large scale storm takes place over several hours, including morning

hours, clear sky conditions are unlikely to be present in the area of the storm, where the GII is of interest. This is clearly seen upon observation of the SEVIRI and final IASI GII: Nearly the entire area of interest, as well as almost the entirety of south and central Europe, is missing data coverage. Only very small regions around the Dutch/German and Danish/German borders are contain available data. These two regions both show a high K-index for both IASI and SEVIR, a Lifted index very close to zero (at the Danish/German border IASI observes negative values while SEVIRI values are positive), and TPW values are fairly low over the Dutch/German borders and intermediate over the Danish/German border. With a data coverage this small, it is hardly reasonable to make any real analysis using the SEVIRI and final IASI GII.

This case is a very representative example of the benefits of obtaining the GII from he first-guess IASI temperature and humidity profiles: While the SEVIRI/final IASI GII provide essentially no coverage of the area of interest, the first-guess IASI GII provides full coverage (regardless of cloud cover) of the analysis area. An obvious concern, which should be raised, is the accuracy of the first-guess IASI GII compared to the final IASI GII - how much is the accuracy of the IASI GII improved by the optimal estimation retrieval algorithm of the temperature and humidity profiles? This is investigated further (and more quantitatively) in a separate analysis in section 5.7, however judging by the qualitative comparison between final/first-guess IASI GII in the case study above (and the case studies to follow), one notes relatively small differences between the two.

In the following, the first-guess IASI GII is compared to the observed lightning data and severe weather reports.

K-index: The first-guess IASI K-index shows high values over the Denmark, northern Germany, and western Poland, where the large scale thunderstorm propagated during the afternoon and early evening hours. Over the northern France, Belgium, and parts of the Netherlands, where most of the lightning activity happened *before* the IASI GII measurement, values are actually somewhat lower, indicating not as strong instability. Parts of the Baltic Sea and North Sea also experienced lightning activity from the large scale storm - the K-index does predict instability over parts of these areas but not corresponding exactly to where the lightning activity was observed (for instance, activity was observed off the coast of Lithuania, however the IASI K-index is quite low at this location). It is recalled, however, that the K-index was developed to predict convection over continental areas and so this discrepancy is not all too surprising. High IASI K-index values are also observed in southern Germany/the Czech Republic and around the Alps, where lightning activity also was observed (although likely part of a separate storm, cf. the Blitzortung data). Finally, high instability is indicated in eastern Europe over Romania/Serbia/Bulgaria - some lightning activity was observed Romania, although the level of activity indicates a fairly non-severe storm.

Lifted index: The first-guess IASI Lifted index is moderately negative around northern parts of the Netherlands and the German/Danish border. The area of northern Germany, where several tornadoes occurred, shows only slightly negative values. Lower Lifted index values are observed across southern Germany, the Czech Republic, and western Poland, where the smaller thunderstorm occurred in the evening. Finally, low Lifted index values are also observed for the area in eastern Europe around Romania/Serbia, where very little lightning activity did occur. In conclusion, in this case, the Lifted index indicates higher instability for the two smaller thunderstorms (southern Germany/Alps area and easter Europe) compared to the very large scale thunderstorm in northern Europe.

Total Precipitable Water: High first-guess IASI TPW values are observed over large parts of Germany, the western parts of Poland, and Denmark and the surrounding waters. High values are also observed in France, close to the Swiss border. Interestingly, fairly low TPW values are observed over the Netherlands, where large hail occurred around noon. This actually corresponds well with a general observation, that a high TPW *reduces* hail size due to the reduction in updraft velocity[5] - that is, in the event of a hail storm the hail size is typically inverse proportional to the TPW.

Summary and notable observations: As earlier mentioned, this case study serves as a representative example of the limitations of only obtaining the GII in clear-sky environments and illustrates the advantages of obtaining the GII by utilization of the first-guess IASI temperature and humidity profiles. Comparison of the first-guess IASI GII with lightning and severe weather data showed reasonably good prediction skills for the K-index, whereas the Lifted index interestingly showed more instability in the areas where the smaller thunderstorms occurred compared to the large scale storm. An interesting observation was made of relatively

[5]Website of meteorologist Haby, J. - http://www.theweatherprediction.com/habyhints/294/ (reference also found in section 8)

low TPW in the area of the Netherlands that experienced large hail, coherent with the theory of hail size being inversely proportional to TPW.

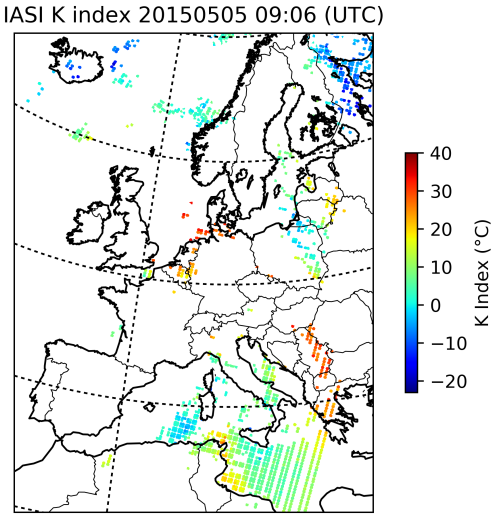

(a) IASI K-index

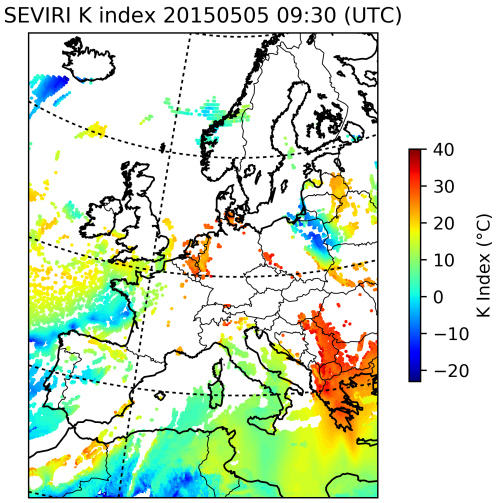

(b) SEVIRI K-index

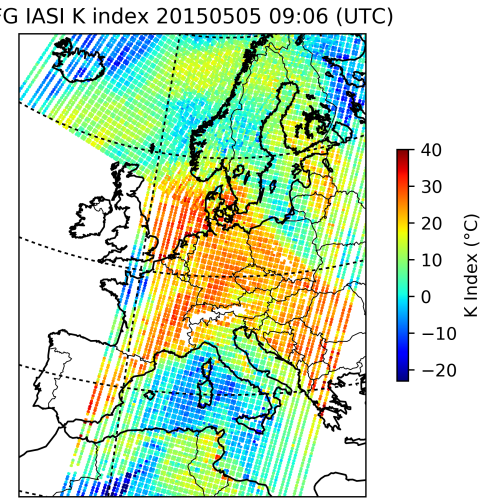

(c) FG IASI K-index

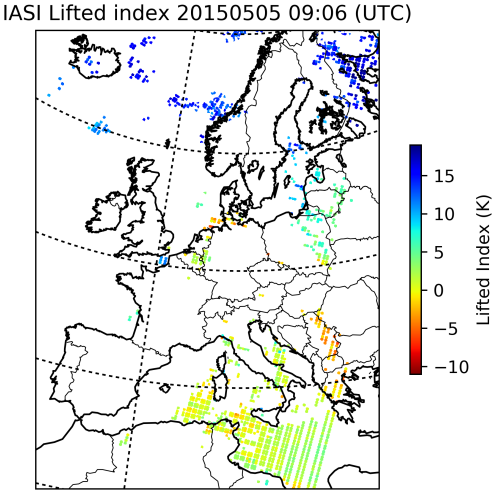

(d) IASI Lifted index

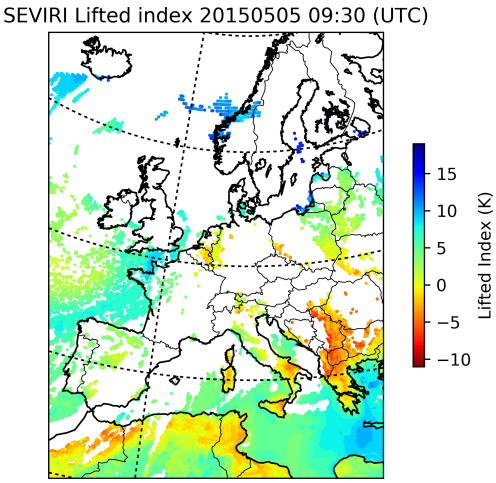

(e) SEVIRI Lifted index

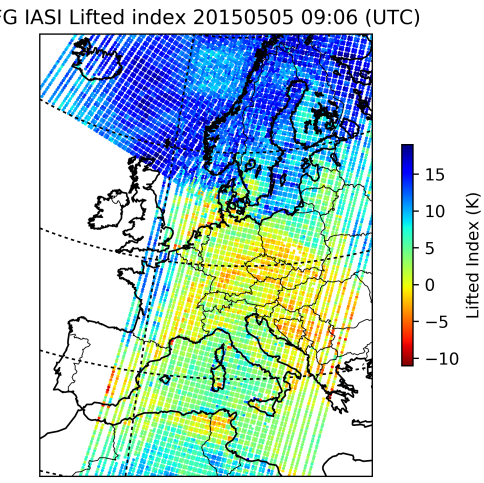

(f) FG IASI Lifted index

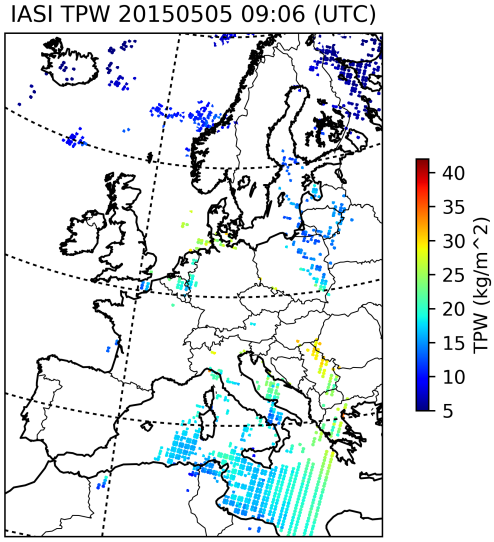

(g) IASI TPW

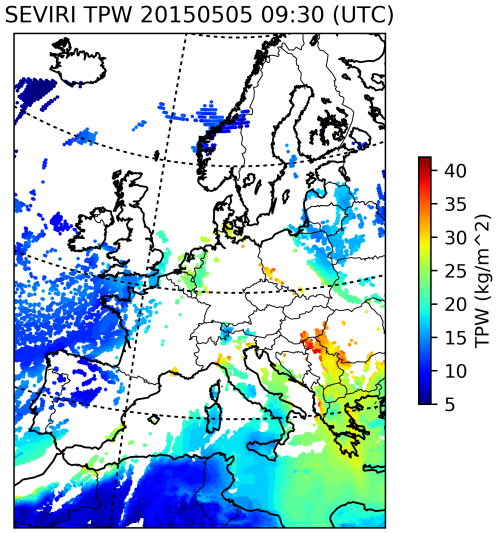

(h) SEVIRI TPW

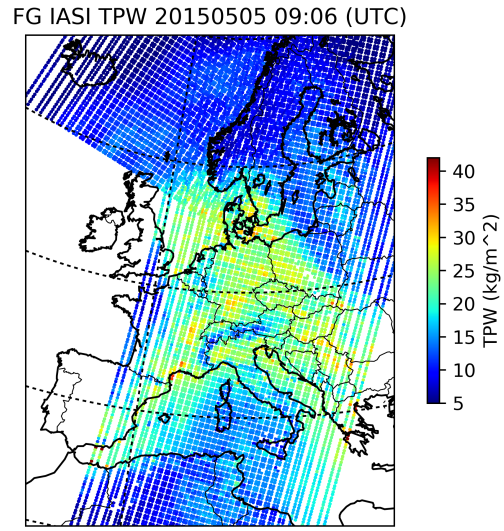

(i) FG IASI TPW

Figure 17: Final IASI, SEVIRI, and first-guess (FG) IASI GII retrievals 2015-05-05.

5.3 Hail storm in Germany 2015-07-07

This case was chosen as it involves a very large scale thunderstorm, which also included very large hail in several areas, causing a large amount of damage to property.

Lightning activity and severe weather reports: Both Blitzortung and GLD data indicate a heavy amount of activity during the day over an area spanning parts of France and northern Italy, almost the entirety of Germany, Switzlerand, and Austria, as well as parts of the Czech Republic and Poland. The main part of this activity is observed in the evening hours, however especially the western parts of this large area shows activity during the afternoon and even in the early morning hours before the GII measurements (in a small area of France). A few other, much smaller areas also show some lightning activity, most notably an area in the vicinity of Rome and another area along the English east coast (however this latter area is mostly outside the IASI sweep).

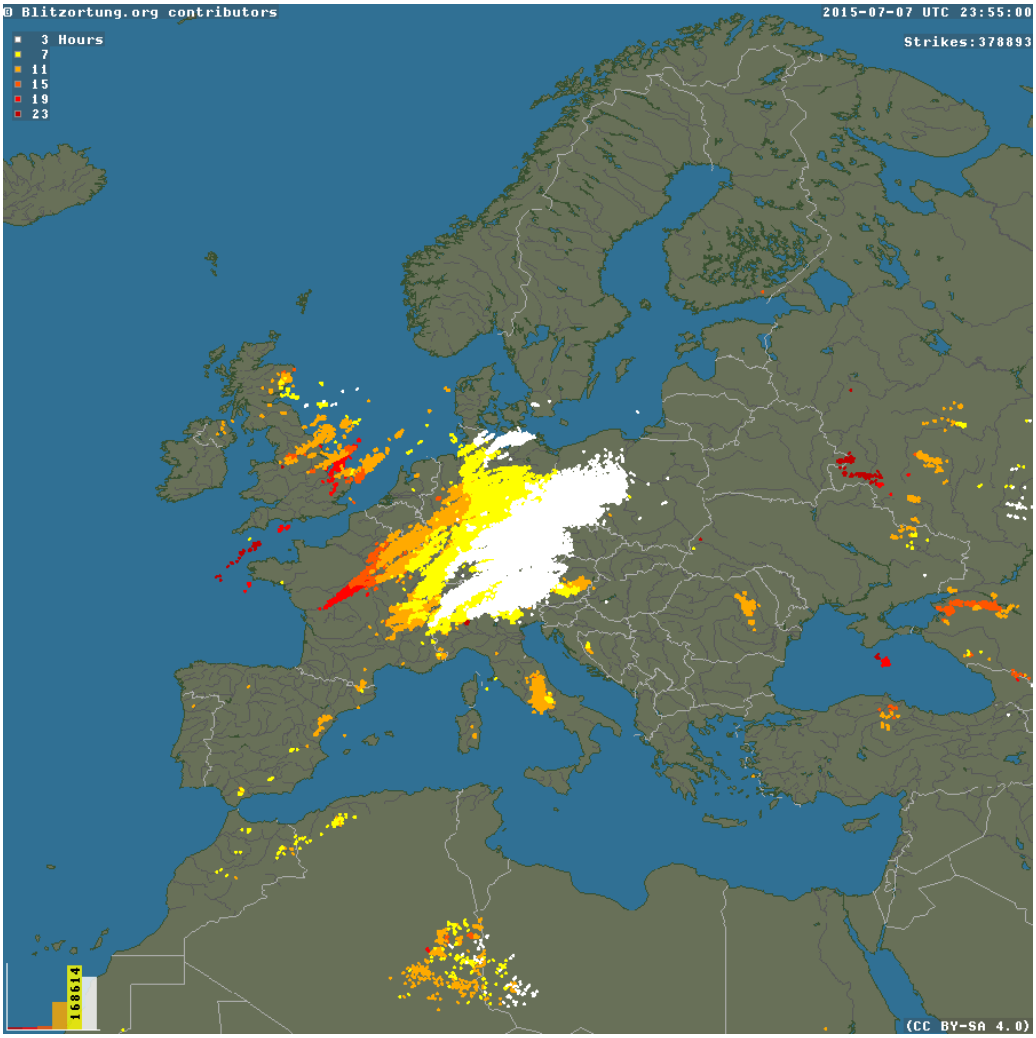

Figure 18: Blitzortung data for the entire day 2015-07-07.

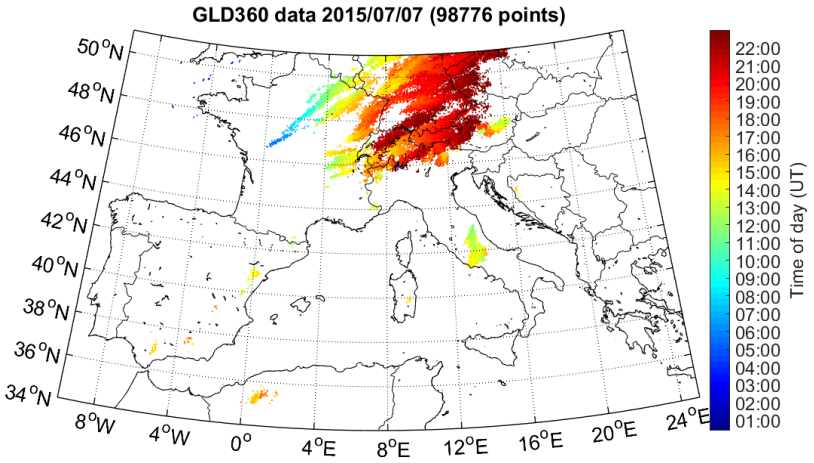

Figure 19: GLD lightning data for the entire day (and full available area) 2015-07-07.

ESWD data shows an enormous amount of reports of strong winds and some damaging lightning in the area of the large scale thunderstorm and (perhaps most notably) a very large number of reports of large hail in the southern and central parts of Germany - the hail reports all lie in the time interval 18:00-21:30.

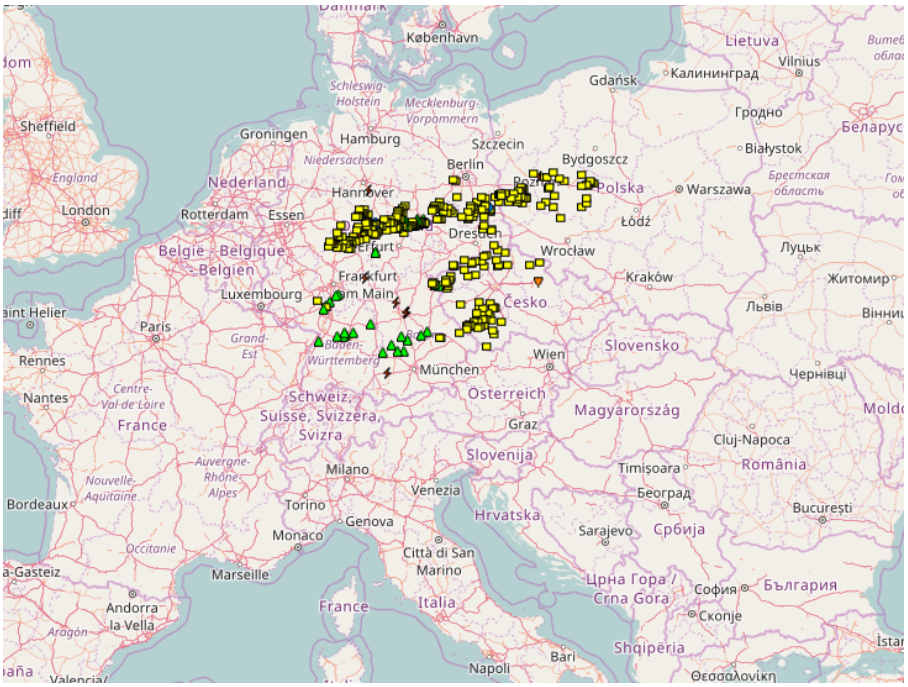

Figure 20: ESWD reports on 20150707 showing hail storms (green triangles), strong winds (yellow squares), damaging lightning (lightning symbol), and a single "dust devil" (orange triangle, not of interest in this study).

K-index: The SEVIRI and final IASI K-index agree fairly well. Both indicate high instability (K-index above 30 °C) in southern Germany and a large part of eastern France, Switzerland, Austria, and northern Italy - all areas over which the large scale afternoon/evening thunderstorm was observed. However they also both show high K-index values over Slovenia and parts of Hungary and Croatia - though these areas are close to the massive area of the large scale thunderstorm, no lightning activity was observed here. In addition, high K-index values are observed over a large area in Romania (though IASI is missing some coverage here) where only very little lightning activity occurred (cf. the Blitzortung data, as the area is outside the GLD availablity area). Both the SEVIRI and final IASI K-index is significantly lower in northern Germany, however with values around 20°C a likelihood of unstable conditions is still suggested. For the area around the German/Polish border,

however, values drop to around 15°C - while values at this level in some cases might be considered as indicating instability, it is remarkable that the K-index is so much lower compared to what is observed around southern Germany, as a quite large amount of lightning data was observed around the German/Polish border. Finally, both the SEVIRI and final IASI K-index predict instability in the area around Rome, where a thunderstorm of smaller scale was observed.
The first-guess IASI K-index adds coverage in the southern Germany/northern Italy area and Romania where some data was missing, however not much information is added. On the western edge of the IASI sweep, the first-guess IASI K-index shows high instability around the south-east coast of England, where lightning activity was observed.

Lifted index: Looking first at the Lifted index of the final IASI GII it is noted that it bears close resemblance to the IASI/SEVIRI K-index in terms of the areas that are indicated as being unstable. The same large area around southern Germany, eastern France, Switzerland, Austria, and northern Italy shows high instability (in the shape of very negative Lifted index values). Furthermore, the area around Romania, which showed high K-index values for both IASI and SEVIRI, also shows negative Lifted index values (although data coverage is quite sparse for IASI). In addition, northern Germany and Poland show much smaller indications of instability (when compared to southern Germany), even though subsequent lightning activity was observed here, as was also the case for the K-index. The Lifted index over the Mediterranean and Tyrrhenian Seas is quite low for the final (and first-guess) IASI GII and slightly higher for the SEVIRI GII, though no lightning activity was observed here, however this discrepancy is somewhat ignored, as the indices are not expected to necessarily yield correct predictions over water. The final IASI Lifted index shows quite negative values in Hungary - interestingly, the Lifted index of this area is slightly higher for the first-guess IASI GII and SEVIRI observes even higher Lifted index (indicating lower levels of instability). The SEVIRI Lifted index also indicates slightly higher values over Romania, compared to the first-guess and final IASI Lifted index.

Total Precipitable Water: Immediately one notices very high TPW values for all three GII retrievals in a region of northern Italy, just south of the Alps. Part of this region was exposed to subsequent thunderstorm activity, however interestingly most of the region actually lies just south of the extent of the large scale evening thunderstorm. Moving slightly further south from here, to the area around Rome, another, separate thunderstorm of much smaller scale did occur in the early afternoon hours. Thus, the region of northern Italy lies between two areas that experienced thunderstorm activity. Interestingly, all three retrieval types observe a small area just west of the small scale afternoon thunderstorm over Rome with a moderately high TPW (higher values are observed for SEVIRI and first-guess IASI compared to final IASI TPW). Thus, there is a small offset between the area of storm activity and the area of high TPW content. A reasonable guess as to why this is observed could be, that the moist region has been transported by wind during the hours between the GII measurement and the thunderstorm activity. Another interesting observation is that the TPW is moderately low (around 25 kg/m^2) in the area of southern Germany, where large hail were reported. As for the case studied in section 5.2 above, this supports the idea of hail size being inverse proportional to TPW.

Summary and notable observations: This case showed a reasonably good coherence between high K-index values and subsequent thunderstorm activity - most of the area of the large scale afternoon/evening thunderstorm showed very high K-index values in the morning hours. Some false alarm areas were observed (areas of high K-index but no subsequent lightning activity) around Croatia and Hungary and relatively low K-index values were observed in northern Germany/Poland, where the thunderstorm actually did extend to. One could speculate, whether the wind could have played a part in this offset between areas of indicated instability and areas of observed lightning activity (as was suggested to be the case in a much smaller scale for the TPW around Rome). Both the K-index and the Lifted index predicted instability in the region around Rome, where a separate storm occurred in the afternoon. In general, the K-index and Lifted index agreed fairly well in this case across all three GII retrieval types, with differences between the retrieval types being fairly local and small in magnitude. The TPW content showed a region in northern Italy of very high humidity just south of the large scale storm and another high TPW region just west of the Rome thunderstorm. In addition, moderately low TPW values were observed in the region where large hail occurred in southern Germany.

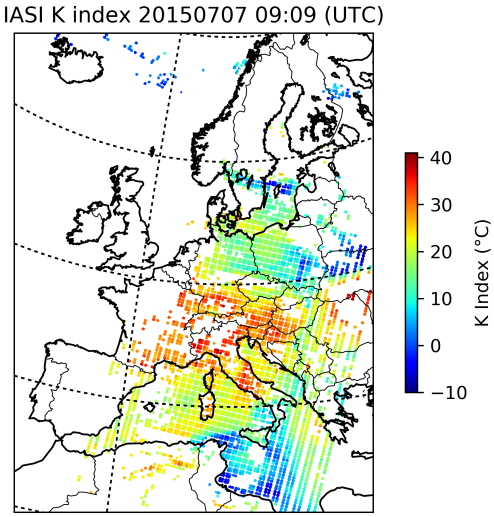

(a) IASI K-index

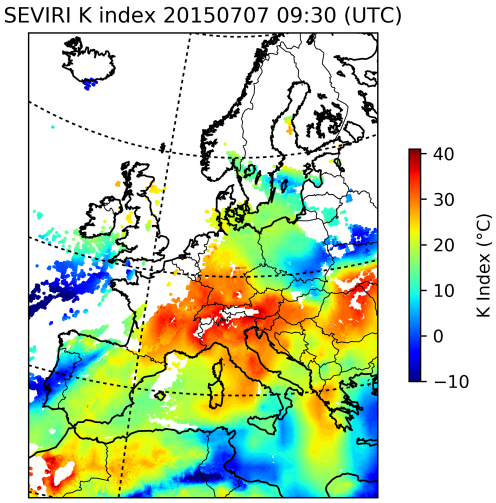

(b) SEVIRI K-index

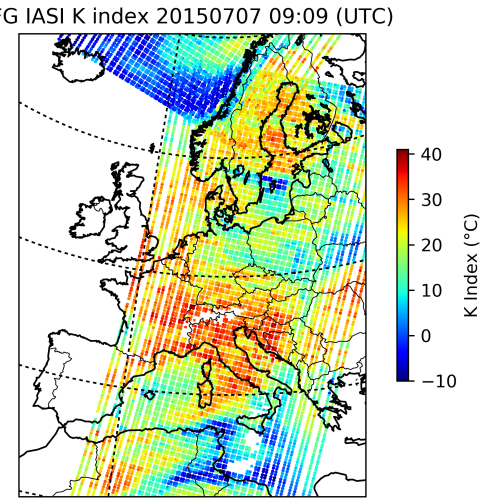

(c) FG IASI K-index

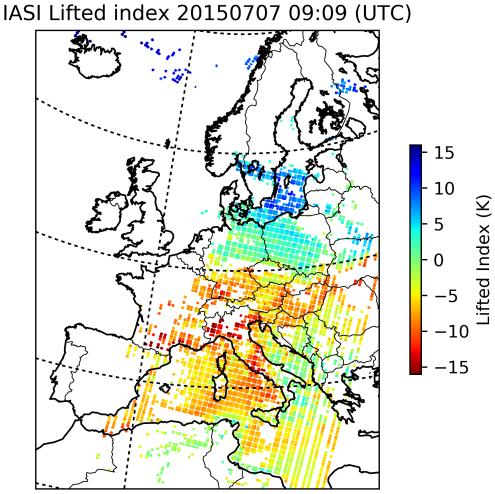

(d) IASI Lifted index

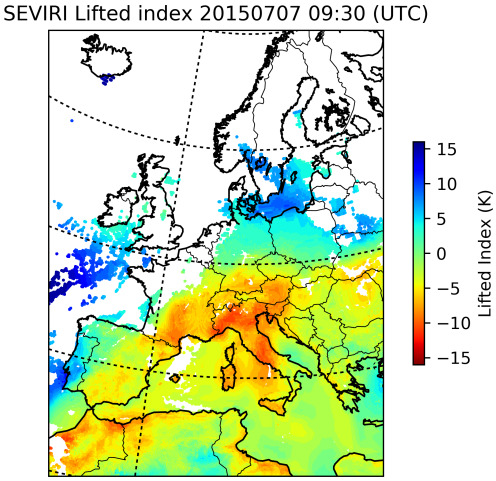

(e) SEVIRI Lifted index

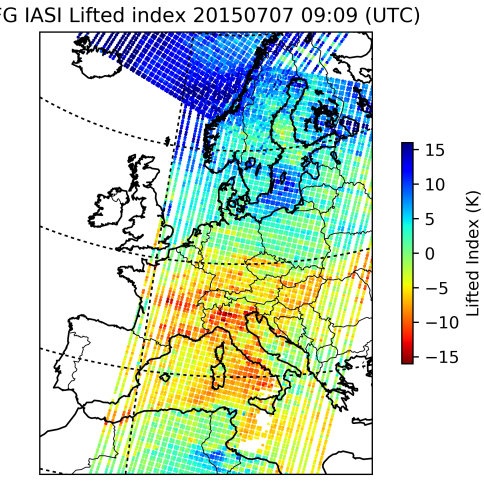

(f) FG IASI Lifted index

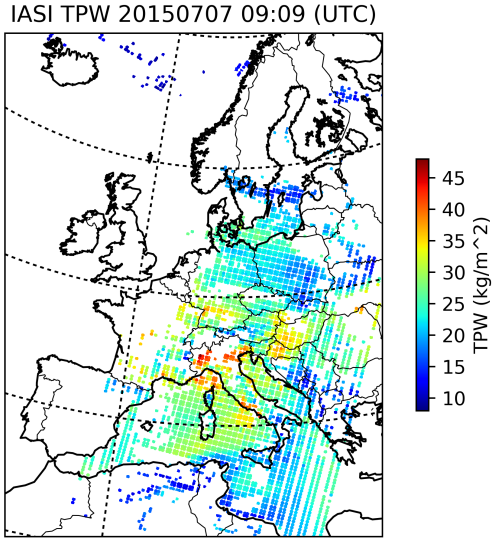

(g) IASI TPW

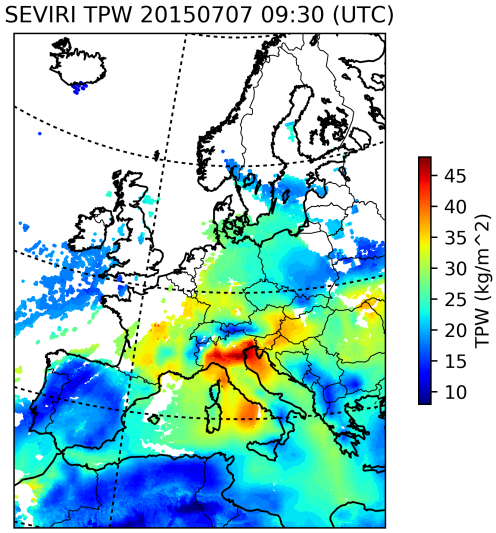

(h) SEVIRI TPW

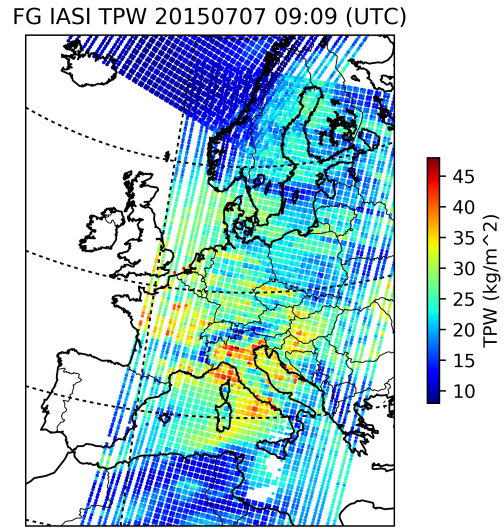

(i) FG IASI TPW

Figure 21: Final IASI, SEVIRI, and first-guess (FG) IASI GII retrievals 2015-07-07.

5.4 Tornado in Venice 2015-07-08

In this case the focus lies on another large scale thunderstorm, that occurred the day after the large scale storm analysed above. Looking at the lightning activity data, it is observed that it spans from the late night (midnight and onwards) to the morning hours and all through the day. Hence, it appears that this storm is actually a continuation of the large scale storm analysed above (in section 5.3). As such, the observation of this severe storm may explain some of the results (and some of the inconsistencies between GII and lightning activity) obtained in section 5.3.
The spatial focus in this case is narrowed slightly in order to get a better view of local GII values within the area of the large scale storm, focusing mainly on the area from Italy to western Ukraine longitude-wise and from Greece to northern Germany latitude-wise.

Lightning activity and severe weather reports:
As mentioned above, the lightning data (Blitzortung and GLD, seen in figures 22 and 23, respectively) reveals that storm activity commences already around midnight and continues all through the day - combining this with the lightning data from the case in section 5.3, it is observed that the thunderstorm simply continues from one day (2015-07-07) to the next (2015-07-08). The storm is observed to propagate (roughly) from west to east. The propagation of the storm is however not quite uniform: Early activity (from midnight to the early morning, *before* the GII measurements) occurs in northern Italy, Switzerland, Germany, the Czech Republic, and Poland. Later on, a few hours before noon, activity is observed around the borders of Italy, Austria, and Slovenia. Then, in the afternoon, activity is observed west of here (in Italy, close to Venice) and also in southern Poland as well as Hungary. Finally, evening activity is observed around Venice and Slovenia, in the area of Croatia/Serbia/Hungary, and around the borders of Slovakia, Poland, and Ukraine. Finally, a very small amount of activity is observed in southern Italy during the late afternoon.

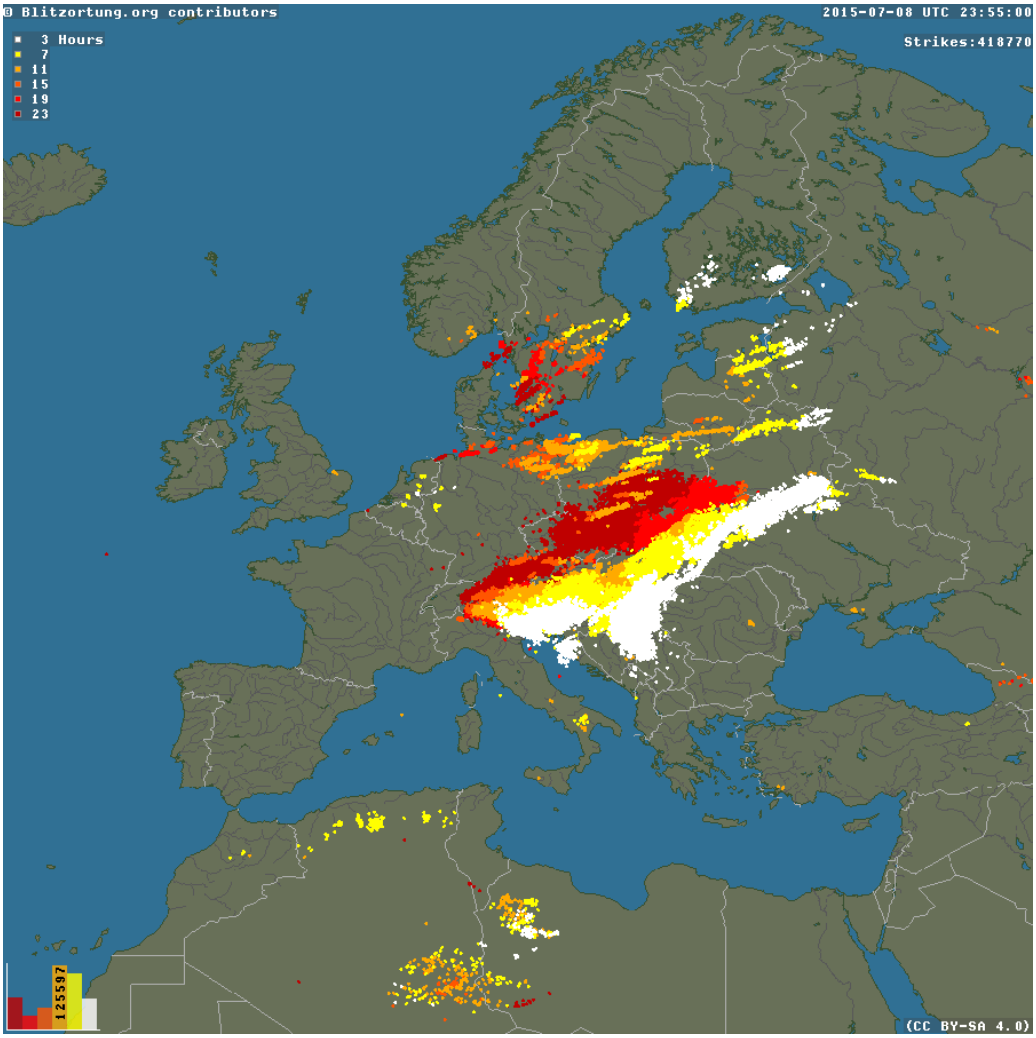

Figure 22: Blitzortung lightning data for the entire day 2015-07-08.

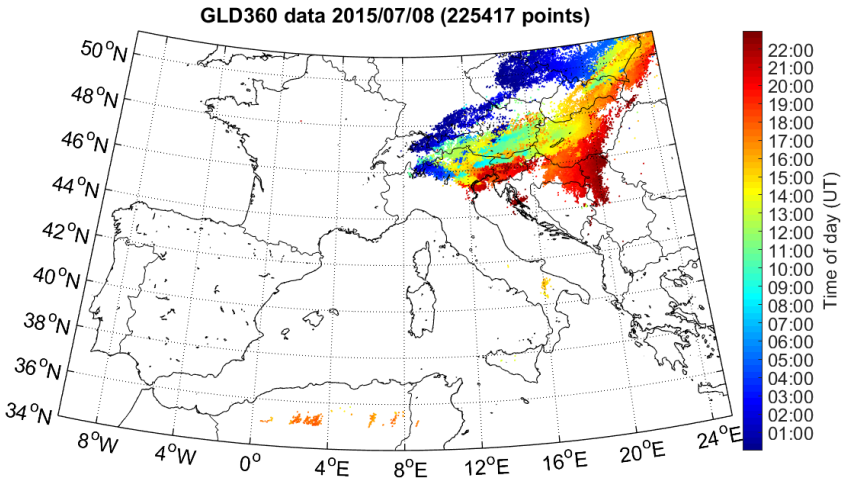

Figure 23: GLD lightning data for the entire day (and full available area) 2015-07-08.

LINET data was available for a small area around Venice, where a tornado occurred along with heavy lightning activity (latitude 45°N - 46.5°N, longitude 10°E - 13°E). The CG and IC observed activity is shown in figure 24.

This close-up view of the lightning activity shows how lightning activity occurred from slightly after midnight and through the entire day in a very small area.

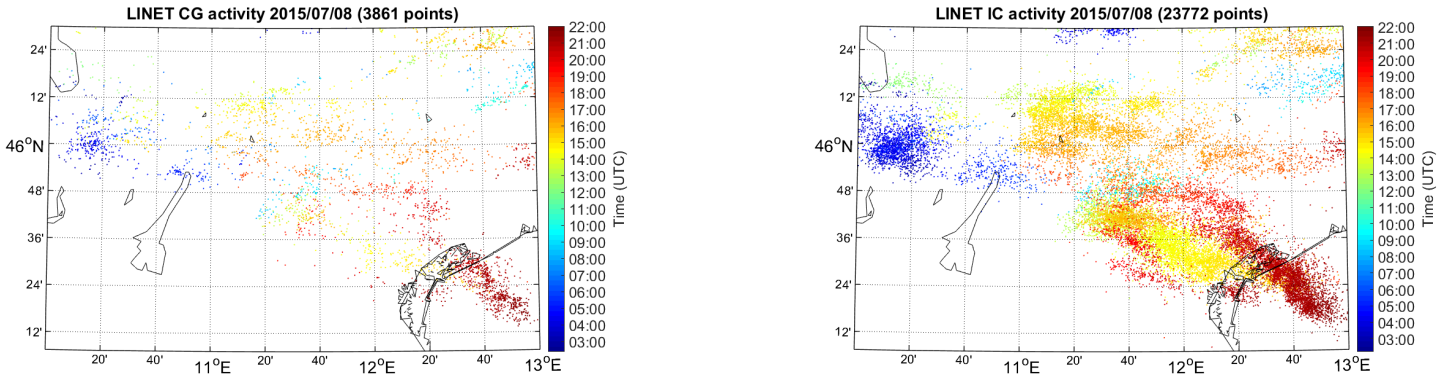

(a) LINET CG activity

(b) LINET IC activity

Figure 24: LINET CG and IC activity for the available area and time period on 2015-07-08.

ESWD data shows a large number of reports of strong winds (mainly in the evening hours) as well as numerous reports of large hail around Slovenia/Croatia, Austria, and Hungary taking place around 14:30-17:00. Finally, a tornado of very high intensity (leaving many people injured and substantial property damage) was observed in the area of Venice in the afternoon (around 16:00).

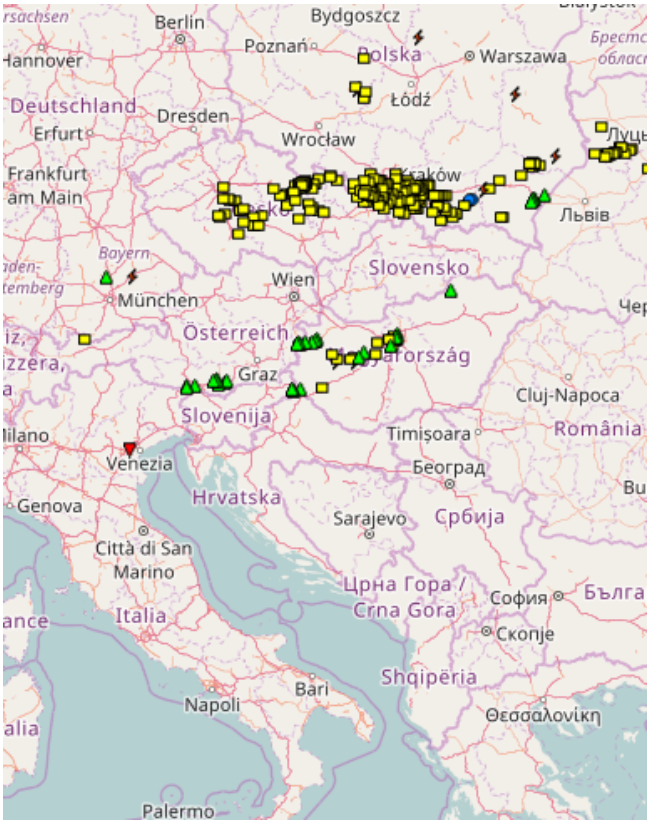

Figure 25: ESWD reports on 20150708 showing hail storms (green triangles), strong winds (yellow squares), damaging lightning (lightning symbol), heavy rainfall (blue circle) and a tornado (red triangle).

K-index: Looking first at the SEVIRI and final IASI K-index one immediately notes that a very large part of central and northern Europe is missing coverage - this was, of course, to be expected, since the lightning

data reveals heavy activity all through the day, including the time around the GII measurements. Comparing the SEVIRI and final IASI K-index in the regions where coverage is achieved, a generally good coherence is observed. Some differences are, however, observed: Around the border of Slovenia and Croatia, where large hail were observed along with lightning activity in the afternoon/evening, the final IASI Lifted index is somewhat higher than what is observed by SEVIRI. Conversely, K-index values are observed slightly higher by SEVIRI compared to the final IASI retrieval along the coast of the Adriatic (Bosnia/Montenegro/Albania as well as Greece). High K-index values are observed for both retrieval types around Hungary, Slovakia, southern Poland, and western Ukraine. Finally, fairly high K-index values are observed over central Italy, although virtually no lightning activity was observed here.
This case is another example of the benefit of all-sky GII retrieval: The first-guess IASI GII adds information for a vast area of central/northern Europe, where the clear-sky retrievals provide no coverage. The first-guess IASI K-index agrees fairly well with the final IASI retrieval, although with some slight differences. In the area around Croatia, Hungary, and to a certain extend Slovakia the first-guess IASI K-index is slightly higher. The first-guess IASI K-index agrees well with the final IASI retrieval in the area around Greece and Albania, where no lightning activity occurred - here, the SEVIRI indicated quite high instability, however both IASI retrievals shows values that are substantially lower. Finally, the first-guess IASI K-index observes observes high instability over the very southern parts of Germany as well as over the Czech Republic, Poland, and the very western parts of Ukraine and Belarus. While souther Germany and the Czech Republic were mainly exposed to early morning thunderstorm activity (before the GII measurements), the other areas all observed activity between noon and late evening time. It seems somewhat reasonable, that the areas, which were exposed to thunderstorm activity only hours prior to the GII measurements, remain unstable for while.

Lifted index: Taking a look at the SEVIRI and final IASI Lifted index, one notes the same pattern for the area around Slovenia/Croatia/Hungary, as was observed for the K-index: both retrieval types indicate instability in the region, however the final IASI Lifted index is substantially lower. Aside from this feature, the two retrievals are very similar. An interesting observation is made for the region along the countries at the Adriatic coast, where a somewhat high K-index was observed. Both the SEVIRI and final IASI Lifted index indicate fairly high Lifted index values - they are still negative, technically indicating instability, however compared to the values observed Slovenia/Croatia/Hungary as well as regions of Italy, where very low Lifted index values occur, the Lifted index for the Adriatic coast area is quite high. It is interesting how Lifted index values seem to indicate quite high instability in central and southern Italy, even though very little activity was observed here. Finally, moderately negative Lifted index values are observed in Poland, Slovakia, and western Ukraine, coherent with K-index observations and subsequent lightning data.
The first-guess IASI Lifted index, again, agrees fairly well with the final IASI Lifted index with the following exceptions: Values in central Italy are somewhat lower for the first-guess IASI retrieval as well as the area around Slovenia/Croatia/Hungary. The added coverage area of the first-guess IASI Lifted index show virtually no instability in southern Germany (values are roughly zero or above). Instability is indicated by moderately negative Lifted index values in Austria, Slovakia, western Ukraine, and parts of the Czech Republic and Poland. Interestingly, the first-guess IASI Lifted index in areas that were exposed to morning time thunderstorm activity (before the GII measurements) show very little indication of instability, compared to what was observed for the K-index. This suggests, that after a thunderstorm has subsided, the Lifted index might return to stable values faster than the K-index, although it must be stressed that strict conclusions should not be made on the basis of just one (or a few) case studies.

Total Precipitable Water: For the TPW content one immediately notices a high deviation between the SEVIRI and final IASI retrieval and the first-guess IASI retrieval: Around the border between Slovenia, Croatia, and Hungary the SEVIRI and final IASI TPW values are very high (> 40 kg/m^2), whereas the corresponding first-guess IASI values are significantly lower (around 30 kg/m^2). The same observation is made in the area round Venice - final IASI and SEVIRI TPW values are significantly higher. In an area just off the coast of central/southern Italy fairly high TPW values are observed for all three retrieval types, with a good agreement. Mainland Italy shows low TPW values, although significantly lower for the first-guess IASI retrieval - especially in the area around Parma, where SEVIRI observes very high values (the IASI retrieval is missing coverage in this area) and the first-guess IASI retrieval observes fairly low values. In the cloud covered areas with no SEVIRI/final IASI coverage, the first-guess IASI TPW shows high TPW values for some areas of the Czech Republic, Poland, wester Ukraine, and Belarus. Interestingly, in the area around Austria and Slovenia, where large hail occurred, the TPW is observed as being fairly low (agreeing with other large hail cases previously analysed). Conversely, in the areas of Croatia and Hungary, where large hail also occurred and where the SEVIRI

and final IASI retrieval obtains coverage, the TPW is somewhat higher. A final, insteresting observation is the quite low TPW values obtained by all three retrieval types along the countries at the Adriatic coast, indicating low levels of moisture, even though the K-index indicated some instability.

Summary and notable observations: First off, it is noted that the instability, which was predicted by the GII retrievals of 2015-07-07 (the case study in **section 5.3**) in the regions of northern Italy, Slovenia, Croatia, Hungary, and Slovakia, despite lightning activity not occurring later on that same day, could possibly be explained by the lightning activity observed on 2015-07-08 (this case study). Although it is the assumption in this report, that the GII may indicate instability in a period ranging from a few hours to around 12 hours, this is purely based on previous studies that have utilized this assumption - it is entirely possible that instability indices may, in some cases, be able to predict further into time.

As for the prediction of the lightning activity on 2015-07-08, both the K-index and Lifted index (across all three retrieval types) indicate instability for the areas of afternoon and evening thunderstorm activity. Interestingly, for the areas where lightning activity occurred in the morning hours, before the GII measurements, the K-index indicates very unstable conditions, whereas the Lifted index indicates mostly stable conditions. Finally, the TPW showed some fairly large deviations for certain areas between the SEVIRI/final IASI retrieval and the first-guess IASI retrieval. Also, for two different areas, both exposed to large hail in the afternoon/evening, two different observations were made - for the area of Slovenia/Austria TPW was observed fairly low (complying with the ideal of large hail size indicating lower TPW values) however for the area of Croatia/Hungary TPW values were somewhat high.

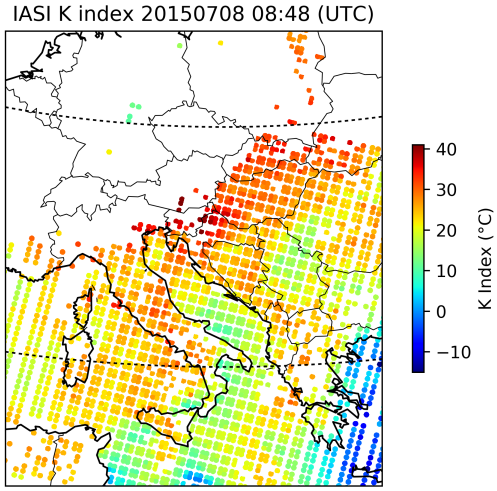

(a) IASI K-index

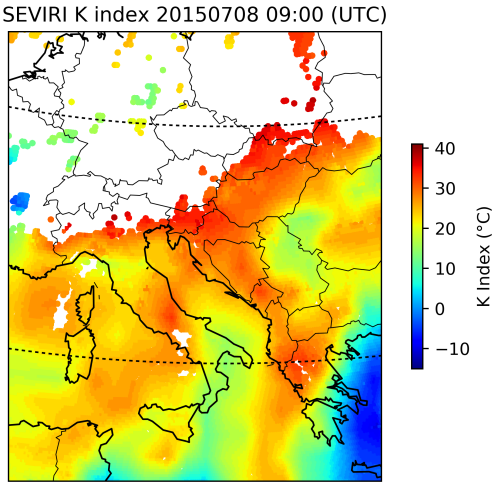

(b) SEVIRI K-index

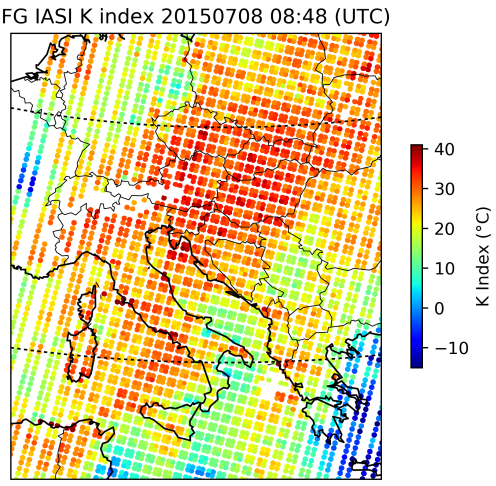

(c) FG IASI K-index

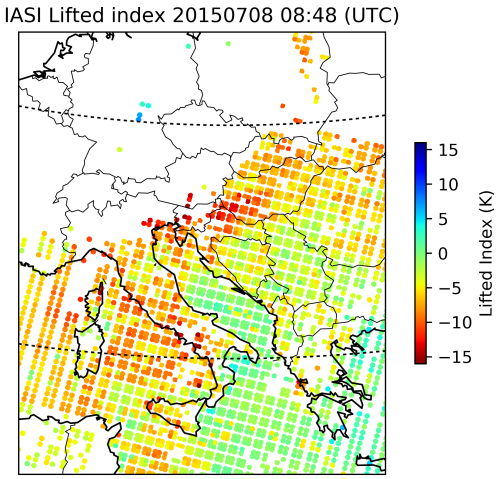

(d) IASI Lifted index

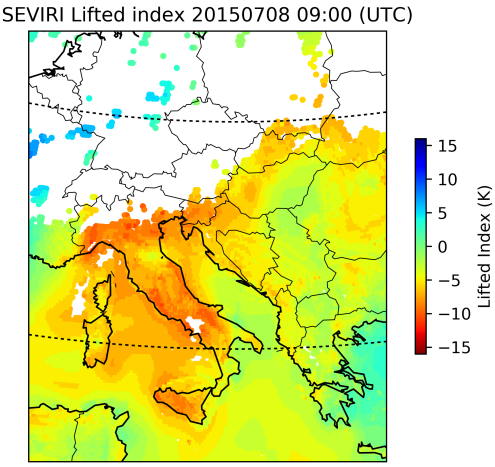

(e) SEVIRI Lifted index

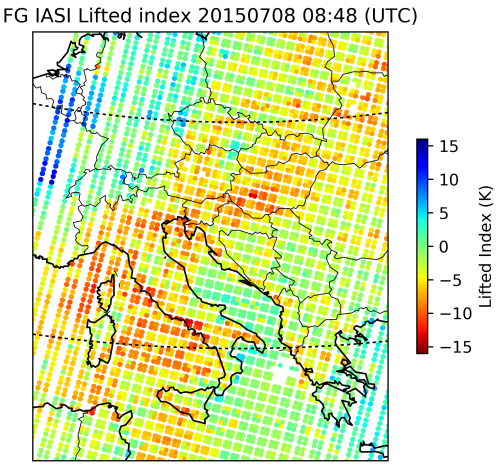

(f) FG IASI Lifted index

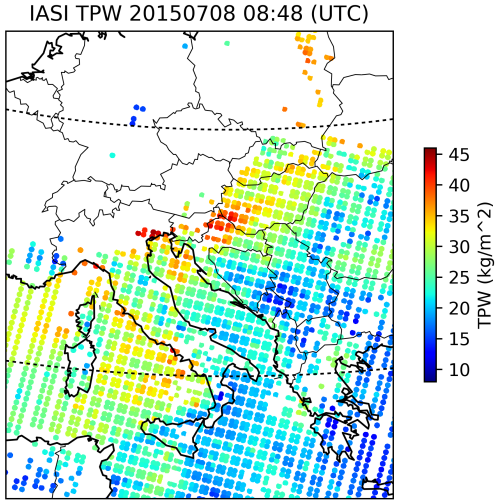

(g) IASI TPW

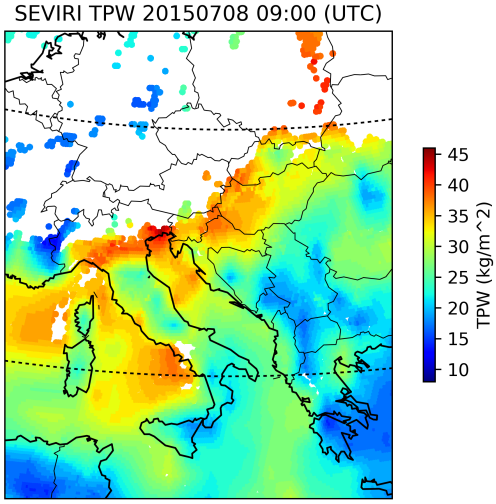

(h) SEVIRI TPW

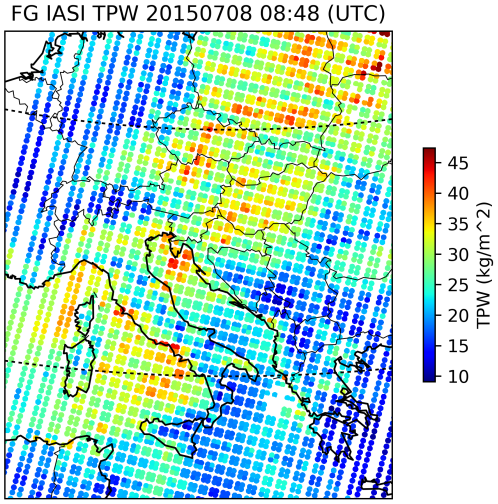

(i) FG IASI TPW

Figure 26: Final IASI, SEVIRI, and first-guess (FG) IASI GII retrievals 2015-07-08.

5.5 Multiple thunderstorms in central & southern Europe 2015-07-24

While the case study of section 5.1 investigated a day where almost the entirety of Europe experienced stable weather this case study investigates a day where nearly the entirety of the southern and central parts of Europe experienced thunderstorm activity.

Lightning activity and severe weather reports: As mentioned, this summer day featured thunderstorm activity in a very large proportion of central and southern Europe. The activity is distributed in many different storms, taking place at various times throughout the day, as opposed to the three cases investigated in sections 5.2-5.4, where lightning activity was observed mainly in one large scale thunderstorm. GLD and Blitzortung data shows lightning activity in the morning hours (before the GII measurements) in southern Italy and the Tyrrhenian Sea to the west, the very eastern Poland, as well as small amounts of morning activity in northern Italy, the Bay of Biscaya, and southern Austria. Activity is observed throughout almost the entire day around the Bay of Biscaya and northern France area. An afternoon and evening thunderstorm is observed in a large area comprising the French/Italian border, Switzerland, part of Austria, northern Italy, and southern Germany. In addition, activity is observed all along the Adriatic coast during the afternoon, with evening activity occurring over Croatia/Slovenia in the evening. Activity is also observed during the afternoon in the entirety of Italy as well as Sardinia and Corsica. Afternoon/evening activity is furthermore observed in the Czech Republic/Slovakia as well as part of Romania and Ukraine.

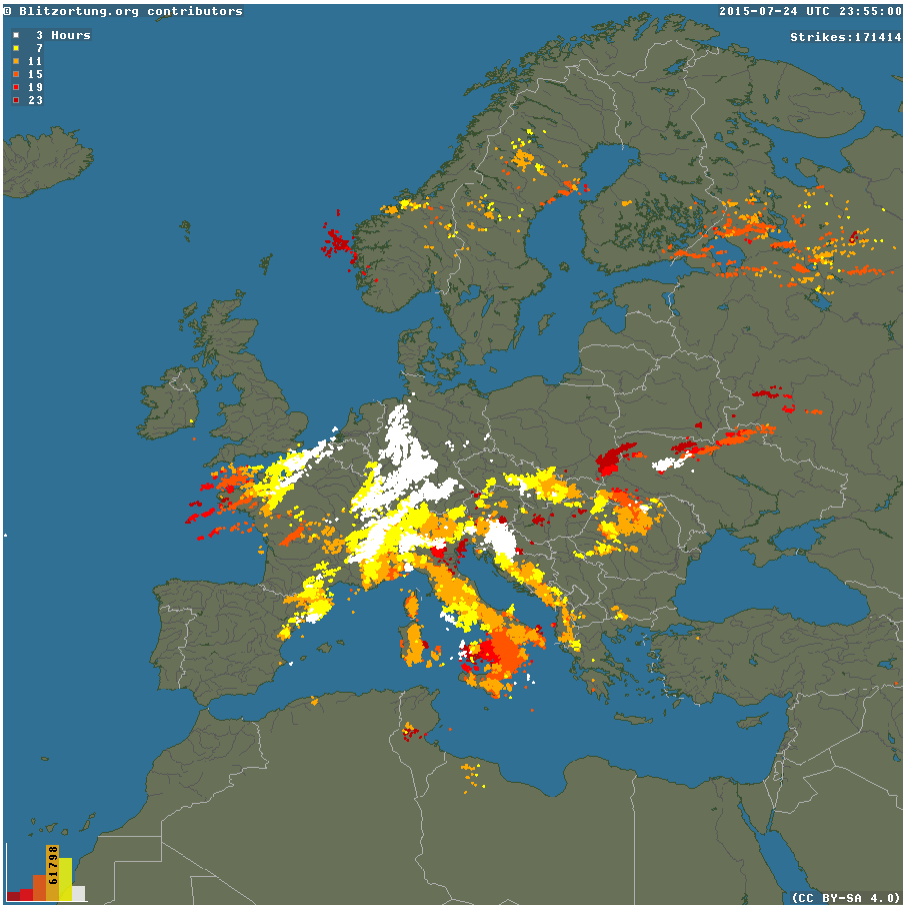

Figure 27: Blitzortung lightning data for the entire day 2015-07-24.

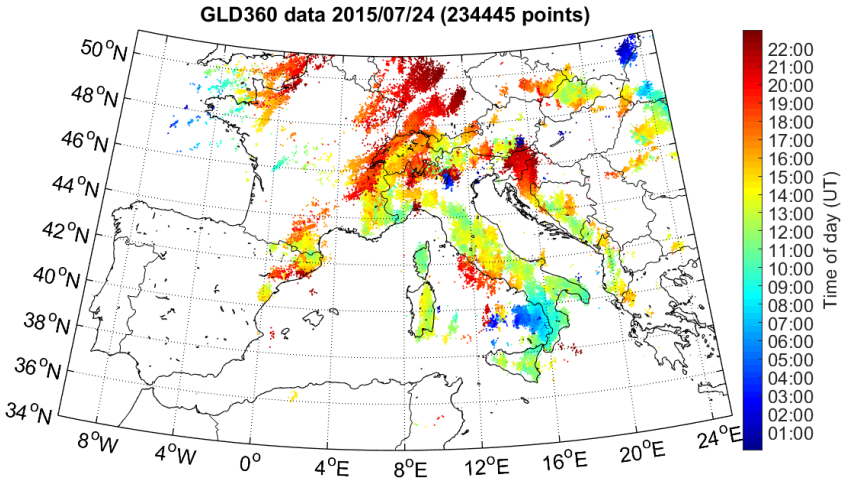

Figure 28: GLD lightning data for the entire day (and full available area) 2015-07-24.

Finally, thunderstorm activity is observed in northern Spain, in the region around Barcelona, and around the French border. In this region, lightning data from the Ebro Valley LMA was also available for this day. This data (seen in figure 29) confirms a large amount of lightning activity in the region roughly between the LMA network and Barcelona.

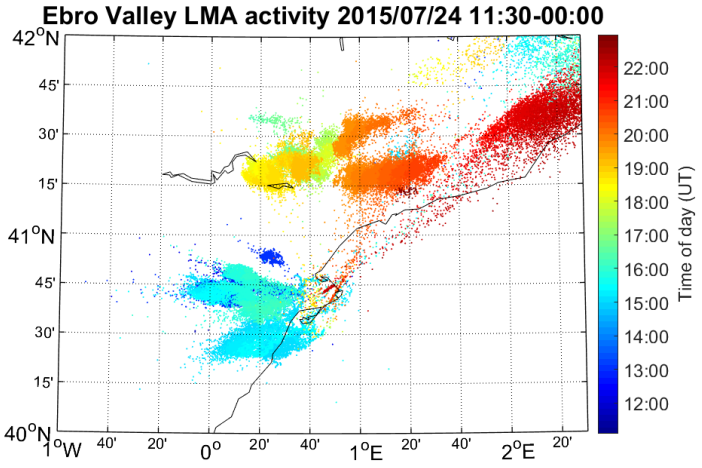

Figure 29: Ebro Valley LMA data for the period 11:30-00:00 on 2015-07-24. Data has been limited to a region in the general vicinity of the LMA network, as the location uncertainty of data that lies far from the network is excessively high (cf. section 3.4).

ESWD data show few notable reports. Strong winds as well as heavy rainfall a few damaging lightning flashes are reported in southern Germany - the rainfall reports just north of Switzerland are reported to have occurred around 19:00 and the damaging lightning and severe wind was reported around 22:00-23:00, corresponding well with lightning activity in the respective areas. Other reports comprise heavy rainfall/severe wind and a single report of hail in the Czech Republic/Slovakia (in the time interval 15:00-18:00) as well as another single report of hail in eastern Hungary (reportedly occurring at roughly 16:30). Both of the reported hail showers do, however, state that the hail were relatively small compared to the hail storms observed in the previous case studies (section 5.2-5.4).

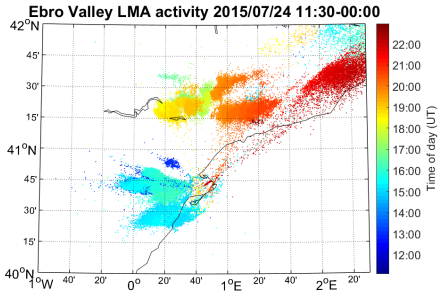

Figure 30: ESWD reports on 20150724 showing hail storms (green triangles), strong winds (yellow squares), damaging lightning (lightning symbol), and heavy rainfall (blue circle).

K-index: Observing first the SEVIRI and final IASI K-index one first notes that most of the regions missing data coverage (due to cloud cover) cohere fairly well with the areas, in which lightning activity was observed in the morning (other areas, such as northern Germany, did not show lightning activity and were presumably under a more stable cloud cover). The entirety of Italy (excluding the regions of missing coverage) shows high K-index values for both retrieval types, however slightly higher values are observed by SEVIRI. A large area around Hungary, Slovakia, Romania, and small parts of Croatia, Austria, the Czech Republic, Poland, Ukraine also show high levels of instability with very near identical values observed by the final IASI and SEVIRI K-index. Moderately high K-index values are furthermore observed in Switzerland and the French/Italian border as well as around Corsica and Sardinia. A region around the Ebro Valley LMA (extending towards and slightly beyond the French border) also shows high instability. The part of Germany central/western Germany, that was not below cloud cover, shows moderate instability (with K-index values around 25 °C). Finally, high K-index values are observed along the Adriatic coastline, extending southwards to Greece, where values then become significantly lower (not how this corresponds very well with lightning activity observations). In all the mentioned areas of high K-index values, lightning activity subsequently occurred (with the only striking exception being Hungary, were only very little activity occurred). Turning the attention to the regions of low K-index (indicating stable conditions), one also observes a good coherence with lightning data: Low K-index values are observed by both the SEVIRI and final IASI retrievals in a large area comprising most of Poland, Belarus, Lithuania, Latvia, and Estonia - a region where no lightning activity was observed. Additionally, very low K-index values are observed around the border between Bulgaria and Romania - also an area of no lightning activity indicated by GLD and Blitzortung.
The first-guess IASI K-index agrees quite well with the final IASI and SEVIRI K-index measurements in clear-sky areas. Further, information is provided for northern parts of Germany, where high K-index values are observed in the west (where lightning activity occurred in the evening) and lower values are seen in the east (where no activity occurred). The north-western part of France shows a high K-index - this corresponds well with the afternoon/evening lightning activity observed in this area. Austria, Slovenia, northern Italy, and Croatia, areas that were partly under cloud cover, all show quite high K-index values, agreeing fairly well with lightning data (with perhaps a slight exception of northern Austria, where little activity occurred). It is again noted, how very high K-index values are observed along the entire Adriatic coastline from north to south with a sudden contrast of very low values observed in Greece, where lightning activity essentially only occurred very close to the border.

Lifted index: The SEVIRI and final IASI Lifted index show negative values (high instability) in the same area comprising Hungary, Slovakia, Romania, and small parts of Croatia, Austria, the Czech Republic, Poland, and Ukraine, in which high K-index values were observed. There are some slight differences between the two retrieval types within this area however, with the final IASI Lifted index showing somewhat lower values than the SEVIRI Lifted index, especially around Romania/Ukraine and Hungary. As was observed for the K-index, both retrieval types indicate instability over the entirety of Italy as well as the area around the Ebro Valley LMA and the Spanish/French border - in the latter area, however, the final IASI retrieval shows significantly lower values. Southern Germany shows values that are slightly negative, corresponding well with what was observed for the K-index. Observing the regions, in which the SEVIRI and final IASI Lifted index values indicate stable conditions, it is observed that these regions agree quite well with what was observed for the K-index - that is, a good coherence is observed between stable areas and areas of no lightning activity. Interestingly, the contrast between the instability indicated in countries along the Adriatic coast north of Greece and the instability

indicated in Greece is not quite as distinguishable in the Lifted index observations - this is the case for all three retrieval types.
The first-guess IASI Lifted index shows slight indications of instability in northern/western France western Germany, where lightning activity was later observed, however not as clearly expressed as was observed for the K-index. In addition, the cloud covered areas in northern Italy, Slovenia, Croatia, and Austria show smaller signs of instability than was observed for the K-index, with values only being slightly negative. Finally, it is noted that areas of high instability (very negative Lifted index values) as observed by the final IASI retrieval generally do not indicate quite as high levels of instability in the first-guess IASI retrieval - examples of this are observed around the Ebro Valley LMA and Spanish/French border area, northern Italy, and the area around Romania/Hungary.

Total Precipitable Water: Immediately one notes quite significant deviations between the SEVIRI and final IASI TPW values - mostly in the Mediterranean and Tyrrhenian Sea (again, as the focus of the analyses is not on instability over oceans this discrepancy is not discussed further - it is, however noted as an interesting observation). Very high TPW values are observed by both retrieval types in an area around western Austria, Slovakia, Hungary, and small parts of Poland and Ukraine, where also very high K-index values and moderately low Lifted index values as well as subsequent lightning activity was observed. High values are also observed in the northern part of Italy. The areas in which heavy rainfall and some hail were reported, just north of Switzerland and around the Czech/Slovakian border, show intermediate and moderately high values, respectively. Finally, fairly high values are also observed by both retrieval types in the area around Ebro Valley - interestingly, the Spanish/French border area show quite low values for the final IASI retrieval, while the SEVIRI TPW remains at a slightly higher level in this area.
The first-guess IASI TPW observations agree quite closely with the final IASI TPW in clear-sky areas. In western France very high TPW values are observed rather locally, while northern France actually show fairly low values (though the bulk of the lightning activity in this area took place in the northern parts). High values are also observed in the cloud covered regions of Ukraine and the very southern Belarus as well as around the coast of Slovenia and Croatia. Relatively low values are observed for the countries along the Adriatic coast, as a sharp contrast to the neighbouring sea, where values are relatively high.

Summary and notable observations: In this case study the K-index showed very promising prediction skills - very strong coherence was observed between all three K-index retrievals and the subsequent observed lightning activity. Also, as opposed to observations of some other cases, the K-index showed few false alarms, meaning that few areas showed a high K-index and no subsequent lightning activity. Similarly, areas of low K-index values generally showed no lightning activity, meaning that the K-index showed few (or virtually no) misses. Interestingly, a stark contrast was seen in the K-index values along the countries of the Adriatic coast, showing high K-index for areas subsequently exposed to lightning activity and low values for Greece, where virtually no lightning activity was observed. This observation indicated that, at least for this case, the K-index was able to distinguish between stable and unstable areas at a fairly local scale.
The Lifted index showed many of the same features observed for the K-index, although with generally smaller contrasts (values in unstable areas weren't *much* more negative than values in stable areas). Also, some deviations between the three retrieval types were observed.
Finally, the TPW values interestingly showed much larger deviations between SEVIRI and IASI retrievals than have been observed for other cases, however these deviations were mainly present over sea areas. TPW values showed moist conditions in most of the areas of subsequent lightning activity, except for the areas around Switzerland/Germany and the countries along the Adriatic coast.

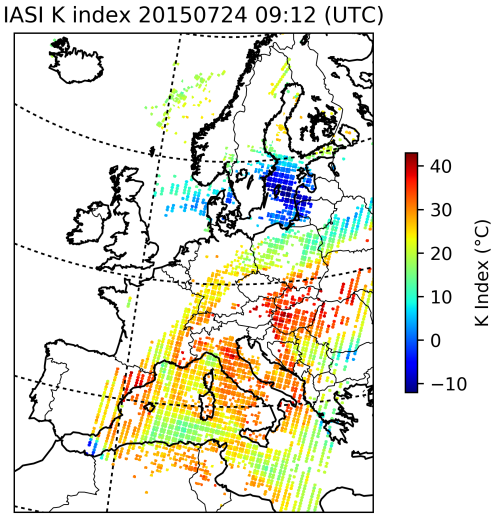

(a) IASI K-index

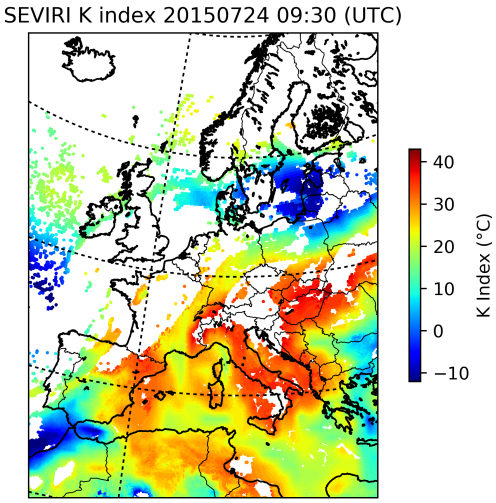

(b) SEVIRI K-index

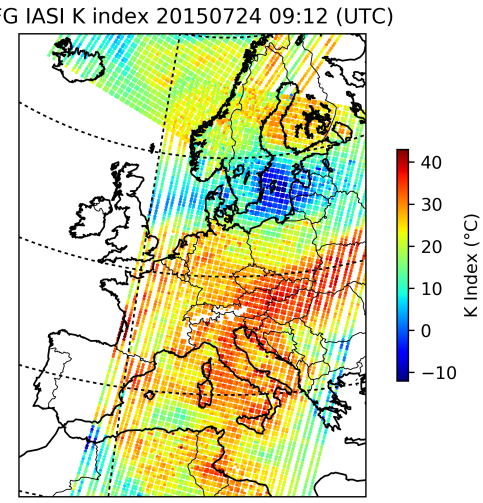

(c) FG IASI K-index

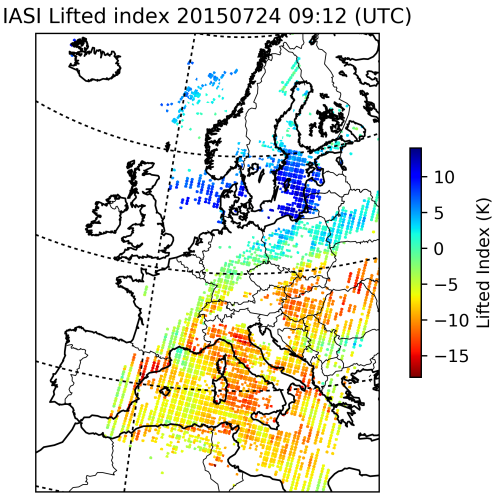

(d) IASI Lifted index

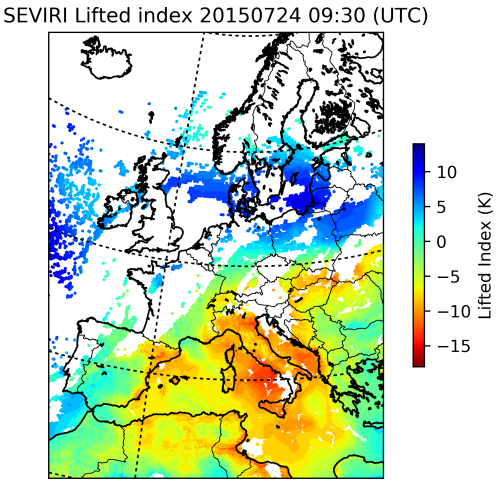

(e) SEVIRI Lifted index

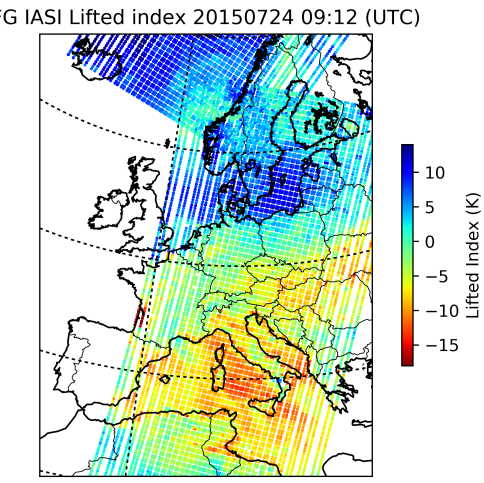

(f) FG IASI Lifted index

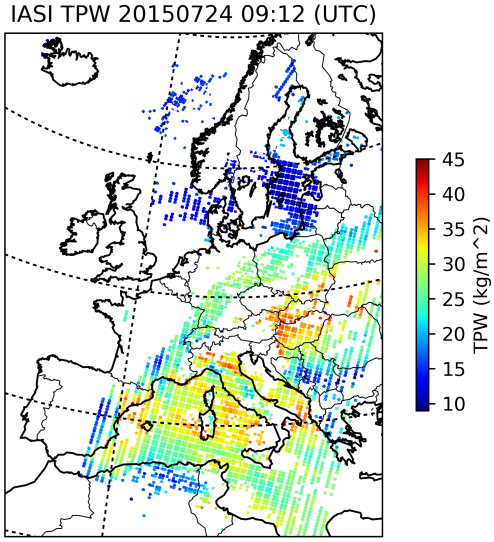

(g) IASI TPW

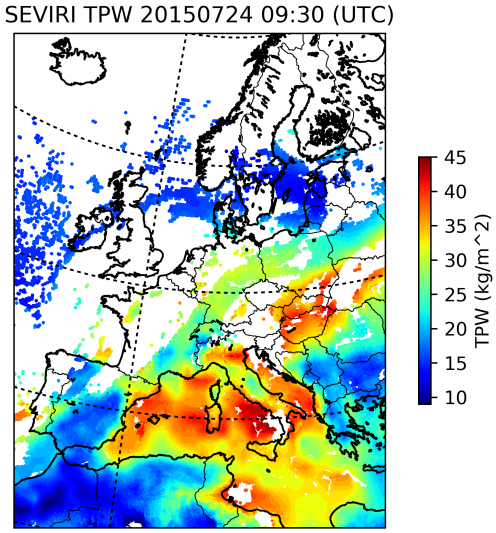

(h) SEVIRI TPW

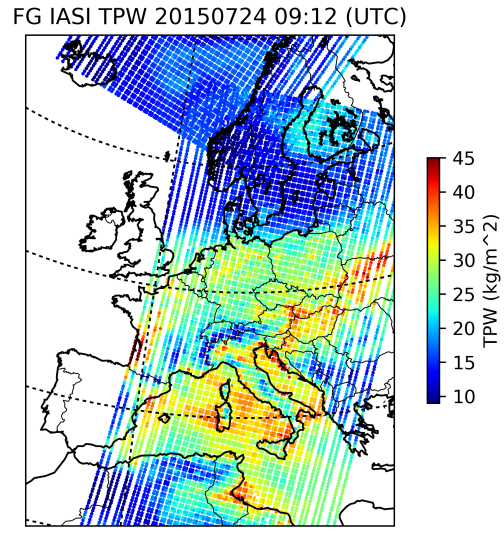

(i) FG IASI TPW

Figure 31: Final IASI, SEVIRI, and first-guess (FG) IASI GII retrievals 2015-07-24.

5.6 Analysis of the temporal development of the SEVIRI GII

This case study is performed with the purpose of investigating the development of the GII, as observed by SEVIRI, during the hours leading up to thunderstorm activity. For this investigation, the case studied in section 5.3 is returned to. The SEVIRI GII (K-index, Lifted index, and TPW) is computed for every other in the time interval 07:00-17:00. The resulting GII plots are seen in figures 32 and 33.

The bi-hourly SEVIRI GII plots first of all show a general tendency, valid for all three indices of the GII - namely, that the instability indices over a given region change quite slowly with time. Although only one case is presented here, similar analyses of the SEVIRI GII were performed for many other case studies and the slow temporal development of the GII was common for all the cases investigated. One obviously undesired feature of the SEVIRI GII, which is displayed by figures 32 and 33, is the limitation due to the retrieval only functioning in clear-sky areas. Tracking either of the three instability indices through the hours from 07:00-17:00 and referring back to the lightning data observed during this day (figures 19 and 18), one notes how, for instance, the area around Rome, where lightning activity was observed in the afternoon, slowly starts to lose coverage (around 13:00). Once the area is out of SEVIRI coverage one can deduce (with reasonable certainty, barring any malfunctions of the SEVIRI data collection or processing) that this region is now covered by clouds - however no instability index values can be obtained for the region.

While it is not completely rejected that some information might potentially be gathered from a study of the temporal evolution of the GII, upon analysis of the bi-hourly SEVIRI GII (as shown above) for several case studies, any significant benefits from such qualitative studies were not observed. It is entirely possible, that through more advanced types of studies of the GII development (perhaps by computing gradients of the indices), the continuous coverage of SEVIRI could improve the prediction skills of the indices. It must again be stressed, however, that problems naturally arise as soon as a cloud develops and SEVIRI coverage disappears.

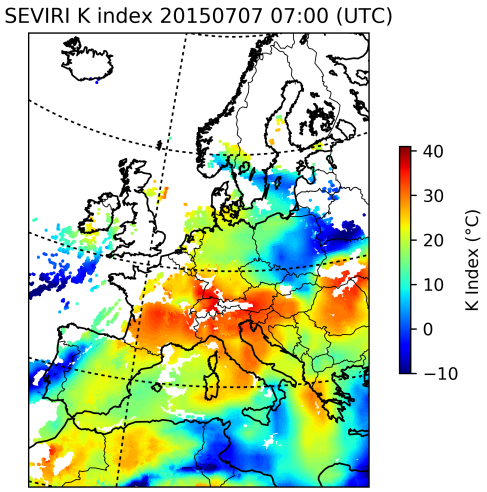

(a) SEVIRI K-index

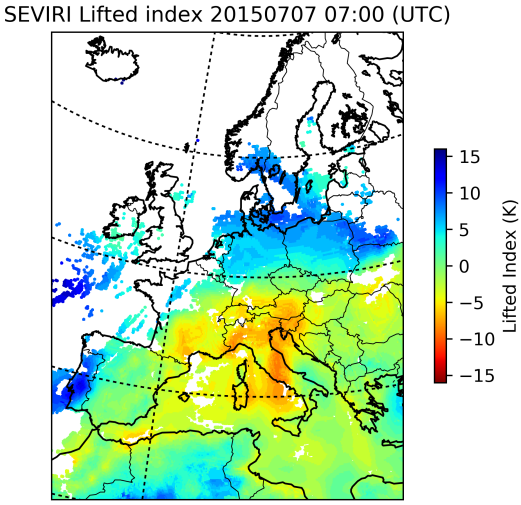

(b) SEVIRI Lifted index

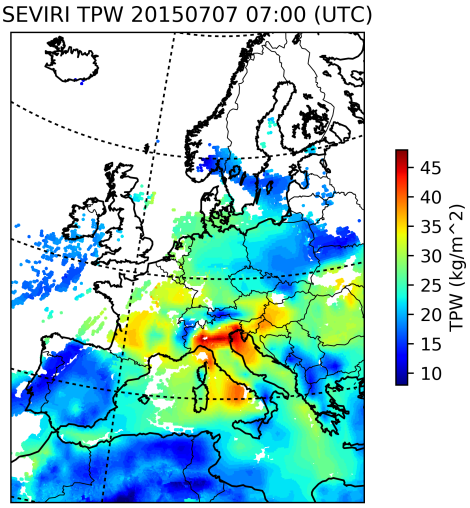

(c) SEVIRI TPW

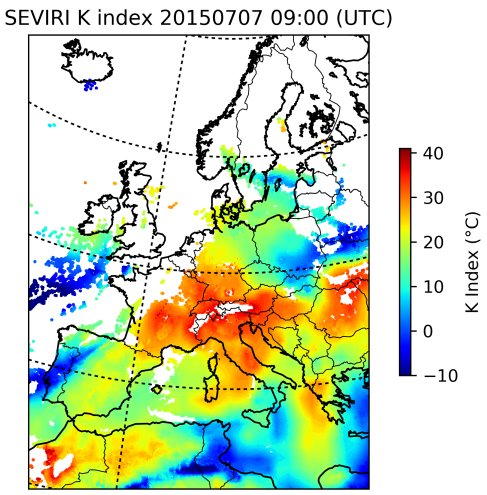

(d) IASI Lifted index

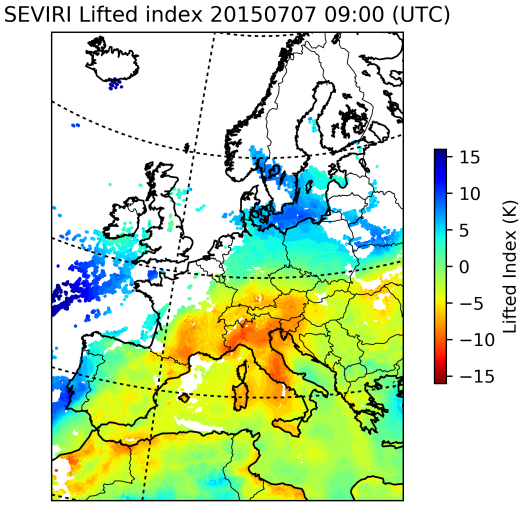

(e) SEVIRI Lifted index

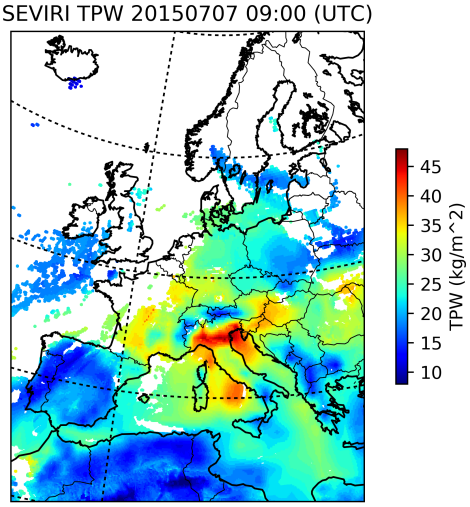

(f) FG IASI Lifted index

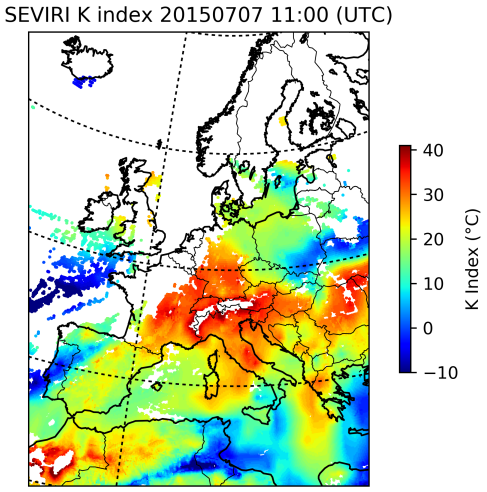

(g) IASI TPW

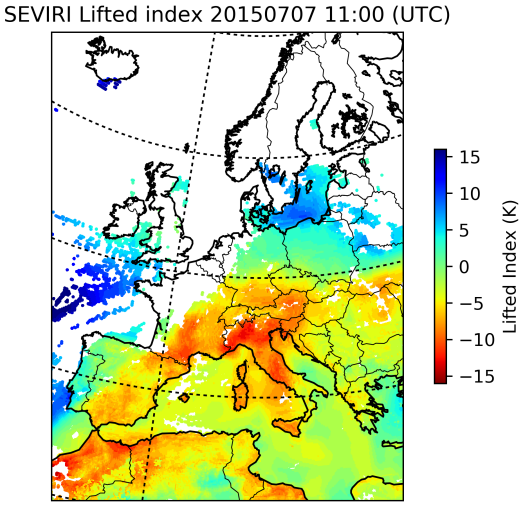

(h) SEVIRI TPW

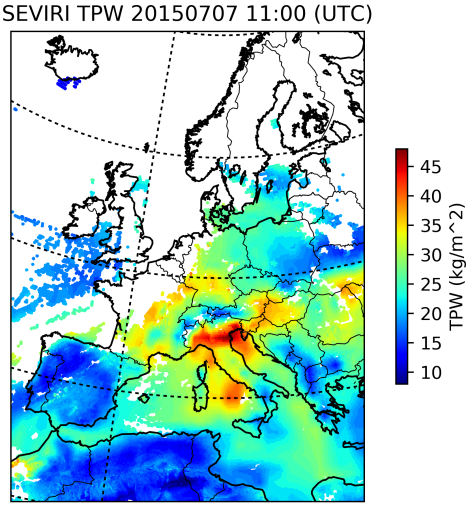

(i) FG IASI TPW

Figure 32: SEVIRI GII observed 2015-07-07 07:00-11:00

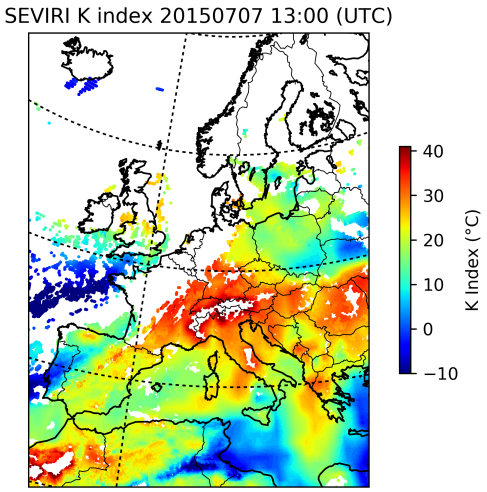

(a) SEVIRI K-index

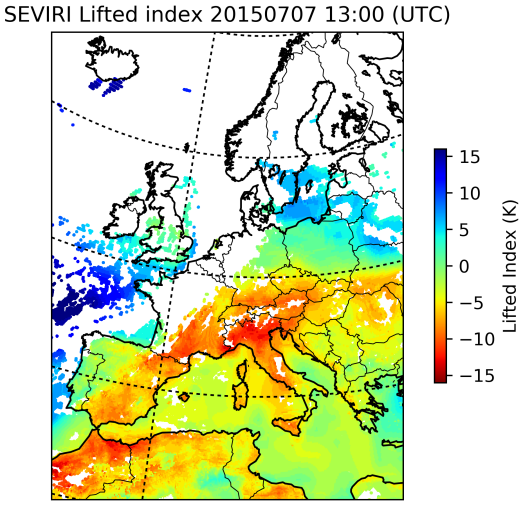

(b) SEVIRI Lifted index

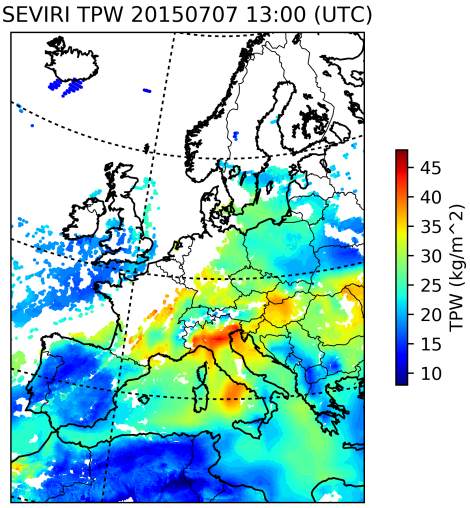

(c) SEVIRI TPW

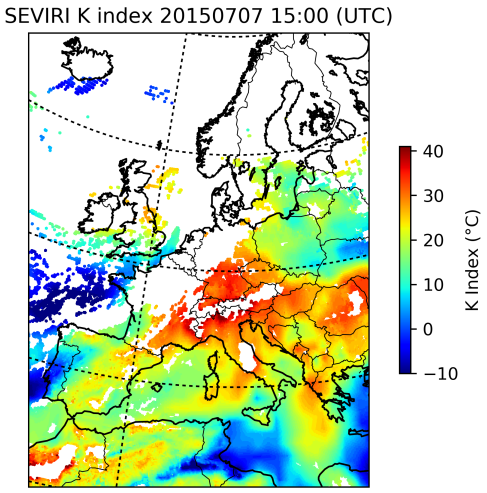

(d) IASI Lifted index

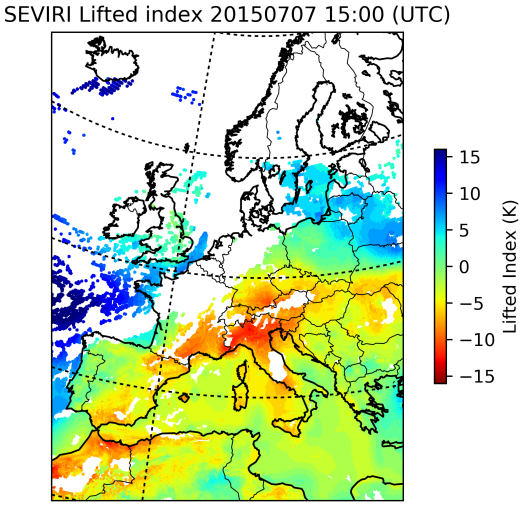

(e) SEVIRI Lifted index

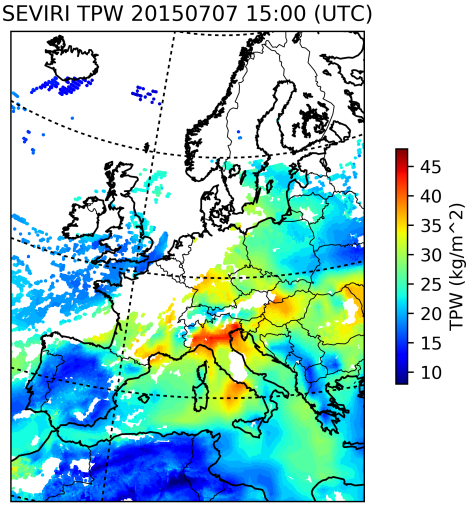

(f) FG IASI Lifted index

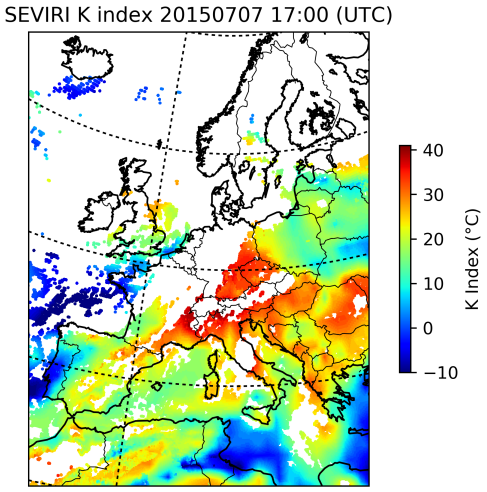

(g) IASI TPW

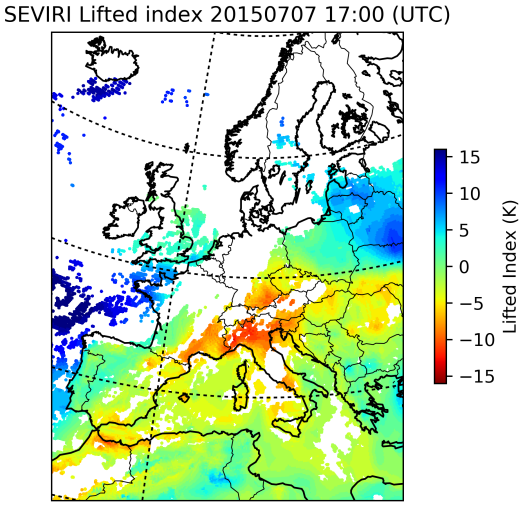

(h) SEVIRI TPW

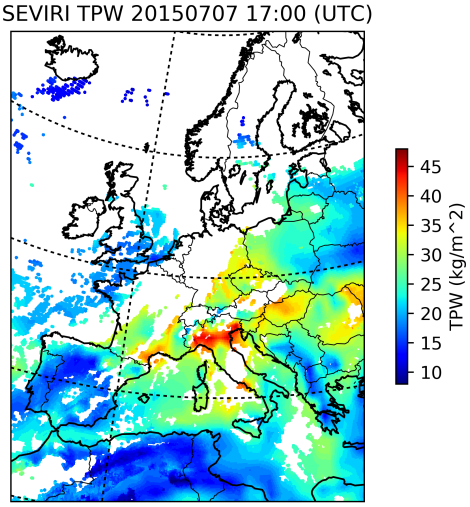

(i) FG IASI TPW

Figure 33: SEVIRI GII observed 2015-07-07 13:00-17:00

5.7 Analysis of difference between first-guess and final IASI GII

2 cases w/ difference plots between IASI/FG IASI KI/LI/TPW (Ebro Valley and Europe Stable cases?)
The benefits of obtaining GII for both cloudy and cloud-free environments are quite obvious - they were illustrated clearly in the case study of section 5.2, where clouds prevented SEVIRI/final IASI GII coverage in nearly the entire area of interest, leaving the first-guess IASI GII as the only option for GII retrieval. If the first-guess IASI GII is to be used consistently as a substitute for the SEVIRI/final IASI GII, however, the effect that the optimal estimation retrieval algorithm is *not* used in generating the first-guess IASI temperature profiles must be investigated. Asserting precise uncertainties of the IASI/SEVIRI temperature profiles and the difference in these uncertainties between the first-guess and final IASI profiles is not possible simply by analytical derivations. Some aspects about the uncertainties are provided in (EUMETSAT, IASI Level 2: Product Generation Specifcation and EUMETSAT, Algorithm Theoretical Basis Document for the MSG GII/TOZ Product). Of course, the main assumption is that the optimal estimation retrieval improves (minimizes) the error of the temperature and humidity profiles. Therefore, in this case study, the difference between the first-guess and final IASI GII is computed in cloud-free areas (where the final IASI GII is available). Note that the difference between the first-guess and final IASI GII lies in the calculation of the temperature and humidity profiles, while it is the GII, resulting from these profiles, that are investigated.

In order to investigate two cases, during which weather conditions were different, the cases studied in section 5.1 (2016-08-13, where stable conditions were dominant) and 5.5 (2015-07-24, where unstable conditions were dominant). The difference between the first-guess and final IASI GII in cloud-free areas was computed for each of the two cases and the result is seen in figure 34. Recall that two consecutive IASI sweeps were used for the case on 2016-08-13.

Observing first the first-guess/final difference of the K-index for the 2016-08-13 case (figure 34 (a)), it is noted that the first-guess K-index is slightly lower than the final K-index (indicated by negative values of the difference) for the majority of the covered area. Meanwhile, for the 2015-07-24 case K-index difference, the first-guess index appears to be lower for about half the coverage area and higher for the other half. Both cases show a K-index difference that varies significantly within a fairly small area - this is for instance seen in figure 34 (d) around Austria/Slovakia and Italy, where values change between roughly $-4°$C and $+4°$C over small distances. This feature seems more prevalent in the 2015-07-24, where thunderstorms occurred in most of southern/central Europe.

Turning the attention to figures 34 (b) and (e), showing the Lifted index difference for the two cases, it is immediately noted, that the differences seem to be more "stable" - as opposed to what was observed for the K-index differences, the Lifted index differences do not show small areas were values cover a very wide range. Instead, the Lifted index differences are distributed in fairly large areas of high values, negative values, nearly-zero values etc.. It is clear that the first-guess IASI Lifted index is much closer to the final IASI Lifted index in the 2016-08-13 case compared to the 2015-07-24 where the final IASI Lifted index interestingly is observed to be significantly lower in regions where thunderstorm activity occurred - thus, it seems as though, at least in this case, the first-guess IASI Lifted index tends to overstate the instability level in areas where instability is present. Such a trend was not quite observed for the K-index differences.

Finally, the TPW differences, shown in figures 34 (c) and (f), show the same pattern of values being more "stable" - this is, however, mostly true for the 2016-08-13 TPW differences, as the 2015-07-24 TPW differences do show some relatively small areas of wide-ranging values (for instance northern Italy and eastern Austria in figure 34 (f)). Interestingly, it seems that for the 2015-07-24 case, the first-guess IASI GII seems to understate the TPW values in areas of subsequent thunderstorm activity. For the 2016-08-13 case, where stable weather was observed in most of Europe throughout the day, the first-guess and final IASI TPW agree fairly well.

Despite some clear differences between the first-guess and final IASI GII in the investigation of the cases above, the first-guess IASI GII still seems useable as a substitute for the final IASI (or SEVIRI) GII. Although differences were especially prevalent in the case study where a large amount of thunderstorm activity was observed (and the areas of high instability are most often the area of prime interest), differences between the two GII retrievals rarely exceeded ± 4 °C (K-index), ± 4 K (Lifted index), or ± 4 kg/m^2 (TPW).

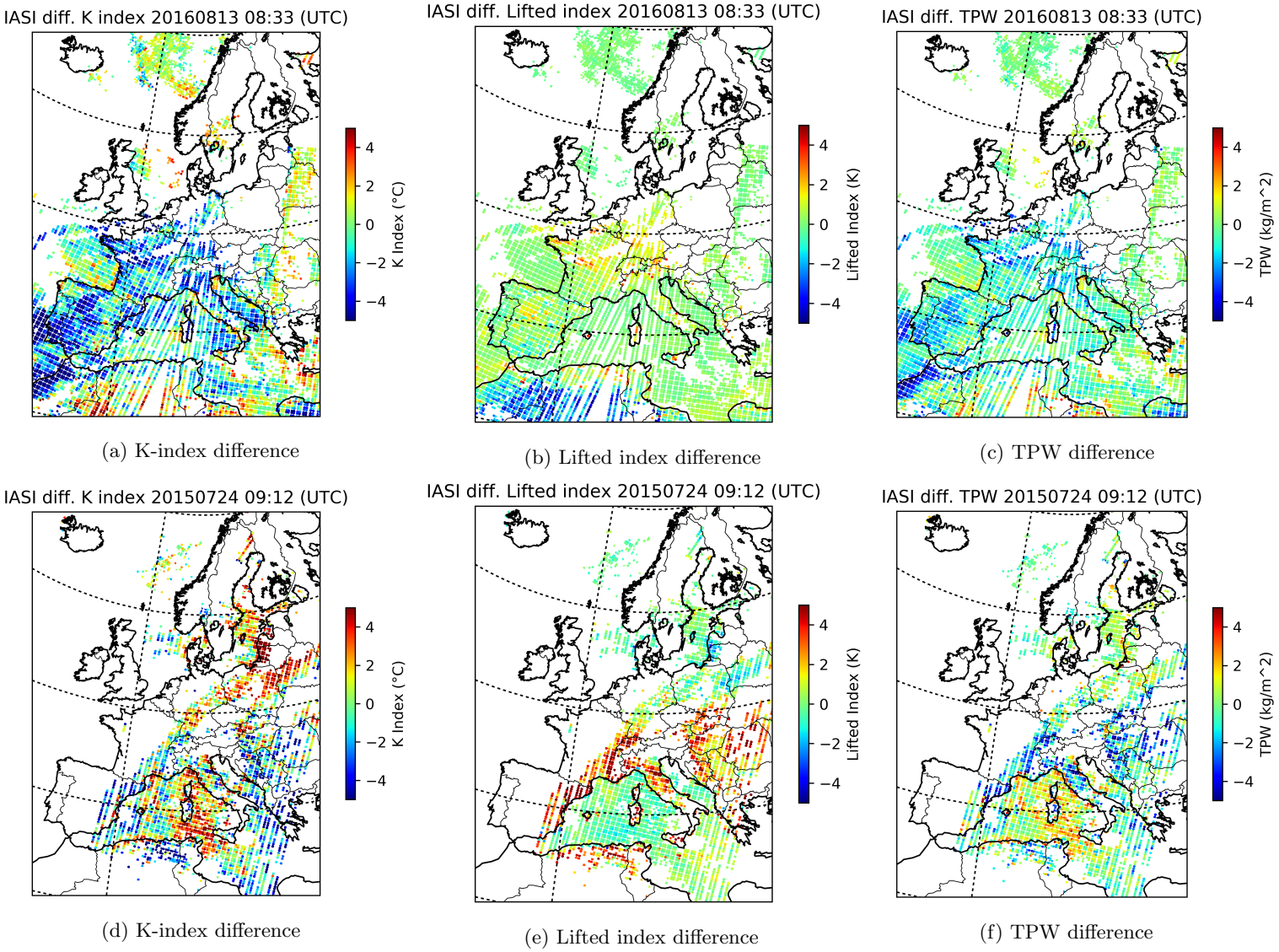

(a) K-index difference

(b) Lifted index difference

(c) TPW difference

(d) K-index difference

(e) Lifted index difference

(f) TPW difference

Figure 34: Differences between first-guess and final IASI KI/LI/TPW. Note that each difference is computed as the first-guess index minus the final index (not the absolute difference).

6 Discussion

The case studies of section 5 presented a lot of interesting observations. Overall, it certainly seems fair to say that the SEVIRI/IASI GII does hold some degree of predictive abilities with respect to severe convective weather events.

Although the K-index in many cases proved highly effective in predicting thunderstorm activity, perhaps best exemplified in the case study of section 5.5, where widespread thunderstorm activity occurred, it did also exhibit a fair amount of false alarms (high K-index values in areas of no subsequent severe weather activity). The opposite feature however, K-index values being low over areas of subsequent lightning activity, was quite rarely observed.

The Lifted index generally agreed fairly well with the K-index in its prediction of unstable areas, although it regularly seemed to show smaller contrasts between stable and unstable areas. As was mentioned in section 2.1, the Lifted index has occasionally been considered a possible indicator of tornadoes. On the basis of these case studies alone, this trait seems hard to confirm (though it cannot be rejected either).

As described in section 2.1, the TPW content is not an instability index in the same sense as the K- and Lifted index. It is a relatively simple air mass parameter indicating the humidity of the atmosphere, an important element of a severe thunderstorm. As such, the TPW does not quite function as a predictor of instability on its own but acts as more as a supplementary source of information about the atmospheric conditions. An interesting observation is seen in the case study of section 5.3, where a region of Romania showed quite high K-index and quite low Lifted index values (indicating high instability) but the TPW values remained relatively low - the area only saw very limited amounts of subsequent lightning activity. It is speculated, whether the TPW might potentially, at least in some situations, act as an indicator of the severity of a storm indicated by the K-index and/or Lifted index.

One of the main questions raised in this report, was whether the GII retrieval based on IASI first-guess temperature and humidity profiles could be utilized on an even footing with the already implemented SEVIRI GII and the IASI GII based on the post optimal estimation retrieval temperature and humidity profiles. If so, this retrieval provides not only a much improved coverage in general but permits GII analysis on days, where clouds are consistently present (such as the case studied in section 5.2). Taking into account the investigation of the difference between the first-guess and final IASI GII of section 5.7 as well as all the qualitative comparisons of all three GII retrieval types in sections 5.1-5.5, it certainly seems reasonable to introduce the first-guess IASI GII as a substitute to the SEVIRI/final IASI GII in situations where cloudy conditions prevent analysis using the latter retrieval types.

A natural trade-off lies in the orbit types of the MSG and Metop satellites: While MSG provides continuous coverage over a very large area (including the entirety of Europe and Africa), Metop provides global coverage, however with only two images per day (one at local morning and one at local evening). As an attempt to assess the value of obtaining a new GII measurement every 15 minutes (as is the case for SEVIRI), the temporal SEVIRI GII development was shown for a single case in section 5.6. This case studied highlighted the general tendency of the GII to evolve quite slowly. Small changes were observed in the indices as time passed, however as the time of thunderstorm activity approaches for a given area, clouds (naturally) start to develop, meaning that the SEVIRI GII can no longer be monitored for the given area.

With the slow rate of change of the GII and all the observations of the case studies considered, it seems that the addition of all-sky GII retrieval from IASI (although likely not as accurate as the clear-sky IASI retrieval due to not undergoing the optimal estimation algorithm) is likely more valuable than having the continuous coverage of the SEVIRI GII. Of course, this conclusion is only based on the case studies of this report and it is entirely possible that another type of analysis scheme could be developed taking into account the temporal changes of the indices of the GII.

Based on the results of this report, possibilities of future studies of the predictive capabilities of the GII (or other instability indices) seem promising. For instance, it would be interesting to perform a more quantitative comparison between the GII and e.g. lightning data, where approximate detection efficiencies and false alarm rates etc. are computed for the different indices based on a much large amount of data.
Successor projects are planned for both MSG and Metop - the Meteosat Third Generation (MTG) and the Metop Second Generation (Metop-SG), respectively, both set to launch in the early 2020's. The MTG will carry an improved version of the SEVIRI instrument (the Flexible Combined Imager, FCI), which features temporal and spatial resolution compared to SEVIRI. It also contains 16 channels, as opposed to SEVIRI's 12. Most interesting is the addition of the InfraRed Sounder (IRS), which is an IASI-like instrument, provding measurements in many more infrared channels. The MTG is not, however, planned to carry any microwave sounders (such as AMSU and MHS aboard Metop), which means that utilizing auxiliary microwave measurements to produce a "first-guess SEVIRI GII" is not a possibility (EUMETSAT, MTG-FCI: ATBD for Global Instability Indices Product).

The Metop-SG will contain an almost identical version of the IASI instrument as well as two new microwave instruments: The MicroWave Sounder (MWS) and the MicroWave Imager (MWI). The improved resolution of the MWS and MWI compared to the AMSU and MHS will provide more accurate first-guess temperature and humidity profiles, which in return provides a more accurate first-guess GII. Details about the instruments can be found on the EUMETSAT website[6].

[6] http://www.eumetsat.int/website/home/Satellites/FutureSatellites/EUMETSATPolarSystemSecondGeneration/EPSSGDesign/index.html

7 Conclusion

The main goals of this project was to investigate characteristics of a series of instability indices (the GII) and to qualitatively analyse their predictive abilities in relation to severe convective weather such as thunderstorms. This was done by means of a series of case studies, which showed fairly good coherence between GII measurements and subsequently observed lightning and severe weather activity, however the predictive abilities of the GII (both as individual indices and as a collective product) was by no means perfect. A detailed summary of the observations of each case study is provided at the end of each case study section and further commented in the discussion in section 6 above. Two retrieval types, the first-guess and the final, for the IASI GII were developed for this report, with the first-guess IASI GII's all-sky coverage being a seemingly valuable addition to GII analysis.
With the launch of the next generation of Metop (Metop-SG, carrying new microwave sounders essential for the first-guess retrieval) it will be interesting to see how much the first-guess IASI GII retrieval can be improved, since section 5.7 did show some deviations from the final (post optimal estimation algorithm) IASI GII.

It is hoped that the experience gained and the tools developed (in the shape of Python processing programs) through the work on this report will contribute to further investigations on instability indices and potentially to the auxiliary data collection of the ASIM data center.

8 Appendix

8.1 Programs for GII processing and visualisation

Data	Data format	Python program
		SEVIRI_GII_read()
SEVIRI GII	BUFR (1 file per 15 minute scan)	
IASI Level 2 product	NetCDF	IASI_GII_process()

Table 3: Basic overview of the programs written to process and visualize the SEVIRI and IASI GII.

8.1.1 SEVIRI_GII_read()

The SEVIRI GII data is delivered in BUFR files (Binary Universal Format for the Representation of meteorological data) - one file contains one full SEVIRI scan, corresponding to 15 minutes of scanning time. A lot of time was spent attempting to properly read the data of the BUFR files and many different methods were tried. Finally, a good solution to the problem was found in the python package *trollbufr*. This package is a part of the *PyTroll* library, an open-source software collaboration project of several national meteorological services and universities (including the Danish Meteorological Institute). A program designed to read the SEVIRI GII files was written. It extracts the relevant data from the BUFR files, reformats them into numpy-arrays, makes a geographical projection and resampling of the data using *pyproj* and *pyresample* (another package in the PyTroll library). Finally, plots of the K-index, Lifted index, and TPW content are constructed and saved (using the simple *pyplot* module).

8.1.2 IASI_GII_process()

The IASI Level 2 Product (containing the temperature and humidity profiles necessary for GII computation) is delivered in the NetCDF format, much simpler to read than the BUFR files. Upon extracting the necessary data from the IASI Level 2 Product into masked numpy arrays, the K-index, Lifted index, and the TPW content is computed following the principles described in section 2.4 (see also the references given in this section for detailed descriptions on the empirical formulas used). The GII computation is performed for both the fist-guess and final temperature and humidity profiles, resulting in both the first-guess and final GII retrievals. Finally, the GII data is projected an resampled using the *pyproj* and *pyresample* modules (the same modules used for the SEVERI plotting routine). Optionally, the user may also choose to compute (and plot) the difference between the first-guess and final IASI GII, creating plots of the type seen in section 5.7.

8.2 Processing and visualisation of lightning data

GLD360, LINET, and Ebro Valley LMA data are all delivered in simple text files (.txt or .dat) and thus are fairly redundant to plot in Matlab, Python or any other language. For this project a Matlab function was created for the reading and plotting of data from each of the three mentioned lightning network. The functions contain essentially the same structure and allow for the user to specify geographical and temporal limits for the data to be plotted.

9 References

[1] Andersen, J. K., Kristensen, M. L., *Comparison and analysis of the Ebro Valley LMA and GLD360 lightning locating systems*, Fagprojekt at Technical University of Denmark, supervisors: Torsten Neubert & Olivier Chanrion, June 2016

[2] Betz, H. D., Schmidt, K., Laroche, P., Blanchet, P., Oettinger, W. P., Defer, E., Dziewit, Z., Konarski, J., *LINET - An international lightning detection network in Europe*, Atmospheric Research, Vol. 91, p. 564–573, 2009

[3] Cummins, K. L., Murphy, M. J., *An Overview of Lightning Locating Systems: History, Techniques, and Data Uses, With an In-Depth Look at the U.S. NLDN*, IEEE Transactions on Electromagnetic Compatibility, Vol. 51, 2009

[4] de Coning, E., Koenig, M., Olivier, J., *The combined instability index: a new very-short range convection forecasting technique for southern Africa*, Meteorological Applications, Vol. 18, p. 421-439, 2011

[5] EUMETSAT, *MTG-FCI: ATBD for Global Instability Indices Product*, Issue v3, January 8th 2013 (Available through `http://www.eumetsat.int/website/home/Satellites/FutureSatellites/MeteosatThirdGeneration/MTGResources/index.html`)

[6] EUMETSAT, *Algorithm Theoretical Basic Document for the MSG GII/TOZ Product*, EUMETSAT Doc. No.: EUM/MET/DOC/11/0247, Version 3, May 24th 2013 (Available through `http://www.eumetsat.int/website/home/Data/TechnicalDocuments/index.html`)

[7] EUMETSAT, *Global Instability Index: Product Guide*, EUMETSAT Doc. No.: EUM/TSS/MAN/15/802106, Issue v1C, September 2nd 2015 (Available through `http://www.eumetsat.int/website/home/Data/TechnicalDocuments/index.html`)

[8] Website of Meteorologist Haby, J., `http://www.theweatherprediction.com/habyhints/294/`, section on Precipitable Water, June 6th 2017

[9] Haklander, A. J, van Delden, A., *Thunderstorm predictors and their forecast skill for the Netherlands*, Atmospheric Research 67–68 p. 273–299, 2003

[10] Koenig, M. & de Coning, E., *The MSG Global Instability Indices Product and Its Use as a Nowcasting Tool*, Weather and Forecasting, volume 24, 2008

[11] Peppler, Randy A., *A Review of Static Stability Indices and Related Thermodynamic Parameters*, Climate and Meteorology Section - Illionois State Water Survey Campaign, sections 3.1-3.2, 1988

[12] Peppler, R. A., Lamb, P. J., *Tropospheric static stability and central North American growing season rainfall*, Monthly Weather Review, Volume 117, p. 1156-1180, 1989

[13] Rodgers, C. D., *Retrieval of Atmospheric Temperature and Composition From Remote Measurements of Thermal Radiation*, Reviews of Geophysics and Space Physics, Vol 14, No. 4, 1976

[14] Thomas, R. J., Krehbiel, P.R., Rison, W., Hunyady, S. J., Winn, W. P., Hamlin, T., and Harlin, J., Accuracy of the Lightning Mapping Array, Journal of Geophysical Research, Vol. 109, D14207, 2004

[15] Uman, M. A., *The Lightning Discharge*, chapters 1-2, Dover publications INC, second edition, 2001

[16] Vaisala, *The Unique Vaisala Global Lightning Dataset GLD360*, available from Vaisala website: `http://www.vaisala.com/en/products/thunderstormandlightningdetectionsystems/Pages/GLD360.aspx`, 2015

[17] Wanke, E., Andersen, R., Volgnandt, T., *Blitzortung.org - A World-Wide Low-Cost Community-Based Time-of-Arrival Lightning Detection and Lightning Location Network*, Project Description Document, available from `http://da.blitzortung.org/cover_your_area.php`, May 11th 2014

DTU Space, Danmarks Tekniske Universitet, Elektrovej
bygning 328, 2800 Kgs. Lyngby

www.space.dtu.dk